Geophys. J. Int. (2003) **152,** 515–565

Gaussian statistics for palaeomagnetic vectors

J. J. Love[1] and C. G. Constable[2]

[1] *US Geological Survey, Denver Federal Center,* PO Box 25046 MS 966, *Denver CO* 80225-0046, *USA*
[2] *Institute of Geophysics and Planetary Physics, Scripps Institution of Oceanography, University of California, La Jolla,* CA 92093-0225, *USA*

Accepted 2002 June 26. Received 2002 June 13; in original form 2001 March 23

SUMMARY

With the aim of treating the statistics of palaeomagnetic directions and intensities jointly and consistently, we represent the mean and the variance of palaeomagnetic vectors, at a particular site and of a particular polarity, by a probability density function in a Cartesian three-space of orthogonal magnetic-field components consisting of a single (unimodal) non-zero mean, spherically-symmetrical (isotropic) Gaussian function. For palaeomagnetic data of mixed polarities, we consider a bimodal distribution consisting of a pair of such symmetrical Gaussian functions, with equal, but opposite, means and equal variances. For both the Gaussian and bi-Gaussian distributions, and in the spherical three-space of intensity, inclination, and declination, we obtain analytical expressions for the marginal density functions, the cumulative distributions, and the expected values and variances for each spherical coordinate (including the angle with respect to the axis of symmetry of the distributions). The mathematical expressions for the intensity and off-axis angle are closed-form and especially manageable, with the intensity distribution being Rayleigh–Rician. In the limit of small relative vectorial dispersion, the Gaussian (bi-Gaussian) directional distribution approaches a Fisher (Bingham) distribution and the intensity distribution approaches a normal distribution. In the opposite limit of large relative vectorial dispersion, the directional distributions approach a spherically-uniform distribution and the intensity distribution approaches a Maxwell distribution. We quantify biases in estimating the properties of the vector field resulting from the use of simple arithmetic averages, such as estimates of the intensity or the inclination of the mean vector, or the variances of these quantities. With the statistical framework developed here and using the maximum-likelihood method, which gives unbiased estimates in the limit of large data numbers, we demonstrate how to formulate the inverse problem, and how to estimate the mean and variance of the magnetic vector field, even when the data consist of mixed combinations of directions and intensities. We examine palaeomagnetic secular-variation data from Hawaii and Réunion, and although these two sites are on almost opposite latitudes, we find significant differences in the mean vector and differences in the local vectorial variances, with the Hawaiian data being particularly anisotropic. These observations are inconsistent with a description of the mean field as being a simple geocentric axial dipole and with secular variation being statistically symmetrical with respect to reflection through the equatorial plane. Finally, our analysis of palaeomagnetic acquisition data from the 1960 Kilauea flow in Hawaii and the Holocene Xitle flow in Mexico, is consistent with the widely held suspicion that directional data are more accurate than intensity data.

Key words: Earth's magnetic field, geomagnetic variation, geomagnetism, palaeointensity, palaeomagnetism, statistical methods.

1 INTRODUCTION

As the result of complex dynamic processes operating in the Earth's core (Busse 1983; Roberts 1992), the geomagnetic field exhibits a wide range of temporal variation: from reversals and excursions to inter-transitional secular variation (Bloxham *et al.* 1989; Merrill & McFadden 1990; Courtillot & Valet 1995). Palaeomagnetic data record this time-dependency over geological and long, historical timescales, by virtue of the magnetization acquired by lava flows, sedimentary rocks, and archaeological artefacts. Ideally, for time-series analyses, palaeomagnetic data would be distributed both regularly in time and with sufficient temporal density so as

to avoid aliasing. But because volcanic eruptions occur sporadically over time, because sedimentation rates are non-uniform in time, and because archaeological artefacts can come from different historical periods of time, palaeomagnetic data are often analysed statistically. Of course, the Earth's magnetic field is vectorial: it has both intensity and direction. Therefore, and again ideally, all palaeomagnetic data would consist of intensity and directional measurements of temporally coincident acquisitions. But because they come from rocks and archaeological artefacts with different physical and chemical properties, and because these materials are formed and subsequently sampled in different ways, palaeomagnetic data from a given site usually consist of only parts of the full 3-D magnetic vector (Butler 1992; Tauxe 1998). If intensity measurements are unavailable, records from fully oriented samples consist of only inclinations and declinations; if samples come from azimuthally-unoriented borecores then declinations are unavailable; if samples are completely unoriented then the data consist of only intensities. Given these mixtures of intensity and directional data groups, it is desirable to characterize the mean and variance of the full magnetic vector field by comparing it to a single, simple probability density function. Yet, the statistical development of a convenient density function for doing just that has been lacking.

For a geomagnetic field of a given polarity, it is common to characterize the variance of palaeomagnetic directions using a Fisher (1953) distribution, and for a bimodal distribution of directions coming from both reverse and normal polarities, the variance is commonly characterized by a Bingham (1964) distribution. What is unsatisfactory is that neither of these directional distributions have any demonstrated relationship with the distributions often used to describe intensity data, such as the normal, log-normal and gamma distributions. Directional and intensity data are usually treated separately, despite the fact that the two data types represent samplings from the very same geomagnetic field. In an effort to address this shortcoming, here we build on the statistical analyses of our predecessors. Instead of treating intensities and directions separately, we treat them jointly, and therefore consistently. This requires the development of a different and more general statistical distribution.

To represent the full-vectorial nature of the palaeomagnetic field at a particular geographic location and of a particular polarity, we consider a unimodal statistical distribution in a Cartesian three-space of orthogonal magnetic-field components consisting of a single Gaussian function with a spherically-symmetrical, isotropic variance. To represent a palaeomagnetic vector field of mixed reverse and normal polarities, we consider a bimodal statistical distribution consisting of two symmetrical Gaussian functions having equal, but opposite, means and isotropic variances, something we call a bi-Gaussian distribution. The projection of the unimodal, 3-D Gaussian distribution onto the unit sphere, a marginalization obtained by integrating over all intensities, is the angular-Gaussian distribution, which has been given in series form by Bingham (1983), and which has been revisited recently by Khokhlov *et al.* (2001) in their analysis of palaeosecular directional variation. In the context of palaeosecular vectorial variation, the 3-D Gaussian distributions considered here are related, at least mathematically, to the statistical models of Constable & Parker (1988), Hulot & LeMouël (1994), Kono (1997), and others, where spherical-harmonic coefficients describing global geomagnetic secular variation are regarded as independent statistical samples from a giant-Gaussian process. With such a global model, the palaeosecular variation at a particular geographic site can be described by a forward calculation. However, relating local secular variation to a global model is a difficult inverse problem. Indeed, Gaussian statistics at a single site need not necessarily arise from a global giant-Gaussian process; such an inference, if it is even appropriate, would require data from many sites. In contrast to such global studies, our concern here is much more local. 3-D Gaussian statistics can be used for studying local palaeosecular variation, with vector data representing a variety of acquisition times and taken from multiple rock depositions and archaeological artefacts. Alternatively, 3-D Gaussian statistics can be used for studying the palaeomagnetic acquisition process itself, with vector data representing a single acquisition time taken from multiple samples of a single rock deposition or a single archaeological artefact.

In this paper we develop a site-local, vectorial statistical theory. We explore the properties of the Gaussian and bi-Gaussian distributions for the palaeomagnetically-relevant spherical three-space of intensity, inclination, and declination. After performing the appropriate marginalizations of the 3-D Gaussian distributions, we demonstrate how to estimate the mean and variance of the magnetic vector field via the maximum-likelihood method, even when the data consist of different mixtures of directions and intensities. In his original paper, Fisher (1953) examined palaeomagnetic data from multiple lava flows, calculating the inter-flow directional dispersion arising from palaeosecular variation, and he examined data from a single lava flow, calculating the intra-flow directional dispersion arising from differences in the palaeomagnetic acquisition process. Following on from Fisher's work, and using the framework of the 3-D Gaussian distributions developed here, we examine palaeosecular vectorial variation over the past 5 Ma, and separately during the normal Brunhes chron, as recorded by inter-flow directional and intensity data taken from Hawaiian and Réunion basalts. We also examine the reliability of palaeomagnetic acquisition by analyzing intra-flow directional and intensity data taken from particular recent lava flows in Mexico and Hawaii.

2 THE DISTRIBUTIONS

The geomagnetic field **B** is a function of both space and time. Our concern here, however, is with the description of the field at a fixed geographic location. We represent a palaeomagnetic vector at a given location by the symbol **x**. In our statistical analysis of the 3-D palaeomagnetic data, each vector **x** is conceived as a realization in probability from a statistical distribution of vectors. In Cartesian coordinates (X, Y, Z), the probability $P(\mathbf{x})$ that **x** lies within the infinitesimal differential volume

$$d^3\mathbf{x} = dX dY dZ \tag{1}$$

is

$$P(\mathbf{x}) = \int p(\mathbf{x})\, d^3\mathbf{x}, \tag{2}$$

where $p(\mathbf{x})$ is the density function

$$p(\mathbf{x}) = \frac{d^3}{d\mathbf{x}^3} P(\mathbf{x}). \tag{3}$$

Of course, the density function is normalized so that upon integration over all space

$$\int_{-\infty}^{+\infty} p(\mathbf{x})\, d^3\mathbf{x} = 1. \tag{4}$$

In the usual way, the expected value E of some function $f(\mathbf{x})$ is the average of all possible values, with proper regard to the probability of their occurrence,

$$E\left(f(\mathbf{x})\right) = \int_{-\infty}^{+\infty} f(\mathbf{x}) p(\mathbf{x})\, d^3\mathbf{x}. \tag{5}$$

2.1 Unimodal Gaussian distribution

We define the unimodal Gaussian probability density function in terms of a mean palaeomagnetic vector $\mathbf{x}_\mu$ and an associated covariance matrix $\mathbf{C}$,

$$p_{g_1}\left(\mathbf{x} \mid \mathbf{x}_\mu, \mathbf{C}\right) = \frac{1}{(2\pi)^{\frac{3}{2}} \mid \mathbf{C} \mid^{\frac{1}{2}}} \exp\left[-\frac{1}{2}(\mathbf{x}-\mathbf{x}_\mu)^T \mathbf{C}^{-1}(\mathbf{x}-\mathbf{x}_\mu)\right]. \tag{6}$$

For the discussion that follows, we shall consider the more restricted case of isotropic variance,

$$\mathbf{C} = \sigma^2 \mathbf{I} = \sigma^2 \begin{pmatrix} 1 & 0 & 0 \\ 0 & 1 & 0 \\ 0 & 0 & 1 \end{pmatrix}. \tag{7}$$

We then have a spherically-symmetrical Gaussian probability density function, where the Cartesian vectorial components have equal scalar variances and where each component is presumed to be independently distributed. As we shall see, this isotropic Gaussian distribution is something of an idealization, since it does not fit all palaeovector data sets. We have chosen to develop the isotropic case because it is simpler than the more general anisotropic case, but despite this, the mathematics that follows is, at times, still rather complicated and messy. We assert that even if it does not fit palaeovector data perfectly, the Gaussian distribution with isotropic variance is useful for purposes of comparison. Henceforth, unless the terminology is otherwise unambiguous, we shall refer to the scalar σ^2 as the 'vectorial variance', and to the scalar σ as the 'vectorial dispersion'.

Illustrated in Fig. 1(a), the Gaussian probability density function is

$$p_{g_1}\left(\mathbf{x} \mid \mathbf{x}_\mu, \sigma^2\right) = p_{g_1}\left(X, Y, Z \mid X_\mu, Y_\mu, Z_\mu, \sigma^2\right). \tag{8}$$

In terms of spherical coordinates, namely intensity, inclination, and declination (F, I, D), for which the differential volume element is transformed according to

$$dX dY dZ \rightarrow F^2 \cos I\, dF\, dI\, dD, \tag{9}$$

the probability density function is

$$\begin{aligned} p_{g_1}\left(\mathbf{x} \mid \mathbf{x}_\mu, \sigma^2\right) &= p_{g_1}\left(F, I, D \mid F_\mu, I_\mu, D_\mu, \sigma^2\right) \\ &= F^2 \cos I q(\mathbf{x} \mid \mathbf{x}_\mu, \sigma^2), \end{aligned} \tag{10}$$

where

$$\begin{aligned} q\left(\mathbf{x} \mid \mathbf{x}_\mu, \sigma^2\right) &= \frac{1}{(2\pi)^{\frac{3}{2}}\sigma^3} \\ &\times \exp\left[-\frac{1}{2\sigma^2}(F\cos I\cos D - F_\mu \cos I_\mu \cos D_\mu)^2\right] \\ &\times \exp\left[-\frac{1}{2\sigma^2}(F\cos I\sin D - F_\mu \cos I_\mu \sin D_\mu)^2\right] \\ &\times \exp\left[-\frac{1}{2\sigma^2}(F\sin I - F_\mu \sin I_\mu)^2\right]. \end{aligned} \tag{11}$$

The Euclidean length of the mean vector $\mathbf{x}_\mu$ is F_μ. The direction of the mean vector is defined by its inclination and declination, I_μ and D_μ. Because we are considering a distribution with isotropic variance, eq. (7), the probability density function is rotationally symmetrical about the mean vector $\mathbf{x}_\mu$. With θ defining the off-axis angle between a particular unit magnetic vector and the mean unit vector,

$$\hat{\mathbf{x}} = \frac{\mathbf{x}}{|\mathbf{x}|} \quad \text{and} \quad \hat{\mathbf{x}}_\mu = \frac{\mathbf{x}_\mu}{|\mathbf{x}_\mu|}, \tag{12}$$

then

$$\cos\theta = \hat{\mathbf{x}} \cdot \hat{\mathbf{x}}_\mu. \tag{13}$$

In summary, the unimodal Gaussian distribution is characterized by a mean magnetic-field vector, represented by $\mathbf{x}_\mu$, together with a dispersion of vectors, with isotropic variance σ^2, about the endpoint

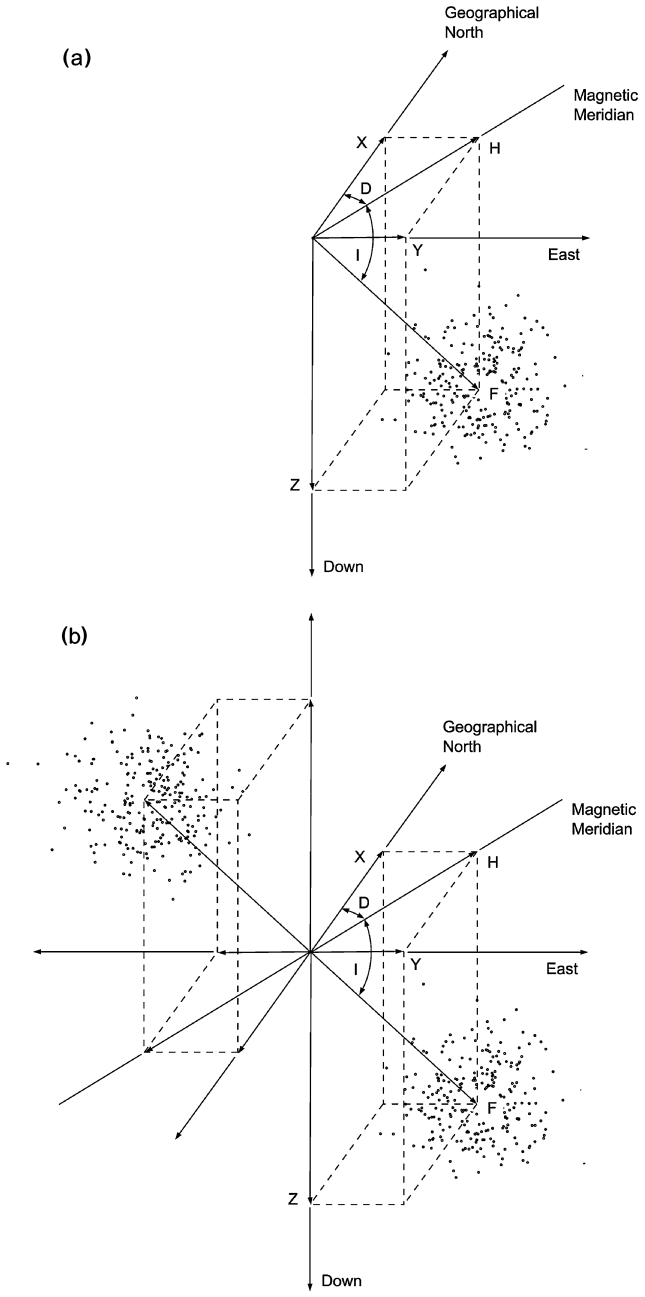

Figure 1. The geometry of the (a) Gaussian and (b) bi-Gaussian distributions. In the usual way (X, Y, Z) define the (north, east, down) magnetic-field components; (F, I, D) are the (intensity, inclination, declination), H is the horizontal component of the field.

of the mean vector. We shall refer to the scalar $(\sigma/F_\mu)^2$ as the 'relative vectorial variance', and to the scalar σ/F_μ as the 'relative vectorial dispersion'.

2.2 Bimodal bi-Gaussian distribution

A simple, although perhaps not sufficiently appreciated, fact is that the sign of the magnetic field **B** is irrelevant to the physical processes operating in the Earth's core (Roberts & Soward 1972). The equations of magnetohydrodynamics are invariant under the transformation

$$\mathbf{B} \to -\mathbf{B}. \tag{14}$$

This means that the statistics of numerous and perfect palaeomagnetic data characterizing the field of one polarity could just as easily characterize the field of the opposite polarity (Merrill *et al.* 1979; Gubbins & Zhang 1993). Indeed, the successful application of palaeomagnetism to plate-tectonic reconstructions, which hypothesizes the statistical dominance of the geocentric axial dipole, indicates, if only in a basic sense, that normal and reverse polarity fields have some similarity. In light of these observations, for studies of the palaeomagnetic field we are motivated to develop a statistical framework that is independent of the sign of the field.

As with the unimodal Gaussian distribution, for the bimodal bi-Gaussian distribution we shall consider the restricted case of isotropic variance. Illustrated in Fig. 1(b), in Cartesian coordinates the bi-Gaussian probability density function is

$$\begin{aligned} p_{g_2}\left(\mathbf{x} \,|\, \mathbf{x}_\mu, \sigma^2\right) &= p_{g_2}\left(X, Y, Z \,|\, X_\mu, Y_\mu, Z_\mu, \sigma^2\right) \\ &= \frac{1}{2}\left[p_{g_1}\left(\mathbf{x} \,|\, \mathbf{x}_\mu, \sigma^2\right) + p_{g_1}\left(\mathbf{x}| - \mathbf{x}_\mu, \sigma^2\right)\right], \end{aligned} \tag{15}$$

and in spherical coordinates it is

$$\begin{aligned} p_{g_2}\left(\mathbf{x} \,|\, \mathbf{x}_\mu, \sigma^2\right) &= p_{g_2}\left(F, I, D \,|\, F_\mu, I_\mu, D_\mu, \sigma^2\right) \\ &= \frac{1}{2}F^2 \cos I\left[q\left(\mathbf{x} \,|\, \mathbf{x}_\mu, \sigma^2\right) + q\left(\mathbf{x}| - \mathbf{x}_\mu, \sigma^2\right)\right]. \end{aligned} \tag{16}$$

Note that p_{g_2} is invariant under the transformations

$$(F_\mu, I_\mu, D_\mu) \to (\pm F_\mu, -I_\mu + 2m\pi, D_\mu + (2n+1)\pi), \tag{17}$$

$$(F_\mu, I_\mu, D_\mu) \to (\pm F_\mu, I_\mu + 2m\pi, D_\mu + 2n\pi), \tag{18}$$

where m and n are integers, although, obviously, negative intensities or inclinations greater than $\pi/2$ (or less than $-\pi/2$) do not correspond to conventional definitions and can therefore be considered to be mathematical artefacts. In summary, then, the bi-Gaussian distribution is characterized by a mean axis-segment, represented by the vectorial pair $\pm\mathbf{x}_\mu$, together with a dispersion of vectors, with isotropic variance σ^2, about the endpoints of the mean axis-segment.

3 MARGINAL AND CUMULATIVE FORMS

As we have said, ideally, palaeomagnetic data consist of coincident intensity and directional measurements. In such circumstances, the unimodal Gaussian distribution, represented by (10), and the bimodal bi-Gaussian distribution, represented by (16), are useful for statistical analyses. However, in practice, palaeomagnetic data usually consist of only parts of the full magnetic vector, in which case we need the appropriately marginalized probability density functions corresponding to the Gaussian distributions. So, for example, for the vast majority of palaeomagnetic data, where only directional measurements are taken from fully oriented samples, namely inclination–declination pairs with no associated absolute palaeointensity (other than a magnetization), we need the joint probability density function for inclination and declination. This density function is obtained by integrating (10), for the Gaussian case, and (16) for the bi-Gaussian case, over all intensities,

$$p_g\left(I, D \,|\, I_\mu, D_\mu, (\sigma/F_\mu)^2\right) = \int_0^\infty p_g\left(F, I, D\right) dF. \tag{19}$$

Likewise, given intensity-inclination data taken, for example, from an azimuthally-unoriented borecore, we need the marginal density function

$$p_g\left(F, I \,|\, F_\mu, I_\mu, \sigma^2\right) = \int_0^{2\pi} p_g\left(F, I, D\right) dD. \tag{20}$$

If only inclinations are available then we need the marginal density function

$$p_g\left(I \,|\, I_\mu, (\sigma/F_\mu)^2\right) = \int_0^{2\pi}\int_0^\infty p_g\left(F, I, D\right) dF\, dD, \tag{21}$$

and so on. In each case, integration is performed over the vectorial components that are either not available or not needed. The required integrations are rather involved, and they are therefore given in the appendices.

When assessing statistical significance with (say) a Kolmogorov–Smirnov test, cumulative probability distributions are needed. So, for example, the cumulative inclination distribution, giving the probability that an inclination lies on the interval $[-\pi/2, I]$, is just

$$P_g\left(I \,|\, I_\mu, (\sigma/F_\mu)^2\right) = \int_{-\frac{\pi}{2}}^{I} p_g\left(I'\right) dI'. \tag{22}$$

As with the marginal distributions, the required integrations for the cumulative distributions are rather involved, and they are, therefore, also given in the appendices. Computer routines for the Kolmogorov–Smirnov significance test can be found in Press *et al.* (1992).

Depending on the available data, combinations of the marginal distributions can be used for estimating the underlying vectorial mean and variance, preferably by maximizing their likelihood as we discuss in Section 5. Examples of the intensity, inclination, declination, and off-axis anglular distributions, are given in Figs 2 and 3 (Figs 4 and 5) corresponding to the 3-D Gaussian (bi-Gaussian) distribution. Amongst all the marginalizations, perhaps the most enlightening, and, it turns out, the most mathematically tractable, are those corresponding to the separate forms for intensity and off-axis angle. It is on these that we now concentrate our discussion.

3.1 Intensity

The intensity probability density function for the 3-D Gaussian distributions is obtained by integrating either (10) or (16) over all angles, in either case the results are identical,

$$\begin{aligned} p_g\left(F \,|\, F_\mu, \sigma^2\right) &= \int_0^{2\pi}\int_{-\frac{\pi}{2}}^{+\frac{\pi}{2}} p_g\left(F, I, D\right) dI\, dD \\ &= \sigma^{-1}\left(\frac{2}{\pi}\right)^{\frac{1}{2}}\left(\frac{F}{F_\mu}\right)\exp\left[-\frac{1}{2}\left(\frac{F}{\sigma}\right)^2 - \frac{1}{2}\left(\frac{F_\mu}{\sigma}\right)^2\right] \\ &\times \sinh\left[\frac{FF_\mu}{\sigma^2}\right]. \end{aligned} \tag{23}$$

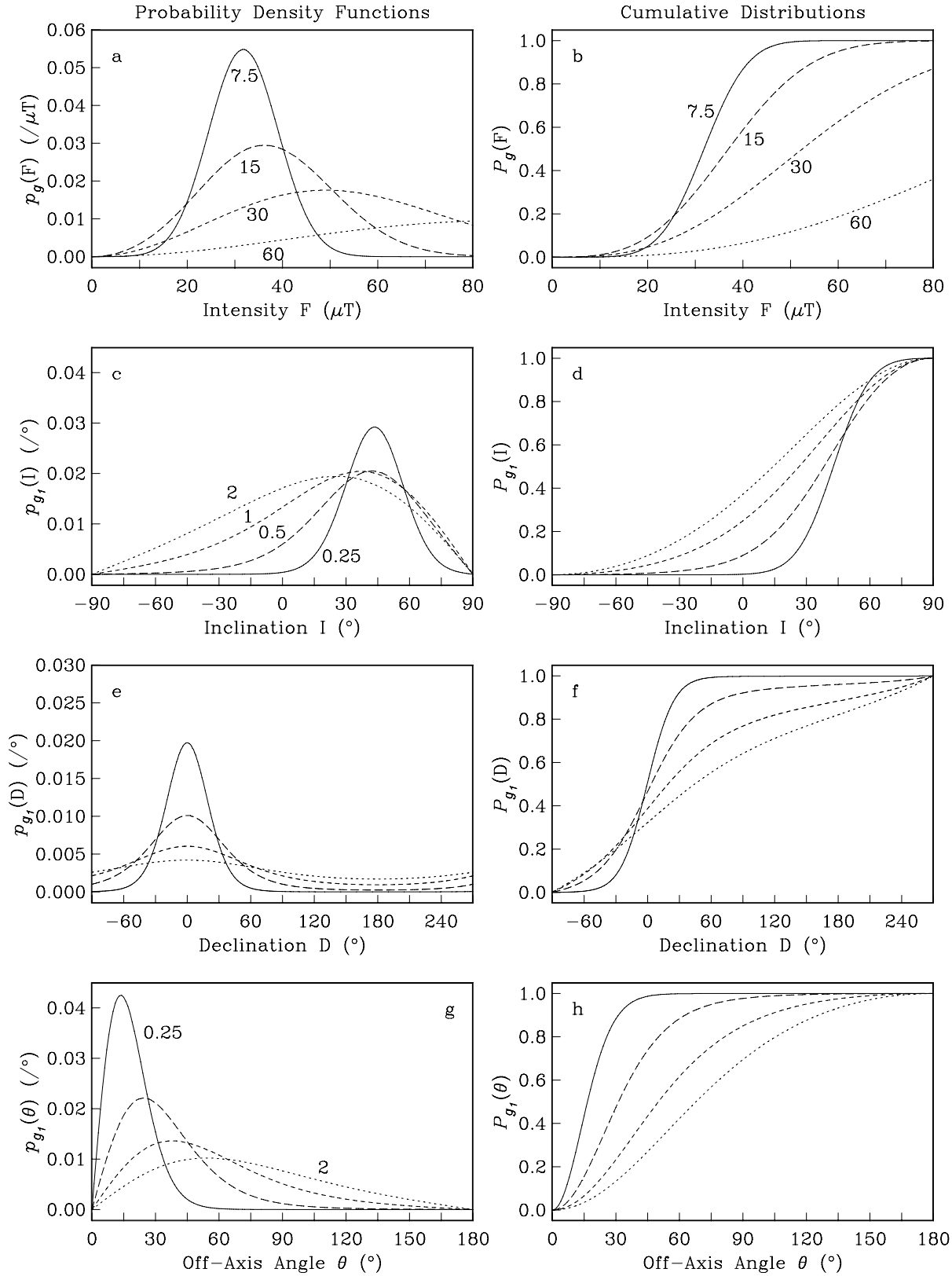

Figure 2. Examples, with different absolute and relative vectorial dispersions, of the marginal probability density functions p_{g_1} and corresponding cumulative distributions P_{g_1} for our Gaussian distribution, eq. (10). (a, b) Intensity F, with vectorial-mean intensity F_μ, and with vectorial dispersions σ of 7.5, 15, 30, and 60 μT shown respectively by solid, long-dashed, short-dashed, and dotted lines. (c, d) Inclination I, (e, f) declination D, and (g, h) off-axis angle θ with vectorial-mean direction $(I_\mu, D_\mu) = (45^\circ, 0^\circ)$, and with relative vectorial dispersions of 0.25, 0.5, 1, 2 shown respectively by solid, long-dashed, short-dashed and dotted lines. Note that with increasing dispersion the intensity and inclination distributions become increasingly asymmetrical, or skewed, about their means, whilst the declination remains symmetrical about its mean.

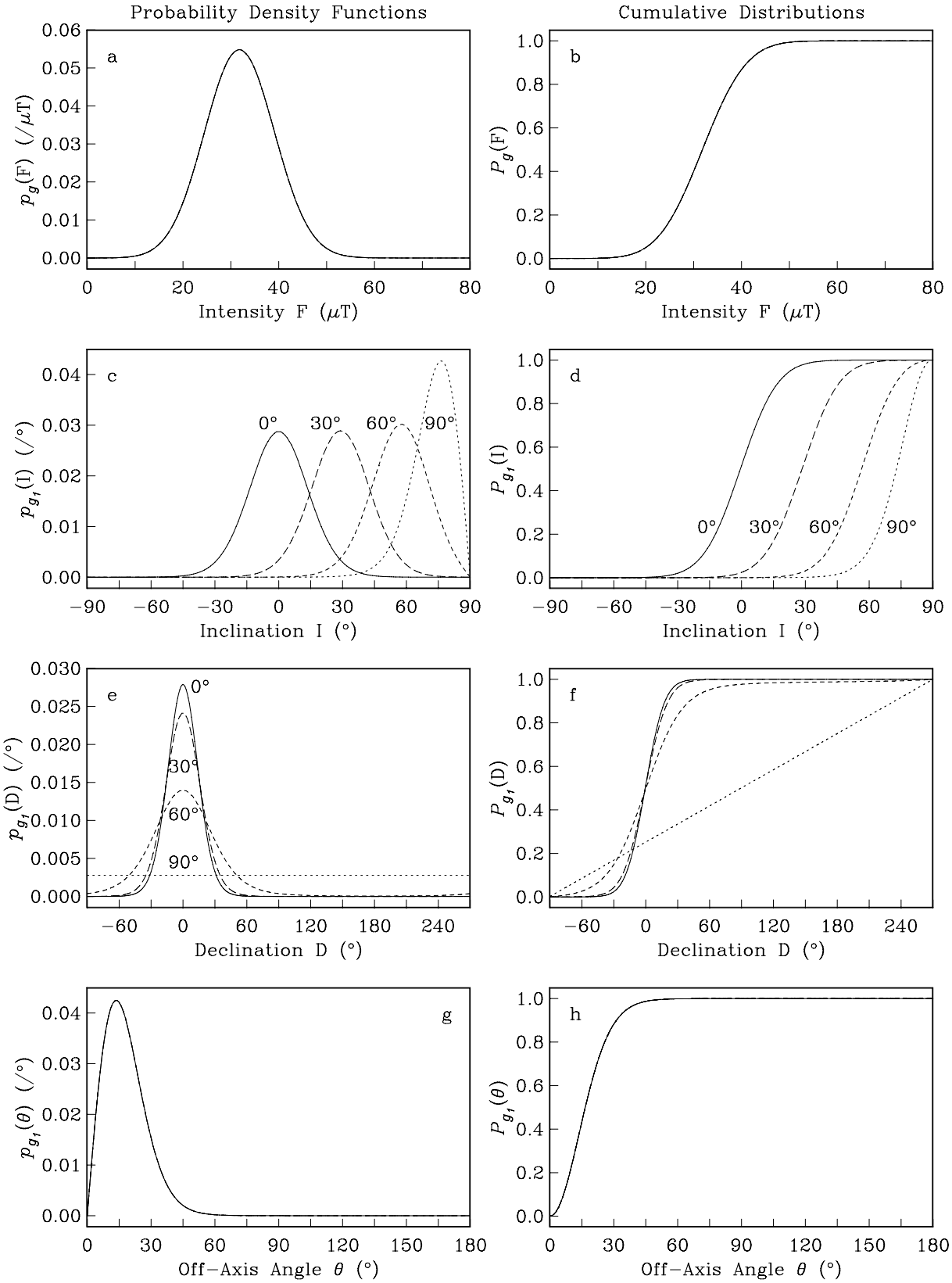

Figure 3. Examples, with different mean inclinations, of the marginal probability density functions p_{g_1} and corresponding cumulative distributions P_{g_1} for (a, b) intensity F, (c, d) inclination I, (e, f) declination D, and (g, h) off-axis angle θ for our Gaussian distribution. For vectorial-mean values of $(F_\mu, D_\mu, \sigma) = (30\ \mu T, 0^\circ, 7.5\ \mu T)$ the solid, long-dashed, short-dashed, and dotted lines are for vectorial-mean inclinations I_μ of 0°, 30°, 60°, and 90° respectively. Note that changing the vectorial-mean inclination has no affect on the intensity and off-axis angular distributions. Compare with Figs 5 and 11 of Constable & Parker (1988).

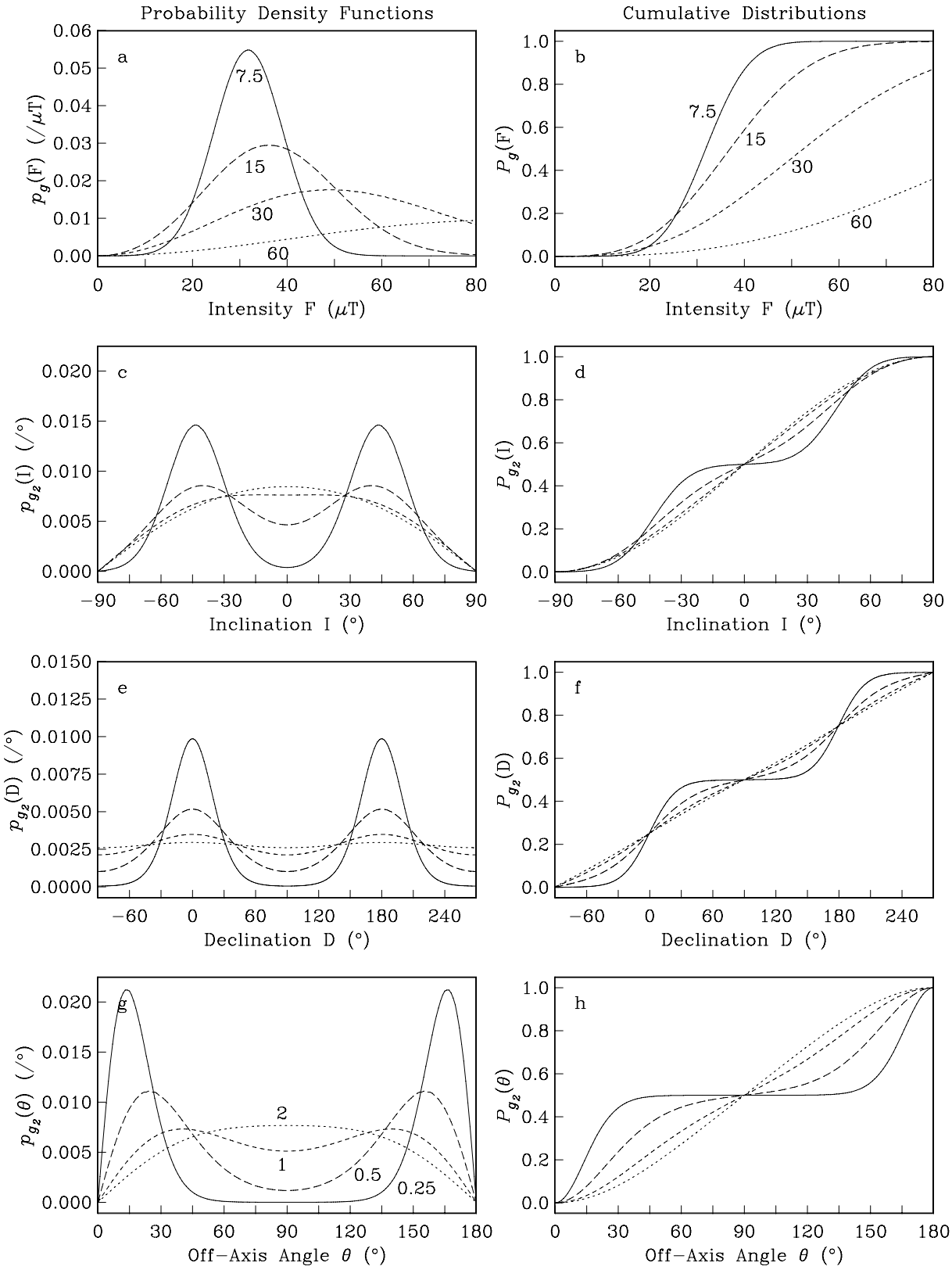

Figure 4. Same as Fig. 2, except for the bi-Gaussian distribution, eq. (16).

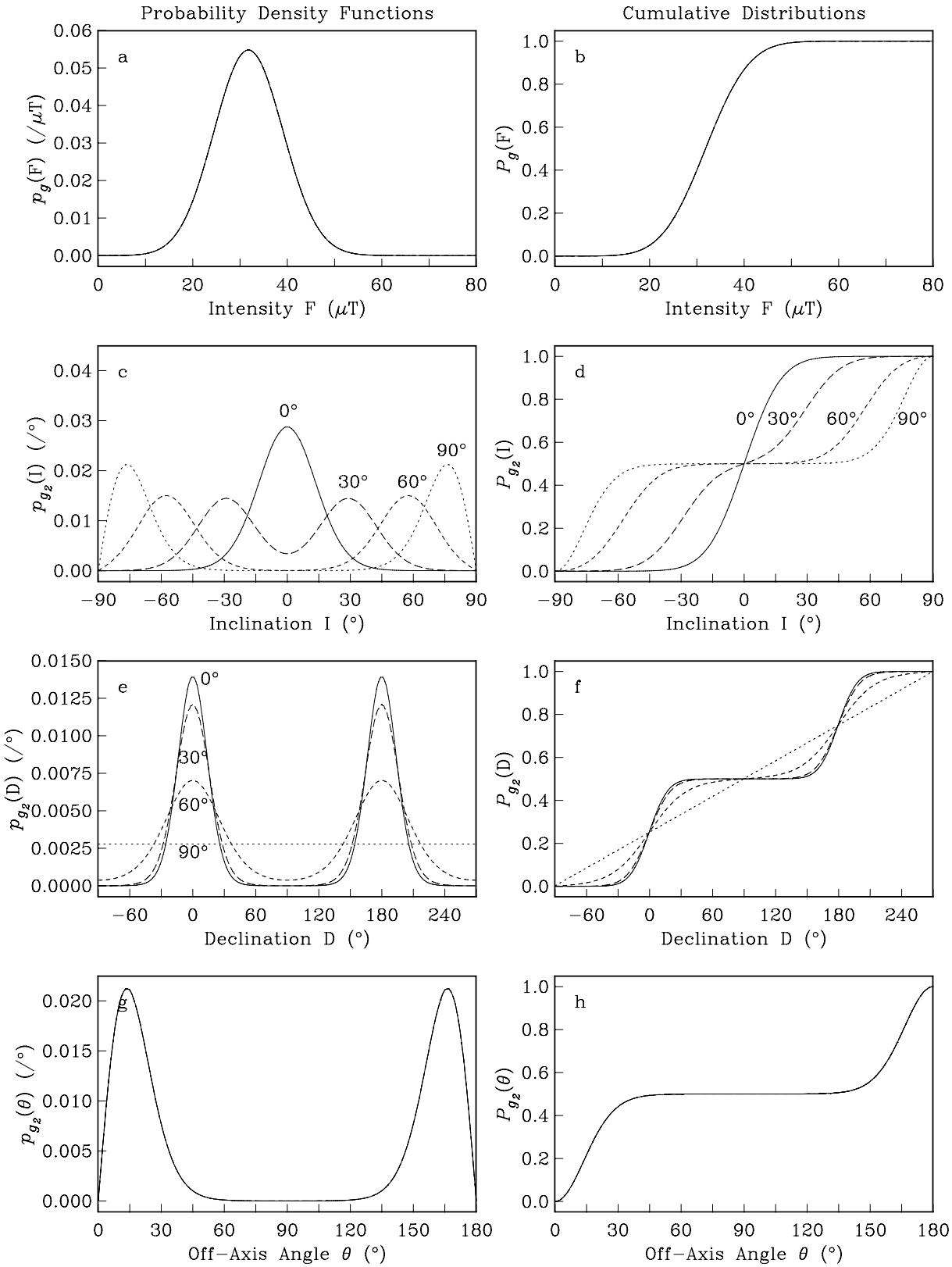

Figure 5. Same as Fig. 3, except for the bi-Gaussian distribution, eq. (16).

The integration is discussed in Appendix D. Like the (off-axis) directional density functions, eqs (27) and (28) given below, eq. (23) is amongst the central mathematical results of this analysis. The limiting forms of this function are discussed in Section 4.

For reference, eq. (23) is a special case of the *n*-dimensional generalized Rayleigh–Rician density function (Miller *et al.* 1958),

$$\left(\frac{F_\mu}{\sigma^2}\right)\left(\frac{F}{F_\mu}\right)^{\frac{1}{2}n}\exp\left[-\frac{1}{2}\left(\frac{F}{\sigma}\right)^2-\frac{1}{2}\left(\frac{F_\mu}{\sigma}\right)^2\right]I_{\frac{1}{2}(n-2)}\left[\frac{FF_\mu}{\sigma^2}\right], \tag{24}$$

where I_ν is a modified Bessel function of the first kind; for reference see Abramowitz & Stegun (1965) or Spanier & Oldham (1987). The Rayleigh–Rician distribution has application to digital communications and the detection of targets amidst Gaussian clutter (DiFranco & Rubin 1968; McDonough & Whalen 1995; Proakis 1995); for a comprehensive mathematical discussion of the Rayleigh–Rician distribution see Miller (1975). For the 3-D ($n = 3$) case considered here, (24) reduces to (23) after use of the identity

$$I_{\frac{1}{2}}(z) = \left(\frac{2}{\pi z}\right)^{\frac{1}{2}}\sinh(z), \tag{25}$$

see 10.2.13 of Abramowitz & Stegun (1965) or 28:13:3 of Spanier & Oldham (1987).

Since the intensity distribution for the unimodal Gaussian distribution is identical to that for the bi-Gaussian distribution, the corresponding cumulative distributions are also identical. The probability that an intensity lies on the interval $[0, F]$ is just

$$P_g\left(F \mid F_\mu, \sigma^2\right) = \int_0^F p_g(F')\,dF', \tag{26}$$

where the integration is given in Appendix D.

3.2 Off-axis angle

For the unimodal Gaussian distribution, the marginal density function for off-axis angle is

$$p_{g_1}\left(\theta \mid (\sigma/F_\mu)^2\right) = \frac{1}{2}\sin\theta\exp\left[-\frac{1}{2}\left(\frac{F_\mu}{\sigma}\right)^2\right]$$
$$\times\left\{\left[1+\left(\frac{F_\mu}{\sigma}\right)^2\cos^2\theta\right]\exp\left[\frac{1}{2}\left(\frac{F_\mu}{\sigma}\right)^2\cos^2\theta\right]\right.$$
$$\left.\times\left[1+\mathrm{erf}\left[\frac{1}{\sqrt{2}}\left(\frac{F_\mu}{\sigma}\right)\cos\theta\right]\right]+\left(\frac{2}{\pi}\right)^{\frac{1}{2}}\left(\frac{F_\mu}{\sigma}\right)\cos\theta\right\}, \tag{27}$$

which is what Bingham (1983) obtained in series form and called the 'angular-Gaussian' distribution, and which has been expressed in a more general anisotropic form by Khokhlov *et al.* (2001) . For the bimodal bi-Gaussian distribution, the marginal density function for off-axis angle is simpler, being just

$$p_{g_2}\left(\theta \mid (\sigma/F_\mu)^2\right) = \frac{1}{2}\sin\theta\exp\left[-\frac{1}{2}\left(\frac{F_\mu}{\sigma}\right)^2\sin^2\theta\right]$$
$$\times\left[1+\left(\frac{F_\mu}{\sigma}\right)^2\cos^2\theta\right]. \tag{28}$$

The integrations for both the Gaussian and bi-Gaussian cases are discussed in Appendix E. Eq. (27) is the Gaussian analogue of the Fisher directional distribution, and eq. (28) is the bi-Gaussian analogue of the Bingham directional distribution. The limiting forms of these functions are discussed in Section 4 below.

For the directional probability density functions (27) and (28), the corresponding cumulative distributions, giving the probability that an off-axis angle lies on the interval $[0, \theta]$, are just

$$P_g\left(\theta \mid (\sigma/F_\mu)^2\right) = \int_0^\theta p_g\left(\theta'\right)d\theta', \tag{29}$$

where the integrations are given in Appendix E. These cumulative distributions are analogous to those for the Fisher distribution, studied by Watson & Irving (1957) and later by McFadden (1980).

4 LIMITING PROPERTIES

It is instructive to compare the marginal density functions corresponding to the 3-D Gaussian distributions with the separate and, at least so far, theoretically unrelated intensity and directional density functions used more commonly by the palaeomagnetic community.

4.1 Intensity: Normal to Maxwell

First, we consider the intensity (Rayleigh–Rician) density function (23) corresponding to our 3-D Gaussian distributions. For the case where the vectorial dispersion is substantially less than the intensity of the mean vector, $\sigma \ll F_\mu$, the intensity probability density function is approximately that for a 1-D normal distribution,

$$p_n\left(F \mid F_\mu, \sigma^2\right) = \frac{1}{\sqrt{2\pi}\sigma}\exp\left[-\frac{1}{2}\left(\frac{F-F_\mu}{\sigma}\right)^2\right], \tag{30}$$

which McFadden & McElhinny (1982), amongst others, have suggested on empirical grounds might be appropriate for palaeointensity studies, after truncation of negative intensities. Eq. (30) is, of course, neither log-normal nor gamma, distributions which have been, respectively, suggested might be appropriate for intensity studies by Tanaka *et al.* (1995a) and Constable *et al.* (1998). Indeed, the fact that a 1-D normal distribution is a limiting case of the 3-D Gaussian (and bi-Gaussian) intensity distribution lends some (small) justification to the use of the 1-D normal distribution for intensity studies. However, if transitional data are included in an analysis, the condition $\sigma \ll F_\mu$ might not be accurately met, in which case (23) should be used for modelling intensity data. Moreover, as we shall see in our discussion of bias, Section 5, the 1-D normal distribution cannot always be used to give accurate estimates of 3-D vectorial quantities. For a graphical demonstration that a normal distribution is an accurate approximation of the Gaussian intensity distribution (Rayleigh–Rician), when $\sigma \ll F_\mu$, see Figs 6(a) and (b).

If we consider the other limiting case where the vectorial dispersion is substantially greater than the intensity of the mean vector, $\sigma \gg F_\mu$, the intensity probability density function (23) is approximately that for a Maxwell distribution,

$$p_m\left(F \mid \sigma^2\right) = \sigma^{-1}\left(\frac{2}{\pi}\right)^{\frac{1}{2}}\left(\frac{F}{\sigma}\right)^2\exp\left[-\frac{1}{2}\left(\frac{F}{\sigma}\right)^2\right]. \tag{31}$$

This distribution often arises in statistical mechanics, being used to describe the speed of gas molecules in thermal equilibrium; for reference see Kittel & Kroemer (1980) or Landau & Lifshitz (1980). The Maxwell distribution is itself a special case ($n = 3$, $F_\mu = 0$) of the generalized Rayleigh–Rician distribution (24). For a graphical

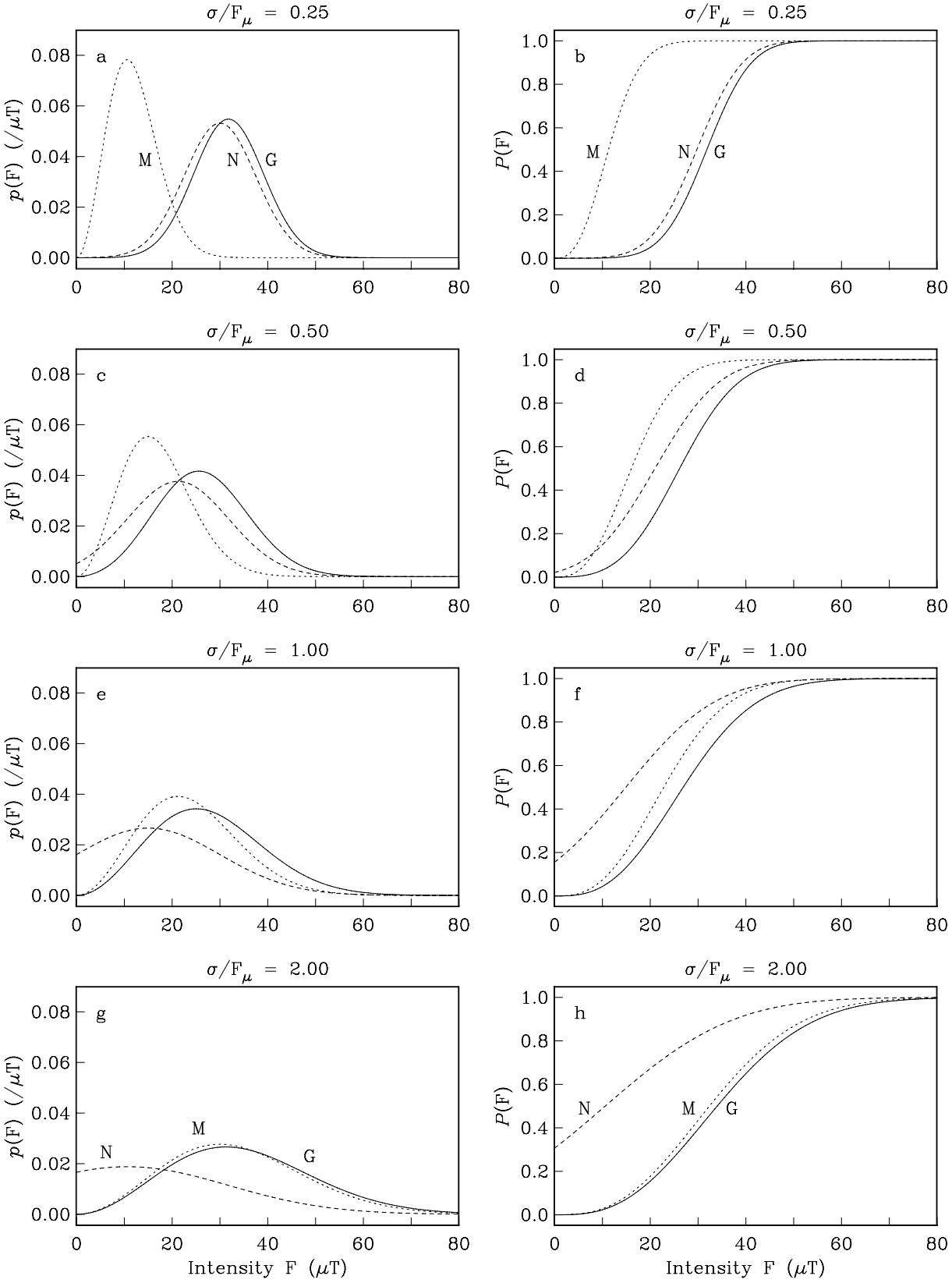

Figure 6. Examples, with different relative vectorial dispersions σ/F_μ of the marginal intensity probability density function $p_g(F)$ and corresponding cumulative distributions $P_g(F)$ for our Gaussian distribution (G). Also shown with dashed lines normal (N), eq. (30), and with dotted lines Maxwell (M), eq. (31), density functions and distributions. In (a, b) we see that in the limit $\sigma/F_\mu \to 0$, the bi-Gaussian intensity distribution approaches a normal distribution; whilst in (g, h) we see that in the opposite limit $\sigma/F_\mu \to \infty$, the bi-Gaussian intensity distribution approaches a Maxwell distribution. For fixity, in each case the product $\sigma\ F_\mu$ is equal to 225 $(\mu T)^2$.

demonstration that a Maxwell distribution is an accurate approximation of the Gaussian intensity distribution (Rayleigh–Rician), when $\sigma \gg F_\mu$, see Figs 6(g) and (h).

4.2 Gaussian off-axis angles: Fisher to uniform

Next, we consider the off-axis angular probability density function (27) corresponding to our unimodal 3-D Gaussian distribution. For the case where the relative vectorial dispersion is substantially less than one, $\sigma/F_\mu \ll 1$, the off-axis angular density function is approximately that for a Fisher (1953) distribution,

$$p_f\left(\theta \,|\, (F_\mu/\sigma)^2\right) = \frac{1}{2}\left(\frac{F_\mu}{\sigma}\right)^2 \left\{\sinh\left[\left(\frac{F_\mu}{\sigma}\right)^2\right]\right\}^{-1}$$

$$\times\ \sin\theta \exp\left[\left(\frac{F_\mu}{\sigma}\right)^2 \cos\theta\right], \tag{32}$$

this being the unimodal directional distribution often used by the palaeomagnetic community; for reference see Mardia (1972) or Fisher *et al.* (1987). Some justification for the use of a Fisher distribution is lent by the fact that it is very nearly equal to the projection of the Gaussian distribution onto the unit sphere. However, the condition $\sigma/F_\mu \ll 1$ might not always be accurately met, in which case (27) should be used for modelling directional data of a given polarity. For a graphical demonstration that the Fisher distribution is an accurate approximation of the Gaussian off-axis angular distribution, when $\sigma/F_\mu \ll 1$, see Figs 7(a) and (b).

For the other limiting case where the relative vectorial dispersion is substantially greater than one, $\sigma/F_\mu \gg 1$, the off-axis angular probability density function (27) is approximately that for a spherically-uniform distribution of directions,

$$p_u(\theta) = \frac{1}{2}\sin\theta. \tag{33}$$

Similar observations apply to the bi-Gaussian distribution, as discussed below. For a graphical demonstration that the spherically-uniform directional distribution is an accurate approximation of the Gaussian off-axis angular distribution, when $\sigma/F_\mu \gg 1$, see Figs 7(g) and (h). We also note that in this limit the Fisher distribution is itself well approximated by a spherically-uniform directional distribution.

4.3 Bi-Gaussian off-axis angles: Bingham to uniform

Finally, we consider the off-axis angular probability density function (28) corresponding to our 3-D bi-Gaussian distribution. For the case where the relative vectorial dispersion is substantially less than one, $\sigma/F_\mu \ll 1$, the off-axis angular density function is approximately that for a Bingham (1964) distribution, also sometimes called a Watson (1965) distribution,

$$p_b\left(\theta \,|\, (F_\mu/\sigma)^2\right) = \frac{1}{2}\left\{{}_1F_1\left[\tfrac{1}{2}; \tfrac{3}{2}; \frac{1}{2}\left(\frac{F_\mu}{\sigma}\right)^2\right]\right\}^{-1}$$

$$\times\ \sin\theta \exp\left[\frac{1}{2}\left(\frac{F_\mu}{\sigma}\right)^2 \cos^2\theta\right], \tag{34}$$

this being the bimodal directional distribution often used by the palaeomagnetic community. The hypergeometric function ${}_1F_1$ is part of the normalizing constant and is given by (A7). For a graphical demonstration that the Bingham distribution is an accurate approximation of the bi-Gaussian off-axis angular distribution, when $\sigma/F_\mu \ll 1$, see Figs 8(a) and (b).

Following from our discussion for the unimodal Gaussian distribution, if we consider the other case where the relative vectorial dispersion is substantially greater than one, $\sigma/F_\mu \gg 1$, the off-axis angular probability density function (28) describes a spherically-uniform distribution of directions, eq. (33); see Figs 8(g) and (h).

5 ANALYSIS OF DATA

In the analysis of palaeomagnetic data, mean vectorial components are usually estimated in one of two ways, either using an arithmetic average (or some variant thereof), or using maximum-likelihood estimation. Arithmetic averages have the advantage of being simple to perform, but unless full-vector data are available, simple averages of non-Cartesian components, and even unit vectors, can give biased estimates of the true mean vector-field. This is true independent of the number of data used. On the other hand, although maximum-likelihood estimates are slightly more difficult to obtain, it is well known that their biases disappear with increasingly numerous data, a property sometimes described as 'consistency in probability' (Cramér 1945; Stuart *et al.* 1999); the only proviso is that the probability density functions being used in the maximum-likelihood estimation must be appropriate to the problem at hand and capable of fitting the data to within some tolerable misfit.

5.1 Averaging full vectors

If full-vector data (intensity, inclination, declination) are available, the simplest method for calculating the mean vector is to convert to Cartesian components, and then perform a vectorial average. The expected value for the X component is just

$$E(X) = \int_{-\infty}^{+\infty} p(X)\, X dX, \tag{35}$$

which, as is well known from vectorial algebra, is an unbiased estimate of the mean component X_μ, even if the underlying 3-D probability density function $p(\mathbf{x})$ is anisotropic. Similar statements can be made for the expected values of the other components, $E(Y)$ and $E(Z)$. Therefore, with full-vector data,

$$E(\mathbf{x}) = \mathbf{x}_\mu, \tag{36}$$

which is exactly the result needed.

5.2 Averaging unit vectors

If only directional data (inclination, declination) are available, the usual method for calculating the mean direction is to convert to Cartesian components, and then perform a simple vectorial average of unit vectors. However, Creer (1983) has noted that this does not always yield a mean direction consistent with that obtained using full vector data. In effect Creer found that, depending on the nature of the secular variation, it often is the case that

$$E(\hat{\mathbf{x}})/|E(\hat{\mathbf{x}})| \neq E(\mathbf{x})/|E(\mathbf{x})|, \tag{37}$$

an inequality that Khokhlov *et al.* (2001) have recently noted can arise from an anisotropic variance of vectors about the mean vector.

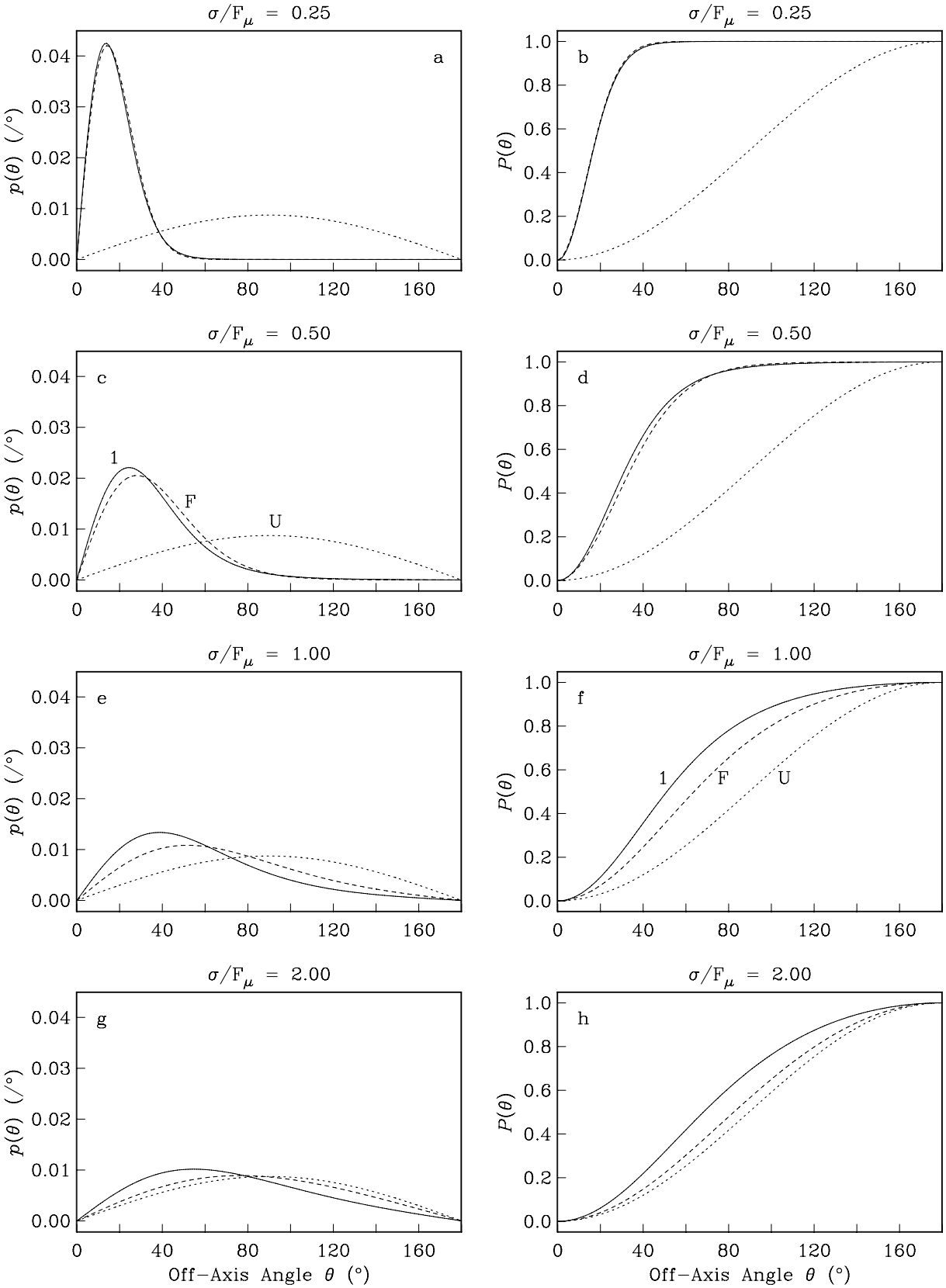

Figure 7. Examples, with different relative vectorial dispersions σ/F_μ of the marginal off-axis angular probability density function $p_{g_1}(\theta)$ and corresponding cumulative distributions $P_{g_1}(\theta)$ for our Gaussian distribution (1). Also shown with dashed lines Fisher (F), eq. (32), and with dotted lines spherically-uniform (U), eq. (33), density functions and distributions. In (a, b) we see that in the limit $\sigma/F_\mu \to 0$, the Gaussian off-axis angular distribution approaches a Fisher distribution; whilst in (g, h) we see that in the opposite limit $\sigma/F_\mu \to \infty$, the Gaussian off-axis angular distribution approaches a spherically-uniform distribution (as does the Fisher distribution). Compare with Fig. 8.

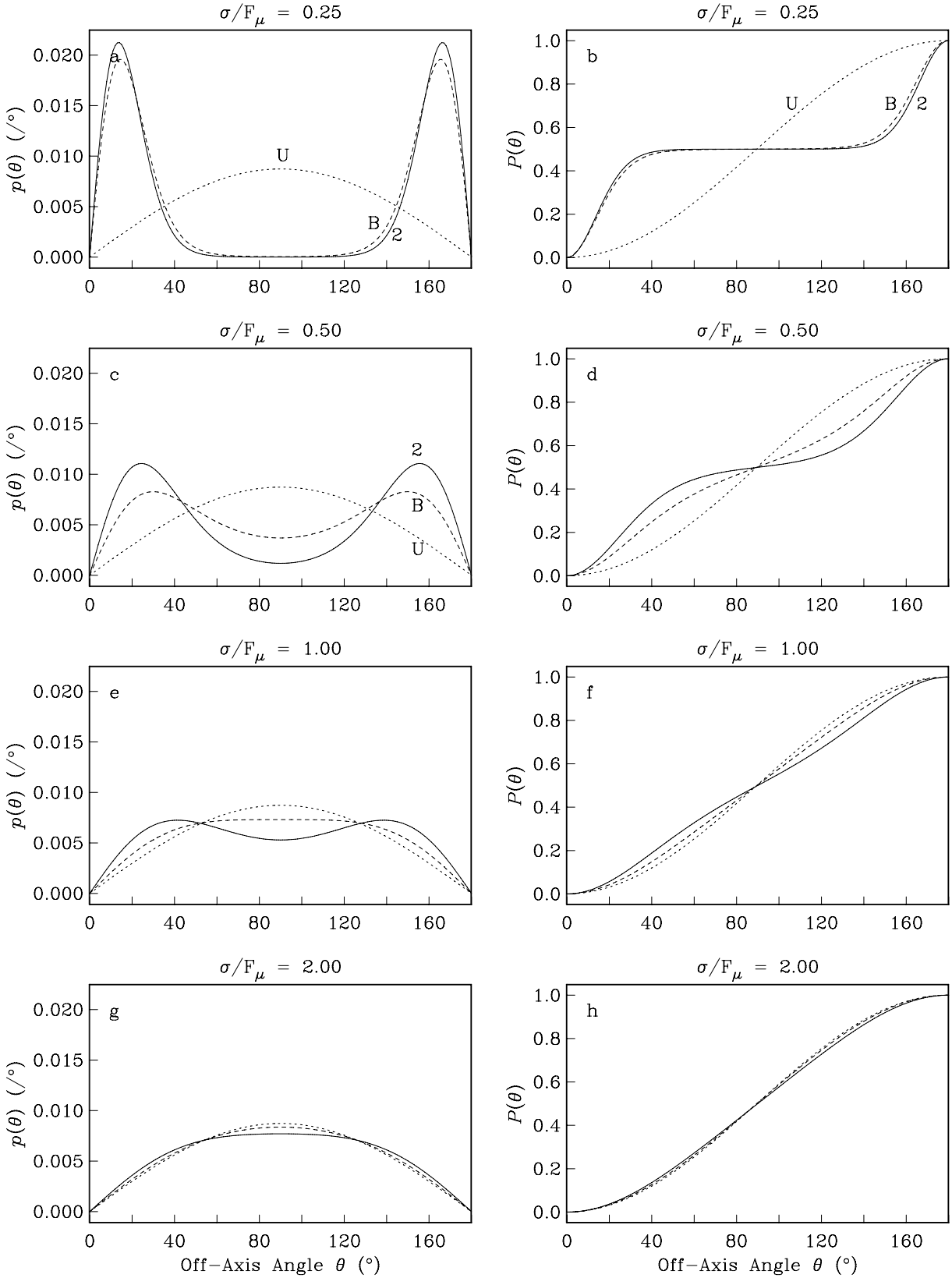

Figure 8. Examples, with different relative vectorial dispersions σ/F_μ of the marginal off-axis angular probability density function $p_{g_2}(\theta)$ and corresponding cumulative distributions $P_{g_2}(\theta)$ for our bi-Gaussian distribution (2). Also shown with dashed lines Bingham (B), eq. (34), and with dotted lines uniform (U), eq. (33), density functions and distributions. In (a, b) we see that in the limit $\sigma/F_\mu \to 0$, the bi-Gaussian off-axis angular distribution approaches a Bingham distribution; whilst in (g, h) we see that in the opposite limit $\sigma/F_\mu \to \infty$, the bi-Gaussian off-axis angular distribution approaches a uniform distribution (as does the Bingham distribution). Compare with Fig. 7.

5.3 Averaging vector parts

It is important to recognize that biased estimates also follow from arithmetic averages of scalar parts of the palaeomagnetic vector field, and this is true even for the isotropic variance considered here. To illustrate these biases, we consider first the case for intensity data. Given a Gaussian or bi-Gaussian distribution, eqs (10) or (16), the expected intensity is just the average, with due respect to probability, of all possible intensities,

$$E_g\left(F \mid F_\mu, \sigma^2\right) = \int_0^\infty p_g(F)\, F dF. \tag{38}$$

The integration is discussed in Appendix D. With the formula for the expected intensity in hand, we can calculate the typical bias between an arithmetic mean of the measured intensities and the intensity of the mean vector,

$$\delta F_g = E_g(F) - F_\mu. \tag{39}$$

In Fig. 9(a) we show the size of this bias as a function of the absolute vectorial dispersion σ, given a variety of mean vectorial intensities F_μ. Note that the bias is always positive, and that for many geophysical studies, a bias of several microTesla is not to be unexpected. We conclude that the mean intensity should not be identified with the intensity of the mean vector.

Next, let us examine the case for inclination-only data. The problem of inverting palaeomagnetic inclination data taken from azimuthally-unoriented borecores for the true, but unknown, mean inclination has been addressed by many authors, usually assuming locally Fisherian statistics (Briden & Ward 1966; Kono 1980; McFadden & Reid 1982; Cox & Gordon 1984). One of the conclusions of these studies is that simply averaging inclination data yields a biased estimate of the inclination of the mean vector, especially when the mean vector is nearly vertical. We measure the bias by the difference

$$\delta I_g = E_g(I) - I_\mu, \tag{40}$$

where the inclination expectations are given in Appendix F. In Fig. 9(c) we show the bias for the Gaussian case, as a function of the relative vectorial dispersion σ/F_μ, given a variety of mean vectorial inclinations I_μ. For many geophysical studies, a bias of tens of degrees or more is not to be unexpected.

From Appendix G we find that, for the Gaussian distribution considered here, the bias in declination estimation resulting from an arithmetic average is zero for all relative vectorial dispersions σ/F_μ,

$$\delta D_g = E_g(D) - D_\mu = 0, \tag{41}$$

provided, of course, that the true mean direction is not vertical, in which case the declination is indeterminate. Finally, in Fig. 9(g) we show the expected off-axis angle for a Gaussian distribution, namely $E_{g_1}(\theta)$, as a function of relative vectorial dispersion. Corresponding mathematical derivations are given in Appendix E.

5.4 Variance of field components

Having found that some arithmetic means are biased estimates of the true underlying mean vectorial components, it is perhaps not surprising that the corresponding variances can also be shown to be biased estimates of the true underlying vectorial variance. For example, given a Gaussian or bi-Gaussian distribution, the variance of the intensity is just

$$\begin{aligned} V_g\left(F \mid F_\mu, \sigma^2\right) &= E_g(F^2) - [E_g(F)]^2 \\ &= \int_0^\infty p_g(F) F^2\, dF - [E_g(F)]^2. \end{aligned} \tag{42}$$

The integration is given in Appendix D. With this, we can compare the standard deviation of the intensity,

$$S_g(F) = [V_g(F)]^{\frac{1}{2}}, \tag{43}$$

with the absolute vectorial dispersion σ. In Fig. 9(b) we see that, for many geophysical studies, these two quantities can differ by several microTesla. In a similar vein, and using derivations given in the appendices, in Fig. 9 we see that the standard deviation of the directional quantities, namely inclination, declination, and off-axis angle, are not simply related to the relative vectorial dispersion σ/F_μ.

5.5 Maximum likelihood

In using palaeomagnetic data to obtain accurate estimates of the properties of the vector field, its mean and its variance, we apply the method of maximum-likelihood; for a general review see Cramér (1945) or Stuart *et al.* (1999). With this approach, the most likely model distribution parameter is estimated from its probability density function, the so-called likelihood function, which is constructed from the joint probability density function for the existing set of data. Toward that end, we assume that the statistics for the palaeovector field are well represented by either a Gaussian or bi-Gaussian distribution. The validity of this assumption can be checked after the fitting to the data has been performed. Given a set of data, in making estimates of the vectorial mean and variance we use the Gaussian density functions and/or their marginal expressions to construct the appropriate likelihood function. In its most general form, for all usually encountered types of data groups, we maximize

$$\begin{aligned} L = &\prod_{j=1}^{N_{FID}} p_g(F_j, I_j, D_j) \prod_{k=1}^{N_{ID}} p_g(I_k, D_k) \\ &\times \prod_{l=1}^{N_{FI}} p_g(F_l, I_l) \prod_{m=1}^{N_F} p_g(F_m) \prod_{n=1}^{N_I} p_g(I_n), \end{aligned} \tag{44}$$

where the individual data density functions are given in the appendices. N_{FID} is the number of data for which intensity-inclination-declination triplets are available; N_{ID} is the number of data for which only inclination-declination pairs are available, etc. Maximizing L, and thus determining a particular estimated vectorial mean and variance, takes account of the correlations that exist within these different spherical-coordinate data groups, at least insofar as Cartesian vectorial components have isotropic variance, eq. (7). The informational content of these correlations is not exploited when different palaeomagnetic measurement types from the same rock deposition or archaeological artefact are treated separately, for example, by calculating a mean direction using unit vectors and, separately, arithmetically averaging the intensities. In the usual way, because it is numerically advantageous, we find the most likely set of distribution parameters by maximizing the logarithm of (44), something we accomplish by a simplex method; for reference see Press *et al.* (1992). The foregoing estimator is general, it can be employed in the analysis of a variety of palaeomagnetic data types used for numerous geophysical applications. Next, we discuss two such applications: palaeomagnetic secular variation and palaeomagnetic acquisition.

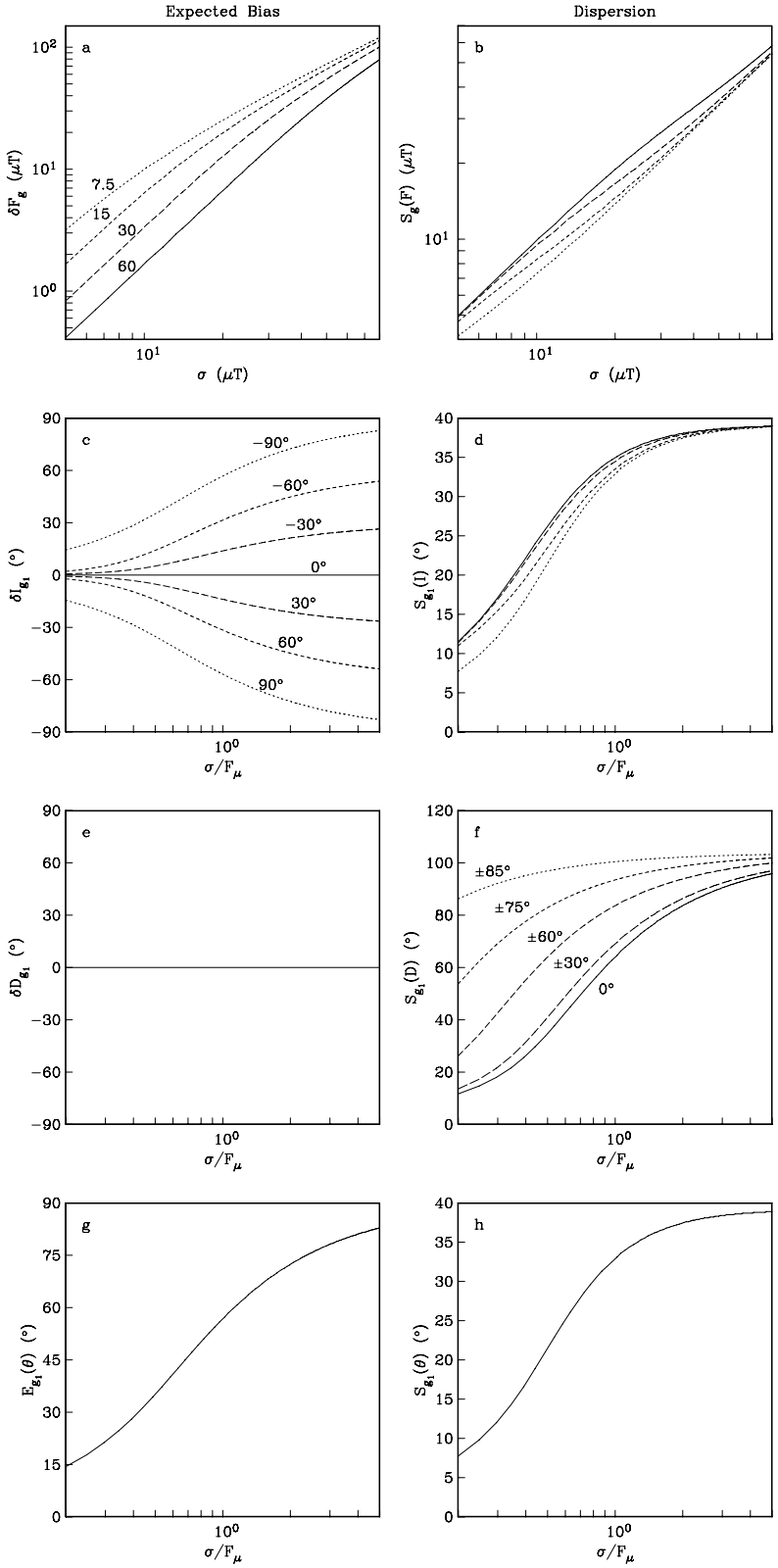

Figure 9. Examples of the bias δ of simple arithmetic averages and the dispersion S of the spherical-coordinate variables for the Gaussian distribution, (10). (a) The intensity bias δF_g as a function of the vectorial dispersion σ for four different vectorial-mean intensities F_μ, namely 7.5, 15, 30, and 60 μT. (b) The corresponding intensity dispersion $S_g(F)$ as a function of the vectorial dispersion and for the same vectorial-mean intensities. (c, d) The inclination bias δI_{g_1}, and the corresponding inclination dispersion $S_{g_1}(I)$, each as a function of the relative vectorial dispersion σ/F_μ, given different mean vectorial inclinations I_μ ranging from vertically up (-90°) to vertically down (90°). (e, f) The declination bias δD_{g_1}, and the corresponding declination dispersion $S_{g_1}(D)$, each as a function of relative dispersion, given different mean inclinations. (g, h) The expected off-axis angle $E_{g_1}(\theta)$ and its dispersion $S_{g_1}(\theta)$, each as functions of relative dispersion.

6 PALAEOMAGNETIC SECULAR VARIATION

In this section we examine palaeomagnetic secular variation recorded in published data measured from basalts from the island groups of Hawaii and Réunion (actually Réunion and its surrounding region). We have chosen to examine data from these two sites for three reasons. The first reason is that the volcanoes at Hawaii and Réunion have been active during similar periods of time: during the past 5 Ma and, in particular, during the Brunhes chron (the past 780 ka). These periods of time are fairly short compared to the timescales associated with tectonic shift and deformation, and it is reasonable to expect that the majority of the lavas from these island groups have remained relatively undisturbed since their deposition, a prerequisite for a study of data recording directional secular variation. Furthermore, over this period of time the conditions at the core–mantle boundary have probably not changed appreciably, and insofar as palaeosecular variation is affected by core–mantle coupling (Cox & Doell 1964; McFadden & Merrill 1995), the data are related to more-or-less stationary physical conditions within the Earth's core. The second reason we have chosen to analyse data from Hawaii and Réunion is that they are on almost exactly opposite latitudes, and therefore, data from these two sites allow us to investigate the long-term geometry and secular variation of the magnetic field. A certain amount of debate has centered around the issue of whether or not it is possible to resolve persistent non-zonal features in the palaeomagnetic field (Johnson & Constable 1995; Kelly & Gubbins 1997; Carlut & Courtillot 1998). However, it is reasonably clear, based on a global distribution of palaeomagnetic data, that, in addition to an (obvious) axial dipole, there is also a persistent axial quadrupole ingredient in the 5 Ma time-averaged field (Wilson 1970; McElhinny *et al.* 1996). Assuming that this is true, then because of their relative geographic locations, data from Hawaii and Réunion should display different vectorial means, and possibly different vectorial dispersions as well. And finally, the third reason we have chosen to examine data from these two sites is that they have been extremely heavily sampled by palaeomagnetists. The intensity and directional data collected from Hawaii and Réunion are sufficiently numerous to make statistical analyses of the full-vector field more robust than for perhaps any other pair of sites on the globe. (The most extensively sampled site is Iceland, but very few absolute intensity measurements are available from there.) The data sets for Hawaii and Réunion (and its surrounding region) are summarized in Tables 1 and 2.

6.1 Data selection and the data set

The data must be sorted and placed into single-flow groups, with care taken to avoid redundancy and sites suffering post-depositional orientational shifts. Of the available palaeomagnetic data from the various Hawaiian Islands covering the past 5 Ma, much of it comes from the Hawaiian Scientific Drilling Project (HSDP) and the near-by Scientific Observation Hole 4 (SOH-4). The HSDP measurements of Holt *et al.* (1996) and Laj & Kissel (1999) contain overlapping inclination data, whilst the latter study also includes intensity data. We have used all of the data from Laj & Kissel that satisfy our selection criteria, as well as those from Holt *et al.* for flows not measured or reported by Laj & Kissel. Likewise, in other cases, where there have been multiple studies of a given flow, we have taken care to avoid redundancy by selecting the measurements made with the most modern or thorough methods. For example, the directional data for the 1840 flow are taken from Tanaka & Kono (1991) instead of Doell & Cox (1963). If (say) an intensity measurement from a flow is reported in a particular paper, but the directions for the same flow are reported in a different paper (possibly by different authors), then we have grouped these data together as a triplet (F, I, D) representing the full magnetic vector field at the time of deposition. For example, Doell & Cox (1963) obtained directional data from the 1907 and 1935 flows, whilst Khodair & Coe (1975) obtained intensity data for the same flows. Grouping such data is important if we are to exploit the informational content of correlations between the different magnetic-field components. In a few cases, separate single-intensity measurements of a given flow have been reported in separate papers but under related authorship (Ueno & Kono 1977; Kono & Tanaka 1977); these data have been averaged to obtain a more robust result. Finally, if the palaeomagnetic data are part of a study concerned with motion along a fault, from deformation, or from a landslide, then we selected only the directional data from the undisturbed sites. For example, in the Hilina fault study by Riley *et al.* (1999) we have kept the Keana Bihopa data, but have excluded the Puu Kapukapu data, since it has undergone subsidence and therefore the data have been subjected to an orientational shift. Although palaeomagnetic data are often used to estimate the change in rock-bed orientation, to use 'corrected' data for palaeosecular variation studies invites the risk of circularity, something we seek to avoid.

Compared to the Hawaiian Islands, there are many fewer palaeomagnetic data covering the past 5 Ma available from the island of Réunion itself, and thus, for augmentation, we have incorporated data from nearby Mauritius, as well as the somewhat more distant islands of Madagascar and Comores. The Madagascar data (Andriamirado 1971) are only roughly dated (0.00–1.60 Ma), and they are therefore used in the bimodal bi-Gaussian analysis covering the past 5 Ma which follows, but not in the unimodal Gaussian analysis of the Brunhes chron. We have grouped directional data from Réunion and Mauritius, reported in Chamalaun (1968) and McDougall & Chamalaun (1969), with intensity data, obtained from the identical flows and reported in Senanayake *et al.* (1982), to form full-vectorial triplets (F, I, D). Although the island of Réunion has been the site of recent volcanic activity, unlike Hawaii no palaeomagnetic data from historical flows have been reported in the literature. Because of this, we have augmented the Réunion data set with two magnetic vectors taken from the modern-field model of Bloxham & Jackson (1992) for the years 1840 and 1990.

For both Hawaii and Réunion, the selection criteria for directional data are similar to those used by others (Prévot & Camps 1993; Quidelleur *et al.* 1994; McElhinny & McFadden 1997). Each palaeomagnetic direction in our data set, inclination and declination (I, D), is an average of measurements from at least two magnetically-cleaned samples per flow, with the precision parameter α_{95}, the semi-angle of the cone of 95 per cent confidence centered on the mean direction, less than 20°. Each absolute intensity (F) in our data set is an average of Thellier- or Shaw-type measurements from at least two samples per flow. In all source papers considered here, authors report not only the mean of multiple measurements of F, but also the number of measurements N and the standard deviation of the different intensity measurements σ_F. The error on the mean is estimated as $\sigma(F) = \sigma_F/\sqrt{N}$. We accept only absolute intensities F where the relative error $\sigma(F)/F$ is less than 33 per cent; but, in fact, the vast majority of the intensity data have relative errors that are much smaller than this cut-off. For the Hawaiian data covering the past 5 Ma (Brunhes, 780 ka), there are 457 (400) intensities, 1691 (1022) inclinations, 1207 (578) declinations, making this one of the largest vector data sets ever considered for a single site. For the Réunion data covering the past 5 Ma (Brunhes, 780 ka) there are 63 (53) intensities, 285 (223) inclinations, 285 (223) declinations,

Table 1. Hawaiian vector palaeosecular-variation data set. Locality is that for the general area. Name denotes the particular site or flow name, as given in the source papers. Lat and Long denote the present latitude and longitude of the site. N_F, N_I, N_D are, respectively, the number of intensity, inclination, and declination data. Age denotes the estimated age range of the sampled flows. Author denotes the source paper.

Locality	Name	Lat °N	Long °E	N_F	N_I	N_D	Age kyr	Author
Hawaii	Historical	19.5	204.5	0	8	8	Brunhes	Doell & Cox (1963)
Hawaii	Puna	19.5	204.5	0	18	18	Brunhes	Doell & Cox (1965)
Hawaii	Kahuku	19.5	204.5	0	28	28	10.00–75.00	”
Hawaii	Hamakua	19.5	204.5	0	11	11	Brunhes	”
Hawaii	Ninole	19.5	204.5	0	25	25	>10.00	”
Hawaii	Pololu	19.5	204.5	0	29	29	200.00–300.00	”
Hawaii	Kau	19.5	204.5	0	54	54	<10.00	Doell (1969)
Kauai		22.1	200.5	0	91	91	1400.00–5600.00	Doell (1972c)
Oahu	Honolulu	21.5	202.0	0	25	25	30.00–850.00	Doell (1972b)
Nihau	Kiekie	21.9	199.8	0	11	11	300.00–700.00	Doell (1972a)
Nihau	Paniau	21.9	199.8	0	5	5	3000.00	”
Nihoa		23.0	198.0	0	14	14	3000.00	”
Oahu	Koolau	21.5	202.0	0	33	33	1800.00–2600.00	Doell & Dalrymple (1973)
Oahu	Waianae	21.5	202.0	0	64	64	2400.00–3600.00	”
Hawaii	Historical	19.5	204.5	6	0	0	0.05–0.10	Khodair & Coe (1975)
Hawaii	Historical	19.5	204.5	5	0	0	0.25	Kono & Tanaka (1977); Ueno & Kono (1977)
Hawaii		19.5	204.5	6	7	7	0.87–>17.86	Coe *et al.* (1978)
Hawaii	Kilauea	19.5	204.5	0	94	94	Brunhes	Holcomb (1980)
Kauai	Kukui	22.1	200.5	10	29	29	3800.00–5100.00	Bogue & Coe (1984)
Kauai	Anahola	22.1	200.5	3	15	15	3800.00–5100.00	”
Kauai	Polihale A	22.1	200.5	0	13	13	3800.00–5100.00	”
Kauai	Kahililoa	22.1	200.5	0	27	27	3800.00–5100.00	”
Oahu	Koolau	21.5	202.0	4	0	0	1800.00–2600.00	Coe *et al.* (1984)
Oahu	Waianae	21.5	202.0	7	0	0	2400.00–3600.00	”
Hawaii	1950, 1972	19.5	204.5	0	2	2	0.03	Castro & Brown (1987)
Hawaii	Historical	19.5	204.5	7	7	7	0.00–1.86	Tanaka & Kono (1991)
Hawaii	Hilo	19.5	204.5	0	11	11	Brunhes	Buchanan-Banks (1993)
Hawaii		19.5	204.5	22	22	22	0.26–13.21	Mankinen & Champion (1993b)
Hawaii		19.5	204.5	6	6	6	13.53–31.10	Mankinen & Champion (1993a)
Hawaii	Kilauea	19.5	204.5	0	73	73	0.00–>2.40	Hagstrum & Champion (1994)
Hawaii	HSDP	19.5	204.5	0	40	0	0.00–420.00	Holt *et al.* (1996)
Hawaii	Mauna Loa	19.5	204.5	0	20	20	1.30	Jurado-Chichay *et al.* (1996)
Hawaii	Kohala	19.5	204.5	7	10	10	60.00–400.00	Brassart *et al.* (1997)
Hawaii	Mauna Loa	19.5	204.5	0	62	62	Brunhes	Champion & Lockwood (1998)
Hawaii	Mauna Loa	19.5	204.5	8	8	8	<35.00	Valet *et al.* (1998)
Hawaii	Keana Bihopa	19.5	204.5	0	21	21	0.35–100.00	Riley *et al.* (1999)
Hawaii	HSDP	19.5	204.5	151	152	0	0.00–420.00	Laj & Kissel (1999)
Oahu	Paheehee	21.5	202.0	0	28	28	3300.00	Herrero-Bervera & Valet (1999)
Oahu	Keaau	21.5	202.0	0	93	93	3300.00	”
Oahu	Kamaileunu	21.5	202.0	0	29	29	3300.00	Herrero-Bervera & Coe (1999)
Oahu	Haleakala	21.5	202.0	0	35	35	3580.00	”
Oahu	Kaena STSR	21.5	202.0	0	55	55	3000.00	Laj *et al.* (1999)
Oahu	Kaena KP	21.5	202.0	0	52	52	3000.00	”
Lanaii		20.8	203.0	0	8	8	780.00–1460.00	Herrero-Bervera *et al.* (2000)
Oahu	Koolau	21.5	202.0	4	14	0	2060.00–3020.00	Laj *et al.* (2000)
Oahu	Kealia	21.5	202.0	1	3	3	2980.00–3020.00	”
Oahu	Kaena STSR	21.5	202.0	2	0	0	3120.00	”
Oahu	Kaena KP	21.5	202.0	1	2	2	3220.00	”
Oahu	Mailiili	21.5	202.0	0	3	3	3270.00–3280.00	”
Oahu	Pahehe	21.5	202.0	2	2	2	3300.00	”
Oahu	Kepuhi Point	21.5	202.0	4	4	4	3890.00–3930.00	”
Kauai	Ohaiula	22.1	200.5	13	28	28	3800.00–5100.00	Bogue (2001)
Kauai	Polihale B	22.1	200.5	6	22	22	3800.00–5100.00	”
Hawaii	SOH-4	19.5	204.5	96	176	0	0.00–98.00	Laj *et al.* (2002)
Hawaii	SOH-1	19.5	204.5	67	102	0	0.00–40.00	Teanby *et al.* (2002)
Hawaii	HSDP	19.5	204.5	19	0	0	420.00–550.00	Tauxe & Love (2003)
Total Brunhes				400	1022	578		
Total				457	1691	1207		

Table 2. Réunion vector palaeosecular-variation data set.

Locality	Name	Lat °N	Long °E	N_F	N_I	N_D	Age kyr	Author
Réunion	Group 1	−21.1	55.5	0	47	47	Brunhes	Chamalaun (1968)
Réunion	Groups 2,3	−21.1	55.5	0	29	29	1000.00–2000.00	”
Mauritius		−20.3	57.5	0	15	15	173.00–5000.00	McDougall & Chamalaun (1969)
Madagascar		−17.0	47.5	0	14	14	0.00–1600.00	Andriamirado (1971)
Comores	Anjouan	−12.2	44.4	0	24	24	Brunhes	Watkins *et al.* (1972)
Comores	Grande Comore	−12.2	44.4	0	13	13	Brunhes	”
Réunion	Grande Chaloupe	−21.1	55.5	0	4	4	2020.00	McDougall & Watkins (1973)
Réunion	Rivière St Denis	−21.1	55.5	0	22	22	2020.00	”
Réunion		−21.1	55.5	0	20	20	Brunhes	Watkins (1973)
Réunion	Rivière de Bellecombe	−21.1	55.5	9	13	13	4.75–11.00	”
Mauritius		−20.3	57.5	6	0	0	200.00–3500.00	Senanayake *et al.* (1982)
Réunion		−21.1	55.5	6	0	0	600.00–2000.00	”
Réunion	Rivière des Remparts	−21.1	55.5	12	17	17	82.00-98.00	Chauvin *et al.* (1991)
Réunion	Modern field 1840, 1990	−21.1	55.5	2	2	2	0.01–0.16	Bloxham & Jackson (1992)
Réunion	Piton des Neiges	−21.1	55.5	28	65	65	70.00–130.00	Raïs *et al.* (1996)
Total Brunhes				53	223	223		
Total				63	285	285		

making this a relatively large data set, although quite a bit smaller than that for Hawaii.

6.2 Biases in the palaeomagnetic record

Because volcanic activity is unrelated to, and therefore uncorrelated with, geomagnetic secular variation, an unbiased sampling by palaeomagnetists of many lava flows coming from many eruptive episodes could yield a set of data that might be considered to be, in some respects, an unbiased record of secular variation. Of course, in reality volcanic activity is highly sporadic and there might, therefore, be some bias in the palaeomagnetic record toward certain periods of time when volcanic eruptions happened to have been unusually prolific. Recognizing such obvious difficulties, some investigators have combined data from stratigraphically-adjacent flows if they were judged to have ‘similar’ directions; the thinking being that serially-similar data must be indicative of a rapid succession of lava depositions preserving more-or-less coincident records of the magnetic field. It should be clear, however, that this interpretation is not necessarily valid. After all, a sequence of similar data could also arise from a quiescent period of secular variation. Indeed, Love (1998) has noted that selective averaging of similar data from stratigraphically-adjacent flows can, itself, introduce bias. Lacking detailed information about the dates of each lava flow, one way to partially alleviate the troublesome affects of sporadic volcanic activity, and hopefully obtain more robust statistical results, is to simply use many palaeomagnetic data coming from many different eruptive episodes. We admit that this is still not a perfect approach, nonetheless, it is the approach we prefer, it being consistent with the basic tenet of statistical analysis: Data should not be chosen on the basis of what they are.

A related nuisance stems from preferential sampling by palaeomagnetists: transitional periods, reversals and excursions, are disproportionately over-represented in the literature. Previous investigators have sought to debias the palaeomagnetic record by picking data recording either transitional or non-transitional stable periods. This requires that the distinction between a transitional and non-transitional period be formally defined, usually done in terms of a cut-off of the virtual geomagnetic pole (VGP) latitude. However, such definitions are entirely arbitrary, they lead to biased data selection, and since this could affect the conclusions of a statistical analysis, they are unsatisfactory. In this study, although we analyse palaeomagnetic data coming from Hawaii and Réunion covering the past 5 Ma, a span which includes several polarity transitions and is therefore subject to sampling bias, we also perform separate analyses on data recording the magnetic field during only the current normal Brunhes chron. Even then, bias is not entirely avoided, brief excursions have been identified within the Brunhes. Nonetheless, this temporal restriction represents an improvement in the situation, since full reversals are more easily identified than brief excursions.

6.3 Normalization

The data come from the general localities of Hawaii and Réunion, however, there are, of course, small differences in the exact location of the various sample sites. To account for these differences in location, we have adjusted all of the intensity and inclination data to a common-site latitude,

$$F \to F \times F_{AD}(\Lambda_C)/F_{AD}(\Lambda_S), \tag{45}$$

$$I \to I + I_{AD}(\Lambda_C) - I_{AD}(\Lambda_S), \tag{46}$$

where Λ_C and Λ_S are the common- and true-site latitudes, where F_{AD} and I_{AD} are the intensity and inclination of an axial dipole given by

$$\tan I_{AD} = 2 \tan \Lambda, \tag{47}$$

$$F_{AD} = g_1^0 (1 + 3 \sin^2 \Lambda)^{\frac{1}{2}}, \tag{48}$$

and where g_1^0 is a constant. These between-site adjustments of the data are small; hypothetical adjustments for the unknown non-dipolar field would be insignificant. We adjust the Hawaii and Réunion data to common-site latitudes Λ_C of $\pm 19.5^\circ$N.

6.4 Hawaiian Secular Variation: 5 Ma

We begin our likelihood analysis by considering the Hawaiian data covering that past 5 Ma. The data set consists of a mixture of data groups: intensities with directions, directions only, intensities with inclinations, intensities only, and inclinations only. To obtain the vectorial mean and variance, we model the data with a bimodal

Table 3. Vector palaeosecular-variation maximum-likelihood estimation for both Hawaii and Réunion. Data types denotes the kind of data used in the estimation, so, for example, F, I, D means that all available intensity, inclination, declination data were used; I, D means that only inclination and declination data were used, etc. F_μ, I_μ, D_μ, σ, and σ/F_μ denote the maximum-likelihood estimates of intensity, inclination, declination, absolute vectorial dispersion, and relative vectorial dispersion. $p_{KS}(F)$ ($p_{KS}(\theta)$) denotes the Kolmogorov–Smirnov probability that the intensity (off-axis angular) data could have been drawn from a three-dimensional Gaussian distribution with the given estimated parameters. Comparison values are also shown for an axial dipole and global field models using data covering 5 Ma, given site latitude and longitude (19.5°N, 204.5°E) for Hawaii and (−19.5°N, 55.5°E) for Réunion. See Figs 10 and 11.

Maximum likelihood data types	F_μ (μT)	I_μ (°)	D_μ (°)	σ (μT)	σ/F_μ	$P_{KS}(F)$	$P_{KS}(\theta)$
				Hawaii			
F, I, D	34.88	30.22	0.15	9.18	0.2633	0.0000	0.0000
I, D	–	29.94	0.07	–	0.2431	–	–
F, I	34.48	31.13	–	9.66	0.2801	0.0000	–
F	28.65	–	–	14.15	0.4939	0.7170	–
I	–	30.68	–	–	0.2401	–	–
	F	I	D				
Axial Dipole	–	35.32	0.00				
Global Field Model (Kelly & Gubbins 1997)	–	31.01	2.04				
				Réunion			
F, I, D	36.10	−39.84	−0.76	8.56	0.2371	0.0935	0.0019
I, D	–	−39.66	−0.63	–	0.2252	–	0.0279
F, I	35.59	−40.49	–	9.14	0.2569	0.1459	–
F	32.83	–	–	12.23	0.3725	0.7277	–
I	–	−40.05	–	–	0.2350	–	–
	F	I	D				
Axial Dipole	–	−35.32	0.00				
Global Field Model (Kelly & Gubbins 1997)	–	−37.42	−2.54				

bi-Gaussian distribution (16). The likelihood function that accommodates all data-group combinations is

$$L = \prod_{j=1}^{N_{FID}} p_{g_2}(F_j, I_j, D_j) \prod_{k=1}^{N_{ID}} p_{g_2}(I_k, D_k) \times \prod_{l=1}^{N_{FI}} p_{g_2}(F_l, I_l) \prod_{m=1}^{N_F} p_{g_2}(F_m) \prod_{n=1}^{N_I} p_{g_2}(I_n). \quad (49)$$

Results are summarized in Table 3 and shown in Fig. 10, where we compare the model probability density functions p and cumulative distributions P with those of the data themselves. Note that, when showing the data distributions, we have enforced normal-reverse symmetry, that is, symmetry under change in sign of the magnetic field, as in transformation (14). This is done only for purposes of comparison; identical likelihood maximization would be attained without enforcing this symmetry on the data.

In Fig. 10 we see that the variance of intensity (declinations) is larger (smaller) than that for the best-fitting, spherically-symmetrical bi-Gaussian distribution, whilst the inclinations are fitted rather well by the same bi-Gaussian distribution. This observation highlights the complexity of palaeomagnetic secular variation at Hawaii: the local vectorial variance is clearly not isotropic, an observation consistent with that made by others on the basis of Hawaiian directional data (Creer *et al.* 1959; Tsunakawa 1988; Tanaka 1999). Indeed, in response to observations such as these, a number of anisotropic giant-Gaussian forward models, with different standard deviations for the orthogonal Cartesian field components, have been proposed (Quidelleur & Courtillot 1996; Constable & Johnson 1999). We believe that a generalization of the isotropic inverse modelling considered here would probably yield fits to the Hawaiian palaeovector data that are better than those seen in Fig. 10.

To test our estimates against those that might be made with data coming only from an azimuthally-unoriented borecore, in Fig. 10 we also show maximum-likelihood results where we have omitted all declinations. For this case, instead of maximizing (49) we maximized

$$L = \prod_{j=1}^{N_{FID}+N_{FI}} p_{g_2}(F_j, I_j) \prod_{k=1}^{N_{ID}+N_I} p_{g_2}(I_k) \prod_{m=1}^{N_F} p_{g_2}(F_m). \quad (50)$$

We conducted a number of other estimation experiments, systematically omitting different parts of the Hawaiian palaeovector data and then maximizing the relevant likelihood function; results are summarized in Table 3. In general, with one or more vectorial part removed from the fitting experiment, the remaining data are relatively better fitted; for example, fitting the intensities alone yields a Kolmogorov–Smirnov probability of 0.7170, yet when the directions are included in the fitting experiment, the fit to the intensities is severely degraded. Interestingly, the mean inclinations and declinations are relatively consistently estimated, there are, however, more sizable differences between the various estimated intensities of the mean vector as well the vectorial dispersions. Again, these observations are consistent with anisotropic palaeosecular variance at Hawaii.

6.5 Réunion secular variation: 5 Ma

Next, we consider the Réunion data covering the past 5 Ma. There are many fewer data from Réunion than from Hawaii, and, since none of the data were taken from azimuthally-unoriented borecores, they consist of a slightly different mixture of data groups: intensities with directions, directions only and intensities only. To obtain the vectorial mean and variance, we model the data with a bimodal bi-Gaussian distribution using the likelihood function

$$L = \prod_{j=1}^{N_{FID}} p_{g_2}(F_j, I_j, D_j) \prod_{k=1}^{N_{ID}} p_{g_2}(I_k, D_k) \prod_{m=1}^{N_F} p_{g_2}(F_m). \quad (51)$$

Results are summarized in Table 3 and shown Fig. 11, and as with the Hawaiian data, when showing the data distributions, we have enforced normal-reverse symmetry. The Réunion data are better fitted

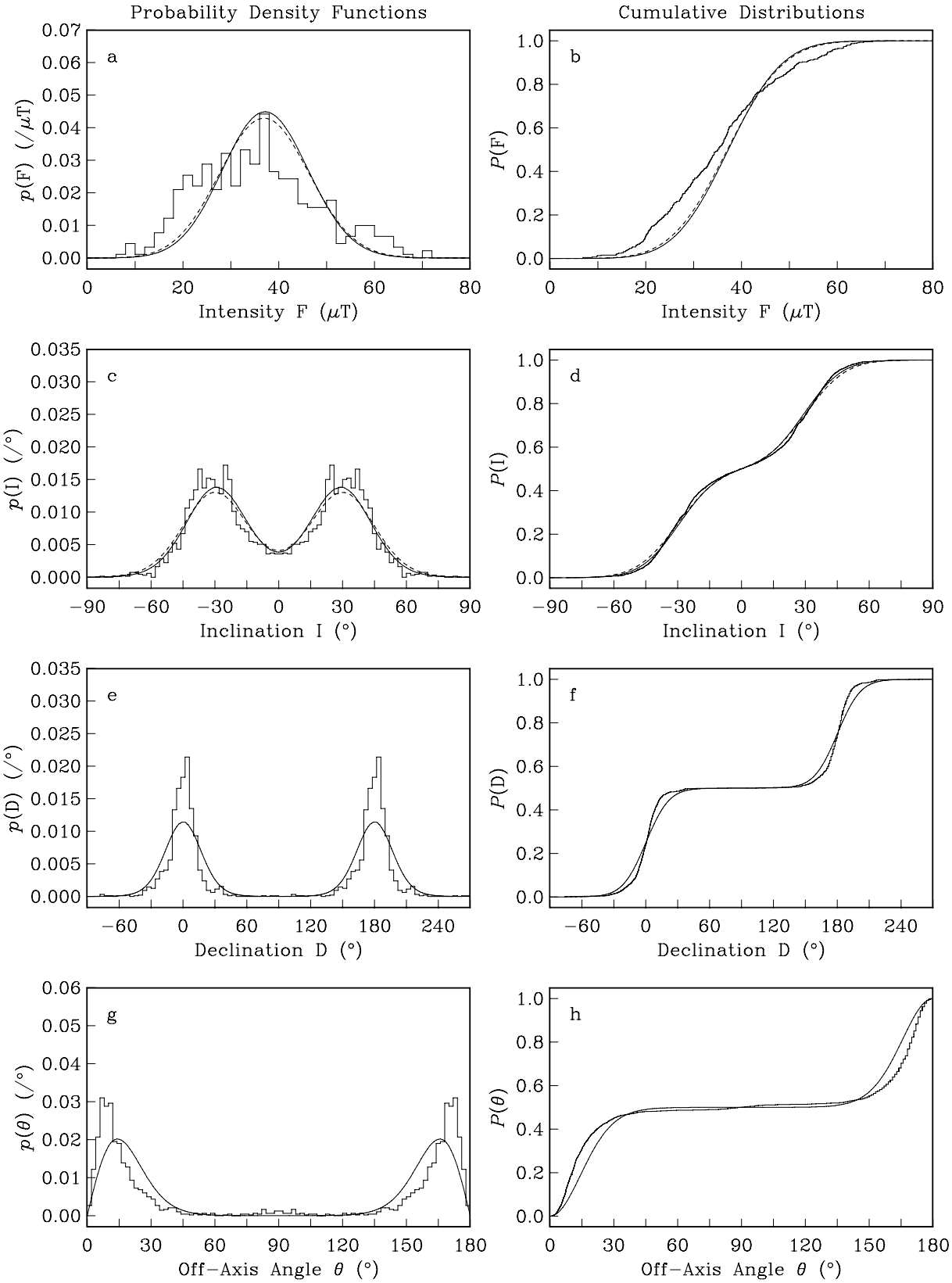

Figure 10. Maximum-likelihood fits for the Hawaiian data covering the past 5 Ma and using a bimodal, 3-D bi-Gaussian distribution, eq. (16), and associated marginal density functions. The marginal probability density functions p and corresponding cumulative distributions P are shown for (a, b) intensity F, (c, d) inclination I, (e, f) declination D, and (g, h) off-axis angle θ. The fits shown by the solid lines correspond to a maximum-likelihood estimation using all the available data groups (F, I, D); the dashed lines correspond to an estimation where the declinations have been omitted. Normal-reverse polarity symmetry of the data bins has been enforced. Numerical values are given in Table 3.

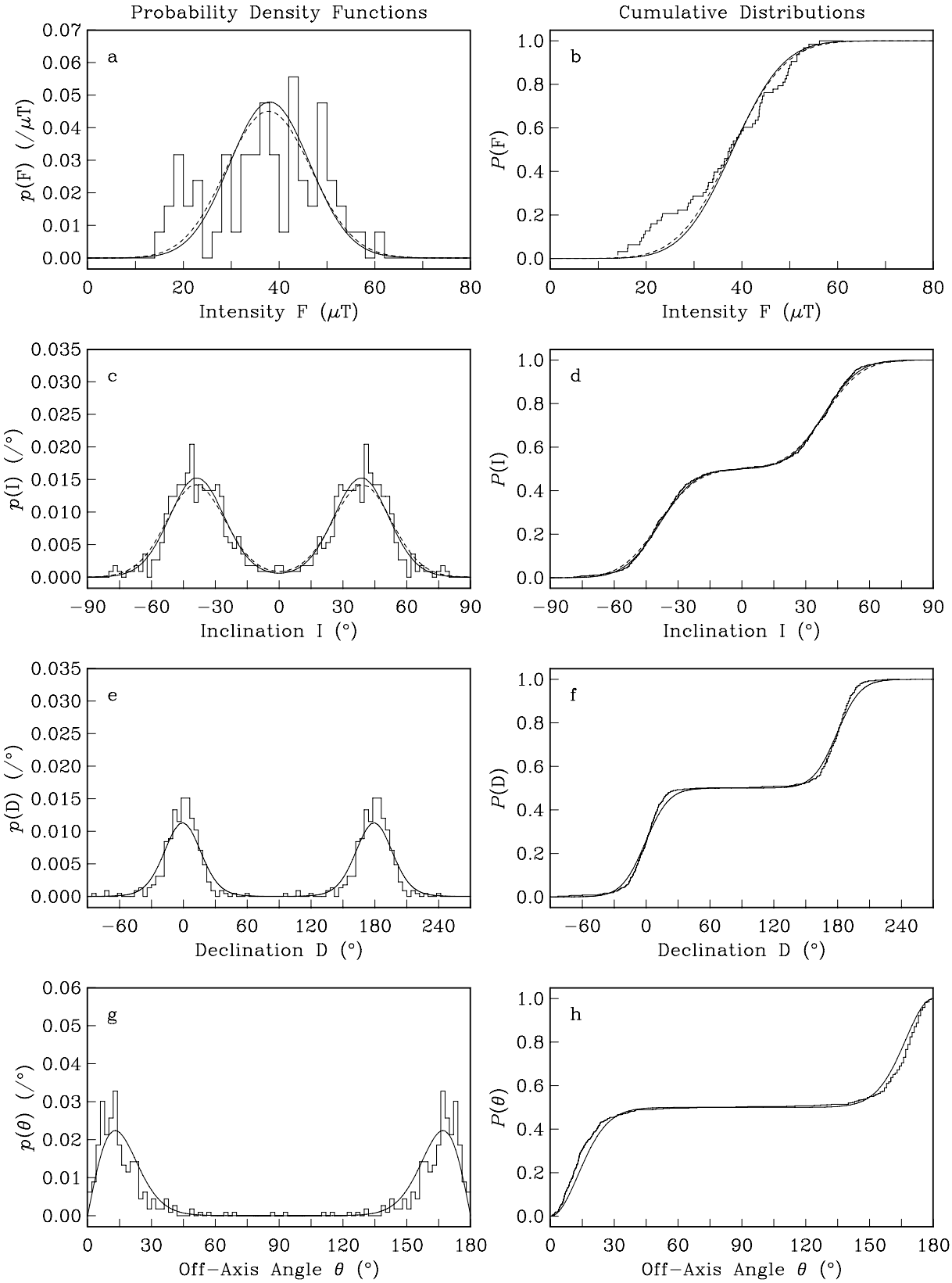

Figure 11. Same as Fig. 10 except for the Réunion data covering the past 5 Ma.

by the bi-Gaussian distribution than are the Hawaiian data, with correspondingly larger Kolmogorov–Smirnov probabilities, but even here there is some noticeable misfit, which, as with the Hawaiian data, might be remedied by allowance for anisotropic variance. Although it is obvious that some signal in the data remains to be modelled, given the extreme simplicity of the assumed bi-Gaussian distribution, and given the incomplete and non-uniform sampling inherent to palaeomagnetic lava data, it is actually rather satisfying that the fits to the Réunion are as good as they are.

6.6 Note on normal-reverse symmetry

For the Réunion data, in Fig. 12 we present the data distributions without enforcing symmetry under change in sign of the magnetic field, as opposed to what we have done previously. Once again, we emphasize that this is irrelevant to the maximum-likelihood estimation using the symmetrical bi-Gaussian distribution, but it affects posterior comparisons of the model distributions with the data distributions. Note that in both our Hawaii and Réunion data sets, normal polarity data are more numerous than reverse polarity data. This kind of polarity asymmetry can arise for three reasons. First, since most palaeomagnetic lava data are collected from surface flows, there is a sampling bias skewed toward more recent episodes of volcanic activity, and especially for Hawaii, these are during the present normal Brunhes chron. Second, a polarity bias might simply reflect differences in volcanic activity: over a certain period of time a reverse (normal) polarity might accidentally be recorded more often than a normal (reverse) polarity. Third, it might be that, over a certain period of time, the field was more often of reverse (normal) polarity than normal (reverse) polarity. If this is the case it might be accidental, reversals do not occur regularly in time, or it might reflect a long-term, slowly-varying state of the magnetic field, giving rise to what is commonly known as a 'polarity bias'. There is, of course, a slight equivocation, since during a particular chron, a normal one (say), there are brief excursional periods, when the field might possibly be better characterized as being of reverse polarity. However, making a fine distinction between normal and reverse polarities, especially during transitional and excursional periods, requires arbitrary definitions which, as we have mentioned, might themselves be biased. Having said all of this, it should be recognized that regardless of whether or not there actually exists a polarity bias, because of invariance under the transformation (14), the particular polarity is itself irrelevant: for either polarity, the physics is the same. Therefore, when comparing model distributions with data distributions it is often preferable, as in Fig. 11, to enforce symmetry under change in sign of the magnetic field. We consider polarity bias to be an important issue, but its study requires a formalism that is different from that developed here.

6.7 Hawaiian secular variation: Brunhes

Because the available palaeomagnetic data might be biased due to preferential sampling of polarity transitions, we consider now the more restricted period of the normal-polarity Brunhes chron. For the Hawaiian data, after maximizing the likelihood function

$$L = \prod_{j=1}^{N_{FID}} p_{g_1}(F_j, I_j, D_j) \prod_{k=1}^{N_{ID}} p_{g_1}(I_k, D_k) \times \prod_{l=1}^{N_{FI}} p_{g_1}(F_l, I_l) \prod_{m=1}^{N_F} p_{g_1}(F_m) \prod_{n=1}^{N_I} p_{g_1}(I_n), \tag{52}$$

for the unimodal Gaussian distribution (10), we obtain the results summarized in Table 4 and shown in Fig. 13. As with the bi-Gaussian fits to the data covering past 5 Ma, for the Brunhes data the misfit to the spherically-symmetrical Gaussian distribution reveals that the variance of the vector data is anisotropic; in fact the degree of anisotropy within the Brunhes appears to be larger than it is for the past 5 Ma, although some of this might by symptomatic of suboptimal temporal sampling. Having said that, in general there is substantial agreement between estimates of the mean vector and vectorial variance using data covering 5 Ma and the subset of data covering the Brunhes. Therefore, at least for the data considered here, it is possible that our expressed concern about bias resulting from preferential sampling of polarity transitions is something of an excessive worry.

6.8 Réunion secular variation: Brunhes

The Réunion Brunhes data are modelled using the likelihood function

$$L = \prod_{j=1}^{N_{FID}} p_{g_1}(F_j, I_j, D_j) \prod_{k=1}^{N_{ID}} p_{g_1}(I_k, D_k) \prod_{m=1}^{N_F} p_{g_1}(F_m), \tag{53}$$

and results are summarized in Table 4 and shown in Fig. 14. As with the Réunion data covering the past 5 Ma, there is still noticeable misfit, mostly in declination, and some of the Kolmogorov–Smirnov probabilities remain rather small, indicative of unmodelled signal in the data (probably some anisotropy). However, what the Kolmogorov–Smirnov probabilities don't measure is the fact that most of the general character of the data is described by the simple unimodal Gaussian distribution; the fit is much better here than it is for Hawaii. The scatter seen in the bins of intensity is probably the result of small data numbers; more intensity measurements from Réunion would certainly be welcome.

6.9 Palaeomagnetic field asymmetry

In Fig. 15 we compare fits to the Hawaiian and Réunion Brunhes data. The two sites are on virtually opposite latitudes, and could, therefore, be expected to display symmetry if (say) the mean field was an axial dipole. Instead, there are significant differences in all local model parameters, both means and variances. Note especially differences in the mean inclination, where, for fits using all available measurements (F, I, D) and, with an appropriate change of inclination sign, the difference is a surprisingly large 9.61°. Asymmetry in palaeomagnetic inclination means from sites on opposite sides of the equatorial plane can be attributed to an axial dipole-quadrupole structure in the time-averaged field, but the inclination differences observed here are greater than those predicted by most mean-field models, such as those compared in Table 4. A more appropriate comparison is between unit directional vectors. With a change in inclination sign, the mean directions from Hawaii and Réunion differ by an angle of 9.92°, which, given the number of data involved in this analysis, is by palaeomagnetic standards a robust demonstration of a persistent departure from a simple geocentric axial dipole. Finally, we note that the intensity data from Hawaii display greater variance than do the intensity data from Réunion, an observation that, by itself, is indicative of asymmetry in the field's behaviour.

6.10 Alternative intensity fits

For further comparison, we performed a number of different maximum-likelihood fits to the Hawaiian and Réunion Brunhes intensity data: using a Rayleigh–Rician distribution (corresponding to the 3-D vectorial Gaussian distributions developed here), a 1-D normal distribution, a log-normal distribution, and a gamma

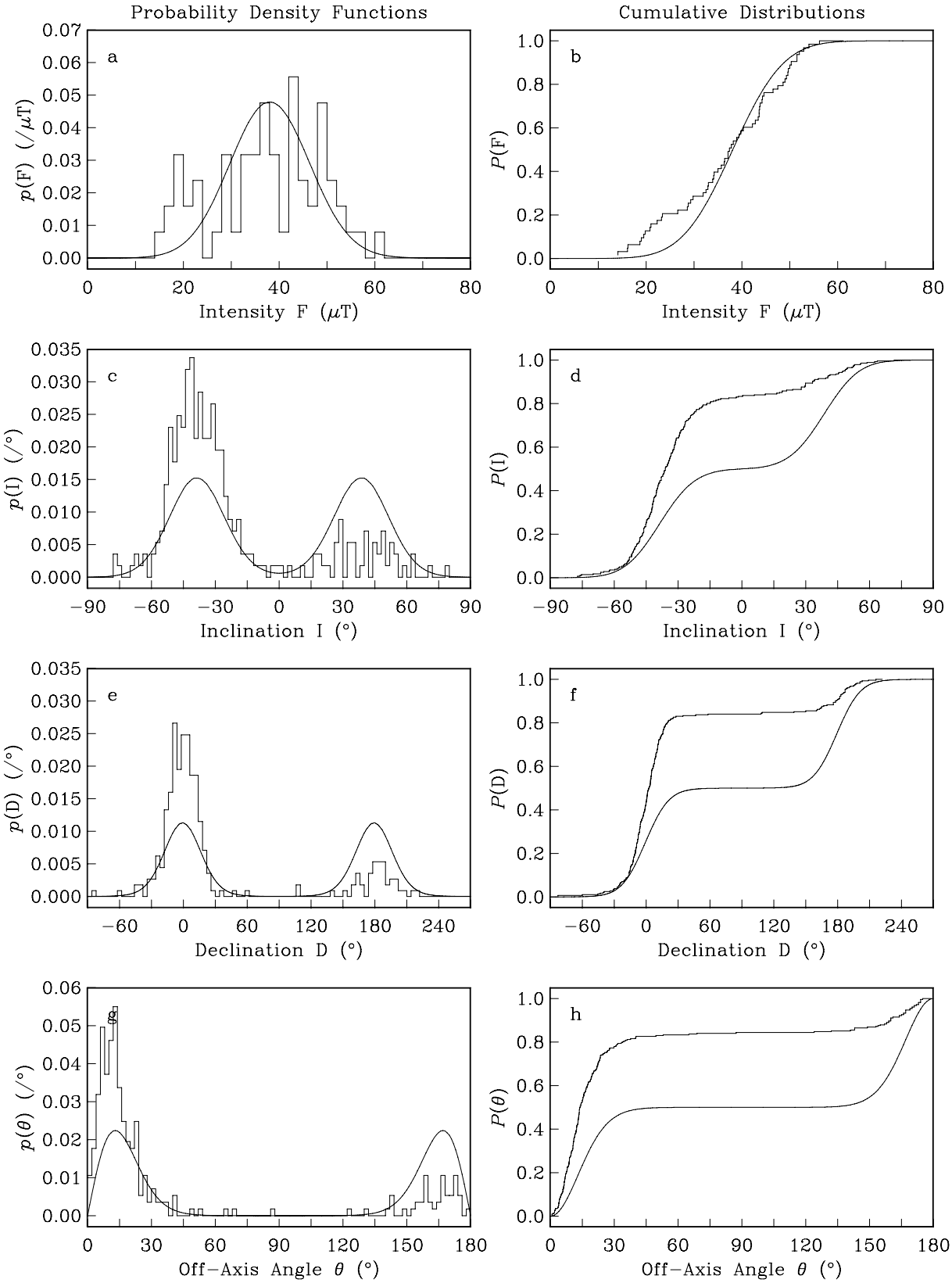

Figure 12. Same as Fig. 11 except that normal-reverse polarity symmetry of the data bins has not been enforced.

Table 4. Same as Table 3, except these results are for the Brunhes. See Figs 13 and 14.

Maximum likelihood data types	F_μ (μT)	I_μ ($\circ$)	D_μ ($\circ$)	σ (μT)	σ/F_μ	$P_{KS}(F)$	$P_{KS}(\theta)$
				Hawaii			
F, I, D	35.78	29.60	2.56	8.75	0.2447	0.0000	0.0000
I, D	–	29.10	2.42	–	0.2142	–	0.0000
F, I	34.79	30.38	–	10.08	0.2897	0.0000	–
F	29.27	–	–	13.86	0.4737	0.4529	–
I	–	29.62	–	–	0.2534	–	–
	F	I	D				
Axial Dipole	–	35.32	0.00				
Global Field Model (Johnson & Johnson 1995) LB1	–	27.08	2.50				
Global Field Model (Carlut & Courtillot 1998) Q94-me	–	31.61	4.46				
				Réunion			
F, I, D	38.81	−39.21	−0.49	7.94	0.2093	0.5144	0.0152
I, D	–	−39.02	−0.39	–	0.2019	–	0.1528
F, I	38.71	−39.55	–	8.63	0.2230	0.7343	–
F	37.45	–	–	10.29	0.2749	0.8815	–
I	–	−39.23	–	–	0.2110	–	–
	F	I	D				
Axial Dipole	–	−35.32	0.00				
Global Field Model (Johnson & Johnson 1995) LB1	–	−34.68	−0.42				
Global Field Model (Carlut & Courtillot 1998) Q94-me	–	−36.63	−0.89				

distribution. In each case we maximized a likelihood function of the form

$$L = \prod_{i=1}^{N_{FID}+N_{FI}+N_F} p(F_i). \tag{54}$$

Results are shown in Fig. 16 and summarized in Table 5. Clearly the Rayleigh–Rician and 1-D normal distributions provide the best fits; for Hawaii the Rayleigh–Rician (1-D normal) distribution gives a Kolmogorov–Smirnov probability of 0.4529 (0.2028), and for Réunion the probability is 0.8815 (0.8983). Neither the log-normal, nor the gamma distributions provide particularly compelling fits.

Although the reader might find the fits given by either the Rayleigh–Rician distribution or the 1-D normal distribution to be acceptable, it is important to recognize that since it follows from a fully 3-D vector field, only the Rayleigh–Rician provides a reasonable measure of the intensity of the underlying mean vector F_μ, and for that matter, the vectorial dispersion σ. A 3-D vectorial average does not correspond to the average of a 1-D normal distribution, the bias being given by (39). If one seeks to estimate the intensity of the mean vector from palaeointensity data, then this is an important distinction to make.

More specifically, for the Hawaiian (Réunion) data, the best fitting Rayleigh–Rician gives a mean-vector intensity of $F_\mu = 29.27$ μT (37.45 μT), which is very different from the 1-D normal expected intensity of $E(F) = 35.81$ μT (40.28 μT). This bias stems from the vectorial variance in the data themselves. Indeed, as we note in Appendix D, as the vectorial dispersion goes to zero, the expected intensity approaches the intensity of the mean vector, eq. (D16). For the Hawaiian (Réunion) data, the best fitting Rayleigh–Rician gives a relative vectorial dispersion of $\sigma/F_\mu = 0.4737$ (0.2749), which is larger than that estimated by using the 1-D dispersion and expected value, $S/E = 0.3455$ (0.2456).

6.11 Alternative directional fits

Next, we performed different maximum-likelihood fits to the Hawaiian and Réunion Brunhes directional data: using the directional (off-axis angular) probability density functions corresponding to the 3-D vectorial Gaussian distribution developed here, and the probability density functions of the Fisher distribution. In each case we maximized a likelihood function of the form

$$L = \prod_{i=1}^{N_{FID}+N_{ID}} p(I_i, D_i) \prod_{l=1}^{N_{FI}+N_I} p(I_k). \tag{55}$$

Results are shown in Fig. 16 and summarized in Table 6. Clearly the directional Gaussian and Fisher distributions provide comparable fits, although for the Hawaiian and Réunion data neither gives high Kolmogorov–Smirnov probabilities. Similar to our point about the intensity experiments discussed above, although the reader might be inclined to use the directional distributions corresponding to either a 3-D Gaussian or a Fisher distribution, only the former gives a meaningful estimate of the relative vectorial dispersion σ/F_μ.

For the Hawaiian (Réunion) data, the best fitting 'angular-Gaussian' distribution gives a Fisher-like dispersion parameter of $(F_\mu/\sigma)^2 = 21.79$ (24.53), which should be compared with the estimates deduced using a Fisher distribution of $\kappa = 21.00$ (20.00). Also note in Table 6 that the dispersion parameter calculated using straightforward arithmetic means, and which requires both inclinations and declinations, is 39.75 (23.69); the former value is drastically different from the maximum-likelihood estimates, which, in addition to inclination-declination data, also accommodate inclination-only data.

7 PALAEOMAGNETIC ACQUISITION

In order to obtain an accurate estimate of the palaeomagnetic field at a particular instant in time, an average is usually constructed from laboratory measurements of multiple samples of an individual rock deposition or archaeological artefact. Because of the complexities of the acquisition process, and those of the laboratory methodology, individual palaeomagnetic measurements, from separate samples of the same rock deposition or artefact, are never truly identical; they display a variance about a mean. In this section we examine estimation of the mean acquisition palaeovector and the vectorial variance about the mean. We analyse published directional and intensity data taken from two recent lava flows in Mexico and Hawaii. The data set is summarized in Table 7.

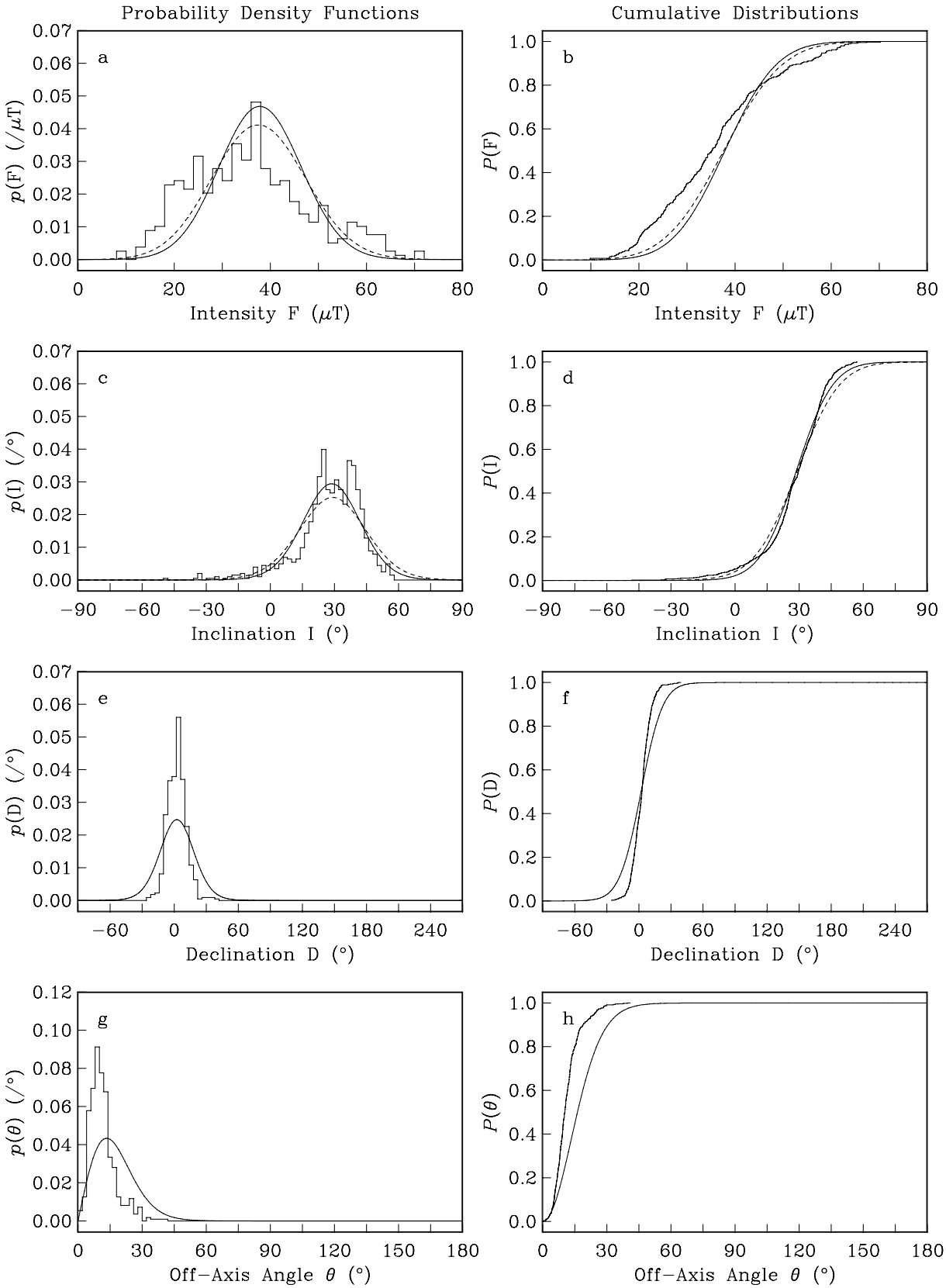

Figure 13. Maximum-likelihood fits for the Hawaiian data covering the Brunhes and using a unimodal, 3-D Gaussian distribution, eq. (10), and associated marginal density functions. The marginal probability density functions p and corresponding cumulative distributions P are shown for (a, b) intensity F, (c, d) inclination I, (e, f) declination D, and (g, h) off-axis angle θ. The fits shown by the solid lines correspond to a maximum-likelihood estimation using all the available data groups (F, I, D); the dashed lines correspond to an estimation where the declinations have been omitted. Numerical values are given in Table 4.

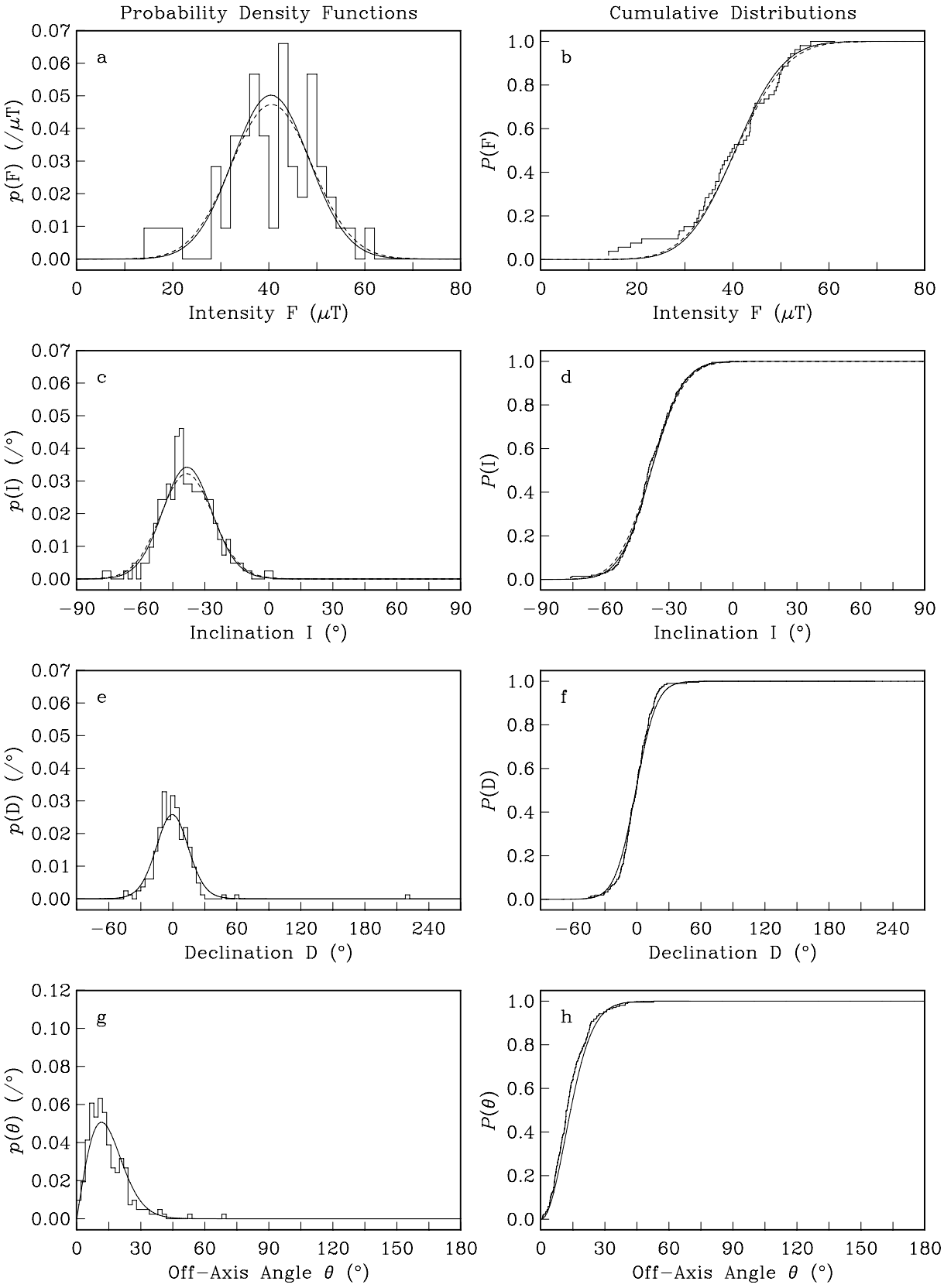

Figure 14. Same as Fig. 13 except for the Réunion data covering the Brunhes.

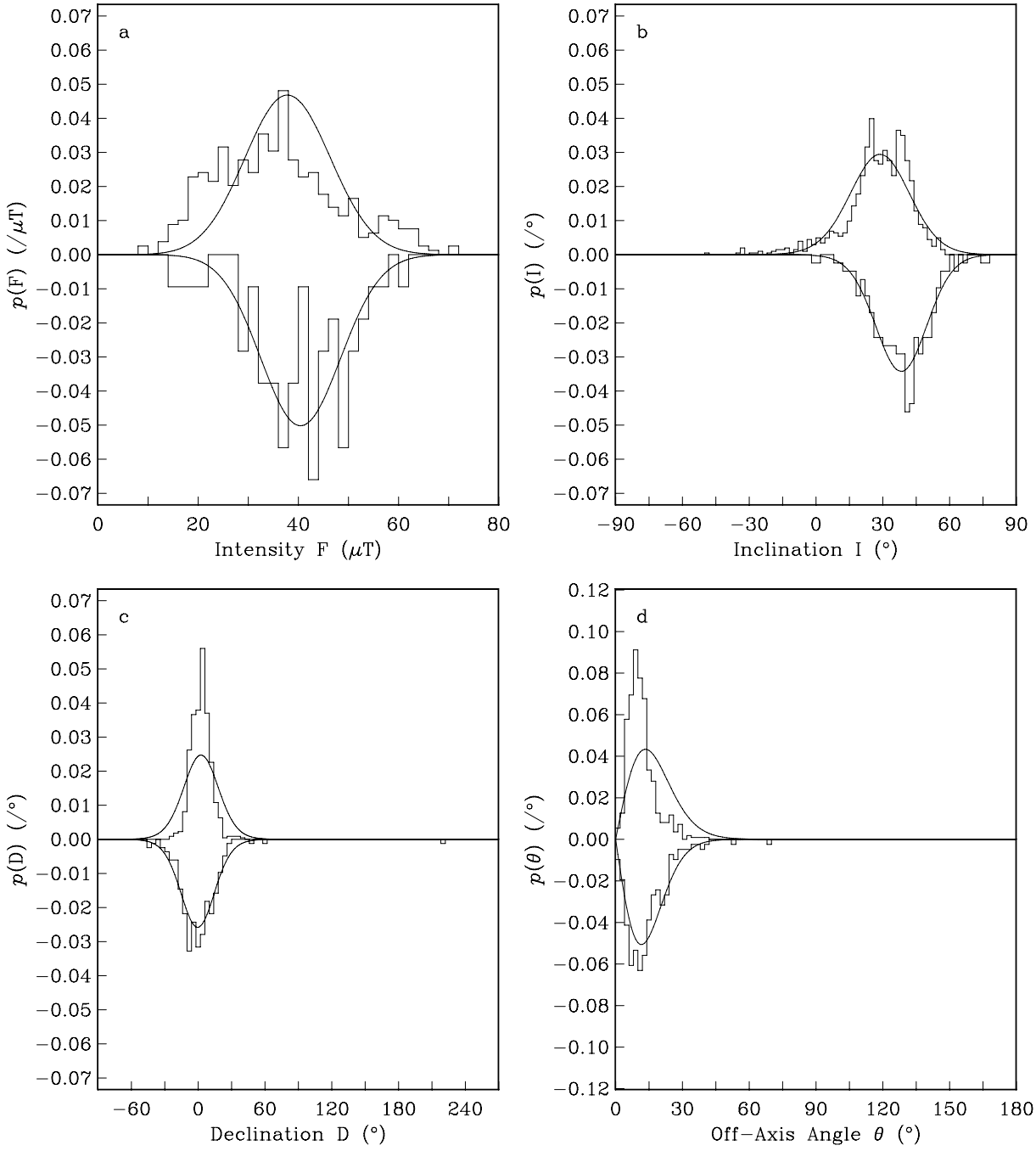

Figure 15. Comparison of maximum-likelihood fits of the unimodal, 3-D Gaussian distribution to the (positive, top) Hawaiian Brunhes data and (negative, bottom) Réunion Brunhes data. The sign of the Réunion inclination data has been changed so that they can, more clearly, be compared to the Hawaiian data. All the available data groups (F, I, D) have been used here. Note that the Réunion data are fitted better than the Hawaiian data, also note the sizable difference in mean inclination between these two sites.

7.1 Data selection and the data set

Most palaeomagnetic studies of particular rock depositions consist of relatively few (typically less than ten) separate measurements. For a robust statistical study of acquisition vectorial statistics, we concentrate on two lava flows that have been sampled relatively numerously for measurement of both direction and intensity, namely the 1960 Kilauea, Hawaiian flow and the Holocene Xitle, Mexican flow. With respect to selecting individual data, we have not applied statistical criteria, like the simple ones used in selecting data for the previous discussion of palaeosecular variation, since the data considered here are individual measurements, as opposed to averages of ensembles of data. Having said this, most of the measurements are relatively modern, and therefore we hope reasonably accurate, with each direction, inclination, and declination (I, D), coming from magnetically-cleaned samples, and with the absolute intensities (F) coming from Thellier- or Shaw-type measurements. Both the Kilauea and Xitle flows have been sampled at various heights across their vertical extents, and the Kilauea flow has been sampled at different localities across its lateral extent. Therefore, the two data

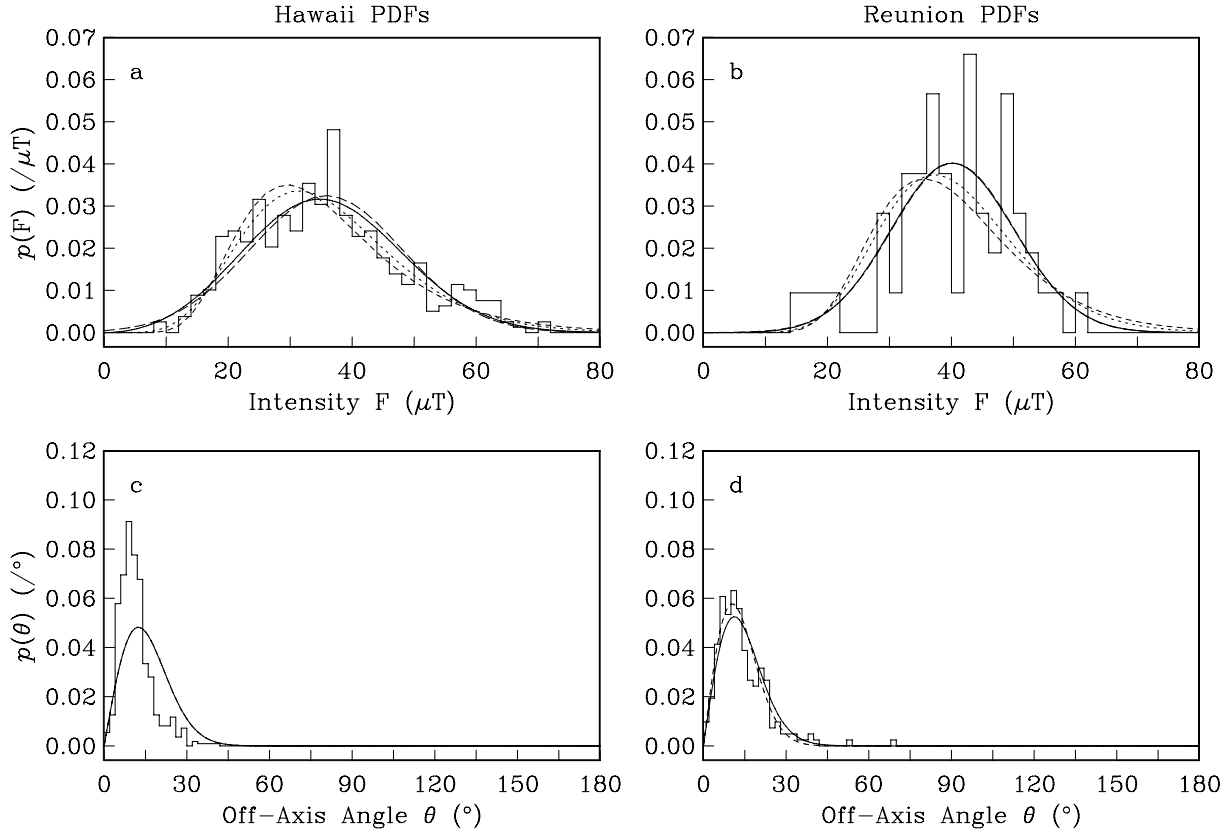

Figure 16. A comparison of maximum-likelihood fits with alternative distributions for palaeosecular-variation data. For the intensity data from (a) Hawaii and (b) Réunion: The Rayleigh–Rician (corresponding to the intensity distribution for the 3-D Gaussian distributions) is shown by a solid line. The 1-D normal distribution, the log-normal, and the gamma distributions are shown by long-dash, short-dash, and dots, respectively. For the directional data (displayed as off-axis angle) from (c) Hawaii and (d) Réunion: The unimodal Gaussian off-axis angular distribution is shown by a solid line. The Fisher distribution is shown by a dashed line. Note that the Rayleigh–Rician and the 1-D normal distributions are nearly identical in (b), and that the Gaussian off-axis angular and Fisher distributions are nearly identical in (c). Numerical values are given in Tables 5 and 6.

Table 5. Intensity palaeosecular-variation maximum-likelihood estimation and comparison for both Hawaii and Réunion. Estimation function denotes the distribution assumed in the maximum-likelihood estimation. F_μ, σ, and σ/F_μ denote the maximum-likelihood estimates of mean vectorial intensity, absolute vectorial dispersion, and relative vectorial dispersion, but only for a Rayleigh–Rician distribution (for the three-dimensional Gaussian). $E(F)$, $S(F)$, and S/E denote the expected intensity, the standard deviation of the intensity, and the relative standard deviation. $p_{KS}(F)$ denotes the Kolmogorov–Smirnov probability that the intensity data could have been drawn from the corresponding distribution and with the given estimated parameters. The conventional averages, denoted by overbars, are straightforward arithmetic averages and variances calculated from the data. See Fig. 16.

Estimation function	F_μ (μT)	σ (μT)	σ/F_μ	$E(F)$ (μT)	$S(F)$ (μT)	S/E	$P_{KS}(F)$
				Hawaii			
Rayleigh–Rician (23)	29.27	13.86	0.4737	35.77	12.36	0.3455	0.4529
1-D Normal	–	–	–	35.81	12.29	0.3432	0.2028
Log-Normal	–	–	–	35.93	13.45	0.3743	0.0079
Gamma	–	–	–	35.81	12.50	0.3491	0.1514
				$\bar{F}$	$\bar{\sigma}$	$\bar{\sigma}/\bar{F}$	
Conventional Averages	–	–	–	35.80	12.30	0.3434	–
				Réunion			
Rayleigh–Rician (23)	37.45	10.29	0.2749	40.30	9.90	0.2456	0.8815
1-D Normal	–	–	–	40.28	9.89	0.2456	0.8983
Log-Normal	–	–	–	40.51	12.19	0.3010	0.3629
Gamma	–	–	–	40.28	11.00	0.2731	0.4166
				$\bar{F}$	$\bar{\sigma}$	$\bar{\sigma}/\bar{F}$	
Conventional Averages	–	–	–	40.29	9.89	0.2456	–

Table 6. Directional palaeosecular-variation maximum-likelihood estimation comparison for both Hawaii and Réunion. Estimation function denotes the distribution assumed in the maximum-likelihood estimation. I_μ, D_μ, $(F_\mu/\sigma)^2$, κ denote the maximum-likelihood estimates of the mean vectorial inclination, declination, Fisher-like dispersion parameter (taken from the three-dimensional Gaussian distribution), and the actual Fisher dispersion parameter. $p_{KS}(\theta)$ denotes the Kolmogorov–Smirnov probability that the directional data could have been drawn from the corresponding distribution. The conventional averages, denoted by overbars, are straightforward arithmetic averages and dispersion parameters calculated from the data. See Fig. 16.

Estimation function	I_μ (○)	D_μ (○)	$(F_\mu/\sigma)^2$	κ	$P_{KS}(\theta)$
			Hawaii		
Gaussian off-axis angle (27)	29.10	2.42	21.79	–	0.0000
Fisher	28.60	2.48	–	21.00	0.0000
	$\bar{I}$	$\bar{D}$		$\bar{\kappa}$	
Conventional Averages	30.86	2.48	–	39.75	–
			Réunion		
Gaussian off-axis angle (27)	−39.02	−0.39	24.53	–	0.1528
Fisher	−39.06	−0.38	–	20.00	0.2654
	$\bar{I}$	$\bar{D}$		$\bar{\kappa}$	
Conventional Averages	−39.07	−0.35	–	23.69	–

sets probably represent a range of rock properties that could affect magnetic remanence.

7.2 1960 Kilauea flow

The data from the Kilauea flow consist of a mixture of data groups: intensities and directions, directions only, and intensities only. We model the data with a unimodal Gaussian distribution, for which the likelihood function is

$$L = \prod_{j=1}^{N_{FID}} p_{g_1}(F_j, I_j, D_j) \prod_{k=1}^{N_{ID}} p_{g_1}(I_k, D_k) \prod_{m=1}^{N_F} p_{g_1}(F_m). \qquad (56)$$

Results are summarized in Table 8 and shown in Fig. 17, where we compare the model probability density functions p and cumulative distributions P with those of the data themselves. The local vectorial variance is clearly not spherically-symmetrical; the directions show a smaller relative vectorial dispersion than do the intensities. Seeking substantiation of this observation, we conducted a number of other estimation experiments, systematically omitting various parts of the Kilauea data and then maximizing the relevant likelihood function. Using intensity (directional) data alone gives a relative vectorial dispersion σ/F_μ of 0.1886 (0.1431). Insofar as these dispersions are a measure of the relative reliability of individual palaeomagnetic estimates of vectorial components, we have quantitative support for vague claims made by other investigators that directional data are somehow more accurate than intensity data. Finally, in Table 8, we compare our palaeomagnetic estimates of the field for 1960 with the modern field model values (as others have done before us); the agreement is sufficiently good to give credence to the palaeomagnetic method.

7.3 Xitle flow

In Fig. 18 and in Table 8 we summarize results from our maximum-likelihood experiments for the Xitle flow data. They are consistent with those obtained for the 1960 Kilauea flow data: a fit to the intensity (directional) data alone gives a large (small) relative vectorial dispersion, an observation that bolsters the claim that directional data are more accurate than intensity data.

7.4 Alternative intensity and directional fits

As with the palaeosecular-variation data, for the purpose of comparison, we performed a number of different maximum-likelihood fits to the 1960 Kilauea and Xitle intensity data: using a Rayleigh–Rician distribution (from the 3-D Gaussian distributions), a 1-D normal distribution, a log-normal distribution, and a gamma distribution. Results are summarized in Table 9. Note that, amongst the various fits, there is much more agreement between the estimated parameters than there is in the analysis of palaeosecular-variation data. This is related to the fact that the relative vectorial dispersion

Table 7. Acquisition data set. Locality is that for the general area. Name denotes the particular site or flow name in the source papers. Lat and Long denote the present latitude and longitude of the site. N_F, N_I, N_D are, respectively, the number of intensity, inclination, and declination data. Date is that for the sampled flows. Author denotes the source paper.

Locality	Name	Lat °N	Long °E	N_F	N_I	N_D	Date	Author
					Hawaii, 1960 Kilauea			
Hawaii		19.5	204.5	2	0	0	1960	Abokodair (1977)
Hawaii	HA32	19.5	204.5	5	6	6	1960	Tanaka (1991)
Hawaii	B3200	19.5	204.5	0	11	11	1960	Hagstrum & Champion (1994)
Hawaii	HA32	19.5	204.5	3	0	0	1960	Tsunakawa & Shaw (1994)
Hawaii	HA3210	19.5	204.5	6	0	0	1960	Tanaka *et al.* (1995b)
Hawaii	H6001, H6002	19.5	204.5	70	78	78	1960	Hill & Shaw (2000)
Total Hawaii				86	95	95		
					Mexico, Xitle			
Mexico	Xitle	19.3	260.8	65	55	55	Holocene	Böhnel *et al.* (1997)

Table 8. 1960 Kilauea, Hawaiian and Xitle, Mexican data-acquisition maximum-likelihood estimation and modern field comparison. Data types denotes the kind of data used in the estimation, so, for example, F, I, D means that all available intensity, inclination, declination data were used; I, D means that only inclination and declination data were used, etc. F_μ, I_μ, D_μ, σ, and σ/F_μ denote the maximum-likelihood estimates of intensity, inclination, declination, absolute vectorial dispersion, and relative vectorial dispersion. $p_{KS}(F)$ ($p_{KS}(\theta)$) denotes the Kolmogorov–Smirnov probability that the intensity (off-axis angular) data could have been drawn from a three-dimensional Gaussian distribution with the given estimated parameters. Comparison values are also shown for an axial dipole and a modern global field model. See Figs 17 and 18.

Maximum likelihood data types	F_μ (μT)	I_μ ($\circ$)	D_μ ($\circ$)	σ (μT)	σ/F_μ	$P_{KS}(F)$	$P_{KS}(\theta)$
			Hawaii, 1960 Kilauea				
F, I, D	34.72	35.80	10.49	5.57	0.1605	0.0691	0.0000
I, D	–	35.81	10.46	–	0.1431	–	0.0000
F, I	34.40	36.04	–	5.89	0.1765	0.1432	–
F	33.91	–	–	6.65	0.1886	0.2185	–
I	–	35.91	–	–	0.1566	–	–
	F	I	D				
Axial Dipole	–	35.32	0.00				
Global Field Model Bloxham & Jackson (1992)	36.09	36.91	10.98				
			Mexico, Xitle				
F, I, D	71.25	30.16	1.87	10.89	0.1529	0.3395	0.0000
I, D	–	30.16	1.87	–	0.1176	–	0.0020
F, I	70.30	30.56	–	12.34	0.1756	0.4049	–
F	68.81	–	–	14.37	0.2089	0.7833	–
I	–	30.36	–	–	0.1373	–	–
	F	I	D				
Axial Dipole	–	35.01	0.00				

σ/F_μ of the acquisition data is small: for Kilauea (Xitle) it is 0.2003 (0.2089), compared to the dispersion for the Hawaiian (Réunion) Brunhes data, 0.4737 (0.2749). The reader will recall, from our discussion in Section 4, that the Rayleigh–Rician distribution is approximately normal for small relative vectorial dispersions, and in such circumstances near agreement in parameter estimation can be expected.

Similar observations pertain to fits to the Kilauea and Xitle directional acquisition data. In Table 10 we compare fits made using the directional distributions from the 3-D Gaussian with those made using a Fisher distribution. Once again, the agreement is very good, better than it was for the palaeosecular-variation data, because the vectorial dispersion σ/F_μ is relatively small. Recall that in Section 4 we showed that the Gaussian off-axis angular distribution is approximately a Fisher distribution for small relative vectorial dispersions.

8 CONCLUSIONS

The Gaussian distribution occupies a prominent position in statistical analysis. This is due chiefly to the central limit theorem, which, roughly speaking, asserts that the distribution of the sum of independent, identically-distributed random variables is approximately Gaussian. Whether or not it is possible to conceive of a set of palaeomagnetic vectors as resulting from such a set of random variables remains something of an open question. There is currently very little linkage between the magnetohydrodynamic theory of the Earth's core and the statistics of secular variation recorded in palaeomagnetic data collected at the Earth's surface, but attempts to correct this shortcoming are underway (Kono *et al.* 2000; Dormy *et al.* 2000; McMillan *et al.* 2001). On the other hand, the theory of palaeomagnetic acquisition is often developed along statistical lines (Néel 1955; Stacey & Banerjee 1974; Dunlop & Özdemir 1997), and in some such domains there might be some physical justification for using Gaussian statistics. Of course, practice is often different from theory, and data which might normally be expected to be Gaussian are not always delivered so cooperatively by nature. Nonetheless, since it follows from the central limit theorem, the Gaussian distribution is very appealing from a general, theoretical standpoint. In contrast to the Gaussian distribution, the Fisher distribution is much more specialized; it arises from first principles in the context of the Langevin theory of paramagnetism (Sears 1953; Chikazumi 1964; Joos 1986), but its broader application to geomagnetism is more difficult to justify. Furthermore, the Bingham distribution, so far as we can tell, was introduced simply because it is mathematically convenient; there is often almost no inherent justification for its use. Of course, neither the Fisher distribution nor the Bingham distribution are appropriate for handling intensity data. For these reasons, and because the Gaussian distribution is so widely applicable, we were motivated to develop the 3-D Gaussian and bi-Gaussian distributions for the palaeomagnetically-relevant spherical coordinates of intensity, inclination, and declination.

To be sure, more work remains to be done. In this paper we have concentrated on Gaussian distributions with isotropic variance, but we have noted, as have others before us, that palaeomagnetic phenomena often display anisotropic statistics. The reader might, therefore, be wondering why we didn't pursue a fully anisotropic theory here. We had two reasons for first developing the isotropic case. The first was purely practical: Although some of the key mathematical formulae, such as the density function for intensity (Rayleigh–Rician), eq. (23), and directions (off-axis angle), eqs (27) and (28), are of closed form and reasonably simple, the underlying mathematics needed for developing the isotropic theory is already rather messy and complicated, as we see in the appendices. Since most science advances incrementally, it is sensible to consider the simpler case first. Indeed, our own reconnaissance of the mathematics of the more general anisotropic case leads us to conclude that its full development would be a much more formidable task. And although Khokhlov *et al.* (2001) have considered the special case of the directional (inclination-declination) Gaussian distribution with

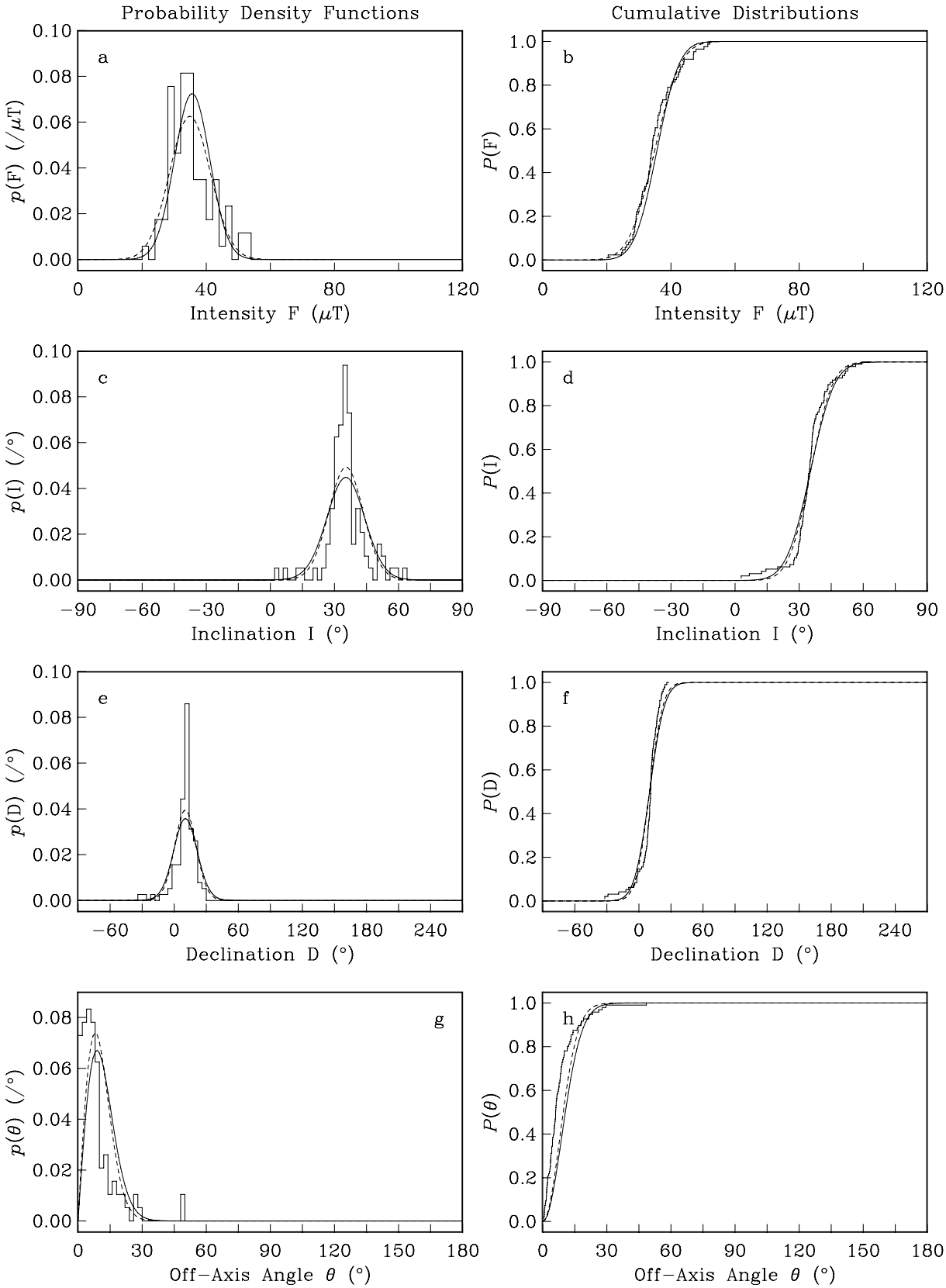

Figure 17. Maximum-likelihood fits for the 1960 Kilauea, Hawaiian data and using a unimodal, 3-D Gaussian distribution, eq. (10), and associated marginal density functions. The marginal probability density functions p and corresponding cumulative distributions P are shown for (a, b) intensity F, (c, d) inclination I, (e, f) declination D, and (g, h) off-axis angle θ. The fits shown by the solid lines correspond to a maximum-likelihood estimation using all the available data groups (F, I, D); the dashed lines in (a, b) correspond to an estimation using intensities only, whilst the dashed line in the other windows (c-h) corresponds to an estimation using directions only. Numerical values are given in Table 8.

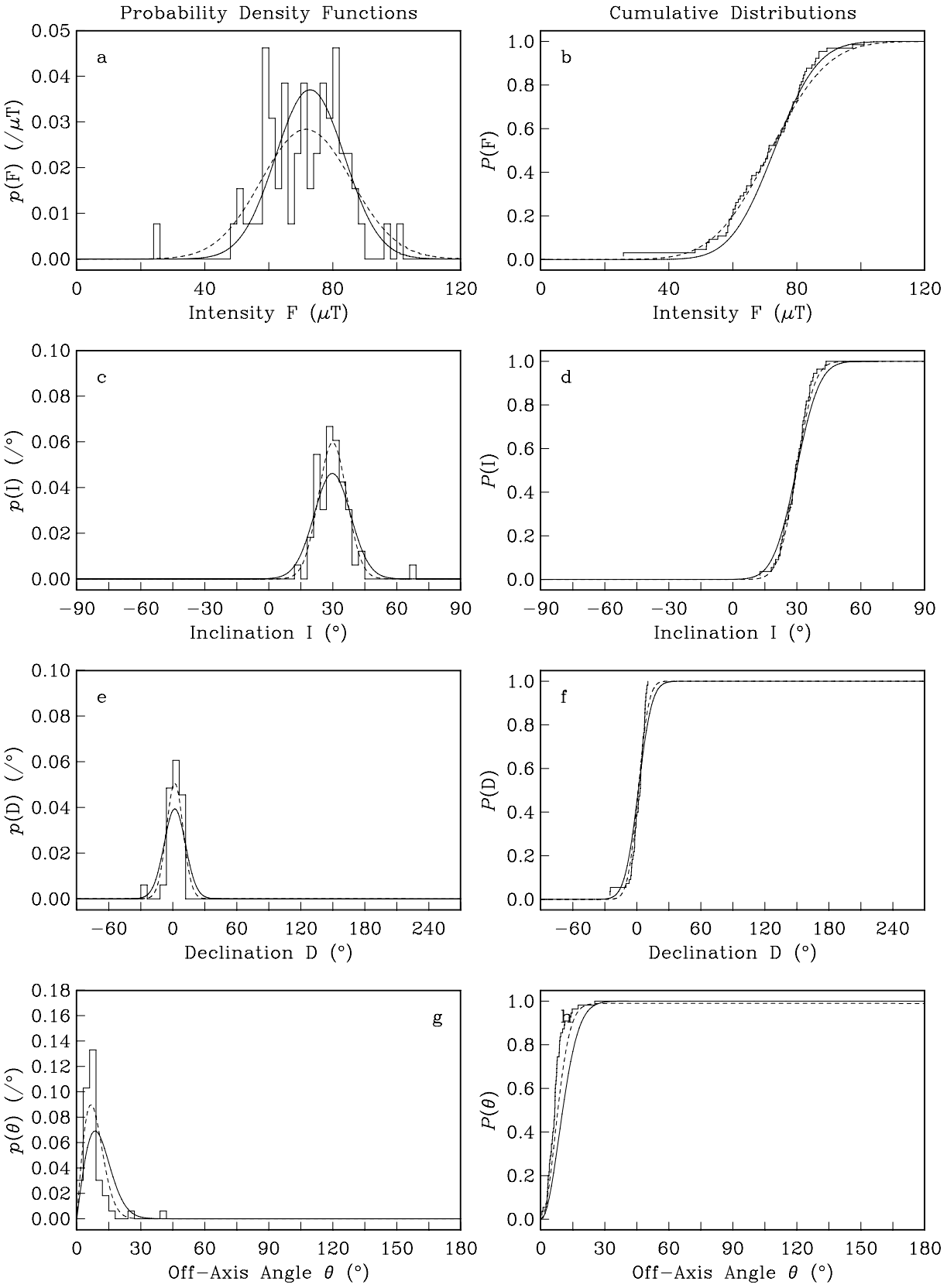

Figure 18. Same as Fig. 17 except for the Xitle, Mexican data.

Table 9. Intensity acquisition maximum-likelihood estimation and comparison for both 1960 Kilauea, Hawaii and Xitle, Mexico. Estimation function denotes the distribution assumed in the maximum-likelihood estimation. F_μ, σ, and σ/F_μ denote the maximum-likelihood estimates of mean vectorial intensity, absolute vectorial dispersion, and relative vectorial dispersion, but only for a Rayleigh–Rician distribution (for the three-dimensional Gaussian). $E(F)$, $S(F)$, and S/E denote the expected intensity, the standard deviation of the intensity, and the relative standard deviation. $p_{KS}(F)$ denotes the Kolmogorov–Smirnov probability that the intensity data could have been drawn from the corresponding distribution and with the given estimated parameters. The conventional averages, denoted by overbars, are straightforward arithmetic averages and variances calculated from the data.

Estimation function	F_μ (μT)	σ (μT)	σ/F_μ	$E(F)$ (μT)	$S(F)$ (μT)	S/E	$P_{KS}(F)$
				Hawaii, 1960 Kilauea			
Rayleigh–Rician (23)	33.91	6.65	0.2003	35.27	6.65	0.1886	0.2185
1-D Normal	–	–	–	35.27	6.66	0.1887	0.2128
Log-Normal	–	–	–	35.26	6.56	0.1861	0.6833
Gamma	–	–	–	35.26	6.52	0.1849	0.7688
				$\bar{F}$	$\bar{\sigma}$	$\bar{\sigma}/\bar{F}$	
Conventional Averages	–	–	–	35.26	6.66	0.1888	–
				Mexico, Xitle			
Rayleigh–Rician (23)	68.81	14.37	0.2089	71.81	14.05	0.1957	0.7833
1-D Normal	–	–	–	71.81	14.04	0.1956	0.7873
Log-Normal	–	–	–	71.93	15.53	0.2159	0.5274
Gamma	–	–	–	71.80	14.65	0.2041	0.0000
				$\bar{F}$	$\bar{\sigma}$	$\bar{\sigma}/\bar{F}$	
Conventional Averages	–	–	–	71.80	14.05	0.1956	–

anisotropic variance, the important dimension of intensity, together with all corresponding marginalizations, still needs to be developed for the 3-D (full-vectorial) anisotropic Gaussian distributions. The second reason we chose to develop the simpler isotropic case is more philosophical: sometimes it is necessary to model every detailed wiggle and wrinkle of a data set in order to extract its informational content, but at other times such completeness is excessive, especially if all the investigator seeks is a semi-quantitative conclusion, or if the data are biased or flawed in some ill-defined way. We say these things with conviction, since we have observed that the Fisher distribution, even though it generally lacks a firm theoretical justification for its application, has proved to be remarkably useful to the palaeomagnetic community. And this is true despite the fact that it actually rarely fits data well! The utility of the Fisher distribution has been as a benchmark for comparison. The Gaussian distributions with isotropic variances considered here, and, in particular, their intensity and directional marginalizations, can fulfill similar comparative roles.

Important practical issues are the nature and size of biases resulting from straightforward, arithmetic averaging of palaeomagnetic vectorial parts. Previous studies have highlighted the biased estimates of the direction of the mean palaeovector given by vectorial averages of unit vector (direction-only) data, and there have been many studies of biased estimates of the inclination of the mean palaeovector given by averages of inclination-only data. What we have demonstrated here is that there are additional biases lurking around the analysis of intensity data. In fact, using only intensity data, common arithmetic estimates of the mean and variance do not correspond to the intensity of the mean vector and the vectorial variance! Even more insidious is the fact that these biases do not diminish with increasingly numerous data. One way around these difficulties is to abandon the simplistic, arithmetic approach and adopt, instead, a maximum-likelihood approach for parameter estimation. This requires an *a priori* assumption about the mathematical form of the underlying probabilistic distribution, here we have considered Gaussian distributions, and it can require marginalizations of the underlying distribution, here we have provided those needed for mixtures of palaeomagnetic data types, be they intensities, inclinations, declinations, or some combination thereof. With maximum-likelihood estimation, insofar as the assumed

Table 10. Directional acquisition maximum-likelihood estimation and comparison for both 1960 Kilauea, Hawaii and Xitle, Mexico. Estimation function denotes the distribution assumed in the maximum-likelihood estimation. I_μ, D_μ, $(F_\mu/\sigma)^2$, κ denote the maximum-likelihood estimates of the mean vectorial inclination, declination, Fisher-like dispersion parameter (taken from the three-dimensional Gaussian distribution), and the actual Fisher dispersion parameter. $p_{KS}(\theta)$ denotes the Kolmogorov-Smirnov probability that the directional data could have been drawn from the corresponding distribution. The conventional averages, denoted by overbars, are straightforward arithmetic averages and dispersion parameters calculated from the data.

Estimation function	I_μ (○)	D_μ (○)	$(F_\mu/\sigma)^2$	κ	$P_{KS}(\theta)$
			Hawaii, 1960 Kilauea		
Gaussian off-axis angle (27)	35.81	10.46	48.83	–	0.0000
Fisher	35.76	10.11	–	46.20	0.0000
	$\bar{I}$	$\bar{D}$		$\bar{\kappa}$	
Conventional Averages	35.76	10.11	–	45.73	–
			Mexico, Xitle		
Gaussian off-axis angle (27)	30.16	1.87	72.31	–	0.0020
Fisher	30.32	1.78	–	71.99	0.0004
	$\bar{I}$	$\bar{D}$		$\bar{\kappa}$	
Conventional Averages	30.31	1.78	–	68.50	–

distribution is appropriate and capable of adequately fitting the data, then reasonable estimates of the vectorial mean and variance are possible, with the size of the biases decreasing with increasingly numerous data.

Palaeomagnetic data from Hawaii and Réunion can be used to discover some of the general properties of the long-term, global geomagnetic field. Although Hawaii and Réunion are on almost opposite latitudes, data from the two sites show significant differences in the mean vector. Furthermore, compared to idealized Gaussian distributions with isotropic variances, the data from Hawaii, in particular, display a large misfit. It has long been known that the directional data have an asymmetrical dispersion, usually characterized as a departure from Fisher statistics. Through our inclusion of intensity data in the analysis, the full 3-D palaeovector field at Hawaii can now be clearly described as anisotropic. On the other hand, we have shown that the data from Réunion are fitted much better by a spherically-symmetrical Gaussian distribution. Neither of these observations, namely differences in the inclination of the mean vector, and differences in the local variances, are consistent with the description of the mean field as being a simple geocentric axial dipole and with secular variation being statistically symmetrical with respect to reflection through the equatorial plane. Instead, the geomagnetic field is spatially asymmetrical in both its long-term average form and in terms of its behaviour.

With respect to palaeomagnetic acquisition, it is often asserted, usually verbally by researchers working in the subject, that palaeointensity data are less reliable than palaeodirectional data. This is a difficult suspicion to verify, if only because the issue has not been especially precisely stated: the two quantities are physically different, and indeed, are measured with different units! Straightforward comparison of their absolute dispersions is not particularly meaningful. Having said this, we acknowledge that the relative reliability of data is an important issue, and to address it, we have isolated the measure of relative vectorial dispersion, namely σ / F_{μ}, as a common parameter that can be obtained from maximum-likelihood fits to either intensity data or directional data. When separately applied to the 1960 Kilauea data from Hawaii and the Xitle data from Mexico, we find that the relative dispersion is larger, for both data sets, for intensity data than it is for directional data. We can, therefore, make some confirmation of the widely held suspicion that intensity data are less reliable than directional data.

ACKNOWLEDGMENTS

This work was supported by the US Geological Survey, and the National Science Foundation through grants #EAR95-26890, #EAR98-05164, and #EAR00-00944. We thank H. Böhnel, A. Chauvin, R. S. Coe, J. T. Hagstrum, E. Herrero-Bervera, M. J. Hill, M. Kono, C. Laj, E. A. Mankinen, G. McIntosh, H. Tanaka, and N. Teanby, for providing numerical data from their published papers; G. E. Backus, J. Forcada, J. S. Johnson, and D. G. McMillan for useful discussions; A. J. Crone, P. S. Earle, and D. M. Perkins for their comments on a draft manuscript; G. Hulot, A. Jackson, and P. L. McFadden for their formal reviews.

REFERENCES

Abokodair, A.A., 1977. The accuracy of the Thelliers' technique for the determination of paleointensities of the Earth's magnetic field, *PhD Thesis,* Univ. of California, Santa Cruz.

Abramowitz, M. & Stegun, I.A., 1965. *Handbook of Mathematical Functions,* Dover, New York.

Andriamirado, C.A.R., 1971. Recherches paléomagétiques sur Madagascar: Résultats et interprétations dans le cadre de la dislocation de la partie orientale du Gondwana, *PhD Thesis,* Univ. of Strasbourg, Strasbourg.

Bingham, C., 1964. Distributions on the sphere and on the projective plane, *PhD Thesis,* Yale University, New Haven.

Bingham, C., 1983. A series expansion for the angular Gaussian distribution, in, *Statistics on Spheres,* pp. 226–231, ed. Watson, G.S., John Wiley & Sons, New York.

Bloxham, J. & Jackson, A., 1992. Time-dependent mapping of the magnetic field at the core–mantle boundary, *J. geophys. Res.,* **97,** 19 537–19 563.

Bloxham, J., Gubbins, D. & Jackson, A., 1989. Geomagnetic secular variation, *Phil. Trans. R. Soc. Lond, Ser. A.,* **329,** 415–502.

Bogue, S.W., 2001. Geomagnetic field behavior before and after the Kauai reverse-normal polarity transition, *J. geophys. Res.,* **106,** 447–461.

Bogue, S.W. & Coe, R.S., 1984. Transitional paleointensities from Kauai, Hawaii, and geomagnetic reversal models, *J. geophys. Res.,* **89,** 10 341–10 354.

Böhnel, H., Morales, J., Caballero, C., Alva, L., McIntosh, G., Gonzalez, S. & Sherwood, G.J., 1997. Variation of rock magnetic parameters and paleointensities over a single Holocene lava flow, *J. Geomagn. Geoelectr.,* **49,** 523–542.

Brassart, J., Tric, E., Valet, J.P. & Herrero-Bervera, E., 1997. Absolute paleointensity between 60 and 400 ka from the Kohala Mountain (Hawaii), *Earth planet. Sci. Lett.,* **148,** 141–156.

Briden, J.C. & Ward, M.A., 1966. Analysis of magnetic inclination in borecores, *Pure appl. Geophys.,* **63,** 133–152.

Buchanan-Banks, J.M., 1993. Geologic map of the Hilo 7 1/2' quadrangle, Island of Hawaii, *USGS Map,* **I-2274,** 1–17.

Busse, F.H., 1983. Recent developments in the dynamo theory of planetary magnetism, *Ann. Rev. Earth planet. Sci.,* **11,** 241–268.

Butler, R.F., 1992. *Palaeomagnetism,* Blackwell Scientic Publications, Cambridge, MA.

Carlut, J. & Courtillot, V., 1998. How complex is the time-averaged geomagnetic field over the last 5 million years?, *Geophys. J. Int.,* **134,** 527–544.

Castro, J. & Brown, L., 1987. Shallow paleomagnetic directions from historic lava flows, Hawaii, *Geophys. Res. Lett.,* **14,** 1203–1206.

Chamalaun, F.H., 1968. Palaeomagnetism of Réunion Island and its bearing on secular variation, *J. geophys. Res.,* **73,** 4647–4659.

Champion, D.E. & Lockwood, J.P., 1998. Paleomagnetic data from basaltic lava flows of the northeastern rift zone of Mauna Loa volcano, Hawaii, *USGS Open-File Rep.,* **98-782,** 1–5.

Chauvin, A., Gillot, P.Y. & Bonhommet, N., 1991. Paleointensity of the Earth's magnetic field recorded by two late Quaternary volcanic sequences at the island of La Réunion (Indian Ocean), *J. geophys. Res.,* **96,** 1981–2006.

Chikazumi, S., 1964. *Physics of Magnetism,* John Wiley & Sons, New York.

Coe, R.S., Grommé, S. & Mankinen, E.A., 1978. Geomagnetic paleointensities from radiocarbon-dated lava flows on Hawaii and the question of the Pacific nondipole low, *J. geophys. Res.,* **83,** 1740–1756.

Coe, R.S., Grommé, S. & Mankinen, E.A., 1984. Geomagnetic paleointensities from excursion sequences in lavas on Oahu, Hawaii, *J. geophys. Res.,* **89,** 1059–1069.

Constable, C.G. & Johnson, C.L., 1999. Anisotropic paleosecular variation models: implications for geomagnetic field observables, *Phys. Earth planet. Inter.,* **115,** 35–51.

Constable, C.G. & Parker, R.L., 1988. Statistics of the geomagnetic secular variation for the past 5 m.y., *J. geophys. Res.,* **93,** 11 569–11 581.

Constable, C.G., Tauxe, L. & Parker, R.L., 1998. Analysis of 11 Myr of geomagnetic intensity variation, *J. geophys. Res.,* **103,** 17 735–17 748.

Courtillot, V. & Valet, J.P., 1995. Secular variation of the Earth's magnetic field: From jerks to reversals, *C. R. Acad. Sci., Ser. II,* **320,** 903–922.

Cox, A. & Doell, R.R., 1964. Long period variations of the geomagnetic field, *Seism. Soc. Am. Bull.,* **54,** 2243–2270.

Cox, A. & Gordon, R.G., 1984. Paleolatitudes determined from paleomagnetic data from vertical cores, *Rev. Geophys. Space Phys.,* **22,** 47–72.

Cramér, H., 1945. *Mathematical Methods of Statistics,* Princeton Univ. Press, Princeton.

Creer, K.M., 1983. Computer synthesis of geomagnetic palaeosecular variations, *Nature,* **304,** 695–699.
Creer, K.M., Irving, E. & Nairn, A.E.M., 1959. Palaeomagnetism of the Great Whin Sill, *Geophys. J. R. Astr. Soc.,* **2,** 306–323.
DiFranco, J.V. & Rubin, W.L., 1968. *Radar Detection,* Prentice-Hall, New Jersey.
Doell, R.R., 1969. Paleomagnetism of the Kau volcanic series, Hawaii, *J. geophys. Res.,* **74,** 4857–4868.
Doell, R.R., 1972a. Paleomagnetism of lava flows from Kauai, Hawaii, *J. geophys. Res.,* **77,** 862–876.
Doell, R.R., 1972b. Paleomagnetism of volcanic rocks from Niihau, Nihoa, and Necker Islands, Hawaii, *J. geophys. Res.,* **77,** 3725–3730.
Doell, R.R., 1972c. Paleosecular variation of the Honolulu volcanic series, Oahu, Hawaii, *J. geophys. Res.,* **77,** 2129–2137.
Doell, R.R. & Cox, A., 1963. The accuracy of the paleomagnetic method as evaluated from historic Hawaiian lava flows, *J. geophys. Res.,* **68,** 1997–2009.
Doell, R.R. & Cox, A., 1965. Paleomagnetism of Hawaiian lava flows, *J. geophys. Res.,* **70,** 3377–3405.
Doell, R.R. & Dalrymple, G.B., 1973. Potassium-argon ages and paleomagnetism of the Waianae and Koolau volcanic series, Oahu, Hawaii, *Bull. Geol. Soc. Am.,* **84,** 1217–1242.
Dormy, E., Valet, J.P. & Courtillot, V., 2000. Numerical models of the geodynamo and observational constraints, *Geochem. Geophys. Geosyst.,* **1**, 10.1029/2000GC000062.
Dunlop, D.J. & Özdemir, Ö., 1997. *Rock Magnetism: Fundamentals and Frontiers,* Cambridge Univ. Press, Cambridge, UK.
Fisher, R.A., 1953. Dispersion on a sphere, *Proc. R. Soc. Lond. Ser. A,* **217,** 295–305.
Fisher, N.I., Lewis, T. & Embleton, B.J.J., 1987. *Statistical Analysis of Spherical Data,* Cambridge Univ. Press, Cambridge, UK.
Gradshteyn, I.S. & Ryzhik, I.M., 1980. *Table of Integrals, Series, and Products,* Academic Press, San Diego.
Gröbner, W. & Hofreiter, N., 1965a. *Integraltafel, zweiter Teil, bestimmte Integrale,* Springer-Verlag, Wien.
Gröbner, W. & Hofreiter, N., 1965b. *Integraltafel, erster Teil, unbestimmte Integrale,* Springer-Verlag, Wien.
Gubbins, D. & Zhang, K., 1993. Symmetry properties of the dynamo equations for paleomagnetism and geomagnetism, *Phys. Earth planet. Inter.,* **75,** 225–241.
Hagstrum, J.T. & Champion, D.E., 1994. Paleomagnetic correlation of Late Quaternary lava flows in the lower east rift zone of Kilauea Volcano, Hawaii, *J. geophys. Res.,* **99,** 21 679–21 690.
Herrero-Bervera, E. & Coe, R.S., 1999. Transitional field behavior during the Gilbert-Gauss and Lower Mammoth reversals recorded in lavas from the Waianae Volcano, O'ahu, Hawaii, *J. geophys. Res.,* **104,** 29 157–29 173.
Herrero-Bervera, E. & Valet, J.P., 1999. Paleosecular variation during sequential geomagnetic reversals from Hawaii, *Earth planet. Sci. Lett.,* **171,** 139–148.
Herrero-Bervera, E., Margas-Viñuela, J. & Valet, J.P., 2000. Paleomagnetic study of the ages of lavas on the island of Lanai'i, Hawai'i, *J. Volcan. Geoth. Res.,* **104,** 21–31.
Hill, M.J. & Shaw, J., 2000. Magnetic field intensity study of the 1960 Kilauea lava flow, Hawaii, using the microwave palaeointensity technique, *Geophys. J. Int.,* **142,** 487–504.
Holcomb, R.T., 1980. Kilauea Voclano, Hawaii: Chronology and morphology of the surficial lava flows, *USGS Open-File Rep.,* **81-354,** 1–321.
Holt, J.W., Kirschvink, J.L. & Garnier, F., 1996. Geomagnetic field inclinations for the past 400 kyr from the 1-km core of the Hawaii Scientific Drilling Project, *J. geophys. Res.,* **101,** 11655–11663.
Hulot, G. & LeMouël, J.L., 1994. A statistical approach to the Earth's main magnetic field, *Phys. Earth planet. Inter.,* **82,** 167–183.
Johnson, C.L. & Constable, C.G., 1995. The time-averaged geomagnetic field as recorded by lava flows over the past 5 Myr, *Geophys. J. Int.,* **122,** 489–519.
Joos, G., 1986. *Theoretical Physics,* Dover, New York.
Jurado-Chichay, Z., Urrutia-Fucugauchi, J. & Rowland, S.K., 1996. A paleomagnetic study of the Pohue Bay flow and its associated coastal cones, Mauna Loa volcano, Hawaii: constraints on their origin and temporal relationships, *Phys. Earth planet. Inter.,* **97,** 269–277.
Kelly, P. & Gubbins, D., 1997. The geomagnetic field over the past 5 million years, *Geophys. J. Int.,* **128,** 315–330.
Khodair, A. & Coe, R.S., 1975. Determination of geomagnetic palaeointensities in vacuum, *Geophys. J. R. Astr. Soc.,* **42,** 107–115.
Khokhlov, A., Hulot, G. & Carlut, J., 2001. Towards a self-consistent approach to paleomagnetic field modelling, *Geophys. J. Int.,* **145,** 157–171.
Kittel, C. & Kroemer, H., 1980. *Thermal Physics,* W.H. Freeman, San Francisco.
Kono, M. & Tanaka, H., 1977. Influence of partial pressure of oxygen on thermoremanent magnetization of basalts, *Phys. Earth planet. Inter.,* **13,** 276–288.
Kono, M., 1980. Statistics of paleomagnetic inclination data, *J. geophys. Res.,* **85,** 3878–3882.
Kono, M., 1997. Paleosecular variation in field directions due to randomly varying Gauss coefficients, *J. Geomagn. Geoelectr.,* **49,** 615–631.
Kono, M., Sakuraba, A. & Ishida, M., 2000. Dynamo simulation and palaeosecular variation models, *Philos. Trans. R. Soc. Lond. Ser. A,* **358,** 1123–1139.
Laj, C. & Kissel, C., 1999. Geomagnetic field intensity at Hawaii for the last 420 kyr from the Hawaii Scientific Drilling Project core, Big Island, Hawaii, *J. geophys. Res.,* **104,** 15 317–15 338.
Laj, C., Guillou, H., Széréméta, N. & Coe, R., 1999. Geomagnetic paleosecular variation at Hawaii around 3 Ma from a sequence of 107 lava flows at Kaena Point (Oahu), *Earth planet. Sci. Lett.,* **170,** 365–376.
Laj, C., Széréméta, N., Kissel, C. & Guillou, H., 2000. Geomagnetic paleointensities at Hawaii between 3.9 and 2.1 Ma: preliminary results, *Earth planet. Sci. Lett.,* **179,** 191–204.
Laj, C., Kissel, C., Scao, V., Beer, J., Thomas, D.M., Guillou, H., Muscheler, R. & Wagner, G., 2002. Geomagnetic intensity and inclination variations at Hawaii for the past 98 kyr from core SOH-4 (Big Island): a new study and a comparison with existing contemporary data, *Phys. Earth planet. Inter.,* **129,** 205–243.
Landau, L.D. & Lifshitz, E.M., 1980. *Statistical Physics,* Pergamon Press, Oxford.
Love, J.J., 1998. Paleomagnetic volcanic data and geometric regularity of reversals and excursions, *J. geophys. Res.,* **103,** 12 435–12 452.
Mankinen, E.A. & Champion, D.E., 1993a. Broad trends in geomagnetic paleointensity on Hawaii during Holocene time, *J. geophys. Res.,* **98,** 7959–7976.
Mankinen, E.A. & Champion, D.E., 1993b. Latest Pleistocene and Holocene geomagnetic paleointensity on Hawaii, *Science,* **262,** 412–416.
Mardia, K.V., 1972. *Statistics of Directional Data,* Academic Press, London.
McDonough, R.N. & Whalen, A.D., 1995. *Detection of Signals in Noise,* Academic Press, San Diego.
McDougall, I. & Chamalaun, F.H., 1969. Isotopic dating and geomagnetic polarity studies on volcanic rocks from Mauritius, Indian Ocean, *Geol. Soc. Am. Bull.,* **80,** 1419–1442.
McDougall, I. & Watkins, N.D., 1973. Age and duration of the Réunion geomagnetic polarity event, *Earth planet. Sci. Lett.,* **19,** 443–452.
McElhinny, M.W. & McFadden, P.L., 1997. Palaeosecular variation over the past 5 Myr based on a new generalized database, *Geophys. J. Int.,* **131,** 240–252.
McElhinny, M.W., McFadden, P.L. & Merrill, R.T., 1996. The time-averaged paleomagnetic field 0-5 Ma, *J. geophys. Res.,* **101,** 25 007–25 027.
McFadden, P.L., 1980. Determination of the angle in a Fisher distribution which will be exceeded with a given probability, *Geophys. J. R. Astr. Soc.,* **60,** 391–396.
McFadden, P.L. & McElhinny, M.W., 1982. Variations in the geomagnetic dipole 2: Statistical analysis of VDMs for the past 5 million years, *J. Geomagn. Geoelectr.,* **34,** 163–189.
McFadden, P.L. & Merrill, R.T., 1995. History of Earth's magnetic field and possible connections to core–mantle boundary processes, *J. geophys. Res.,* **100,** 307–316.
McFadden, P.L. & Reid, A.B., 1982. Analysis of palaeomagnetic inclination data, *Geophys. J. R. Astr. Soc.,* **69,** 307–319.

McMillan, D.G., Constable, C.G., Parker, R.L. & Glatzmaier, G.A., 2001. A statistical appraisal of magnetic fields of geodynamo models, *Geochem. Geophys. Geosyst.,* **2**, 10.1029/2000GC000130.

Merrill, R.T. & McFadden, P.L., 1990. Paleomagnetism and the nature of the geodynamo, *Science,* **248,** 345–350.

Merrill, R.T., McElhinny, M.W. & Stevenson, D.J., 1979. Evidence for long-term asymmetries in the Earth's magnetic field and possible implications for dynamo theories, *Phys. Earth planet. Inter.,* **20,** 75–82.

Miller, K.S., 1975. *Multivariate Distributions,* Robert E. Krieger Publishing, Huntington.

Miller, K.S., Bernstein, R.I. & Blumenson, L.E., 1958. Generalized Rayleigh processes, *Quart. Appl. Math.,* **16,** 137–145.

Néel, L., 1955. Some theoretical aspects of rock magnetism, *Adv. Phys.,* **4,** 191–243.

Papoulis, A. & Pillai, S.U., 2002. *Probability, Random Variables, and Stochastic Processes,* McGraw-Hill, New York.

Press, W.H., Teukolsky, S.A., Vetterling, W.T. & Flannery, B.P., 1992. *Numerical Recipes,* Cambridge Univ. Press, Cambridge, UK.

Prévot, M. & Camps, P., 1993. Absence of preferred longitudinal sectors for poles from volcanic records of geomagnetic reversals, *Nature,* **366,** 53–57.

Proakis, J.G., 1995. *Digital Communications,* McGraw-Hill, New York.

Quidelleur, X. & Courtillot, V., 1996. On low degree spherical harmonic models of paleosecular variation, *Phys. Earth planet. Inter.,* **95,** 55–77.

Quidelleur, X., Valet, J.P., Courtillot, V. & Hulot, G., 1994. Long-term geometry of the geomagnetic field for the last 5 million years: An updated secular variation database from volcanic sequences, *Geophys. Res. Lett.,* **21,** 1639–1642.

Raïs, A., Laj, C., Surmont, J., Gillot, P.Y. & Guillou, H., 1996. Geomagnetic field intensity between 70 000 and 130 000 years B.P. from a volcanic sequence on La Réunion, Indian Ocean, *Earth planet. Sci. Lett.,* **140,** 173–189.

Riley, C.M., Diehl, J.F., Kirschvink, J.L. & Ripperdan, R.L., 1999. Paleomagnetic constraints on fault motion in the Hilina Fault System, south flank of Kilauea Volcano, Hawaii, *J. Volcan. Geoth. Res.,* **94,** 233–249.

Roberts, P.H., 1992. Dynamo theory, in *Chaotic Processes in the Geological Sciences,* pp. 237–280, ed. Yuen, D.A., Springer-Verlag, New York.

Roberts, P.H. & Soward, A.M., 1972. Magnetohydrodynamics of the Earth's core, *Ann. Rev. Fluid Dyn.,* **4,** 117–153.

Sears, F.W., 1953. *An Introduction to Thermodynamics, the Kinetic Theory of Gases, and Statistical Mechanics,* Addison-Wesley Publishing, Cambridge, MA.

Senanayake, W.E., McElhinny, M.W. & McFadden, P.L., 1982. Comparison between the Thelliers' and Shaw's palaeointensity methods using basalts less than 5 million years old, *J. Geomagn. Geoelectr.,* **34,** 141–161.

Slater, L.J., 1966. *Generalized Hypergeometric Functions,* Cambridge Univ. Press, Cambridge, UK.

Spanier, J. & Oldham, K.B., 1987. *An Atlas of Functions,* Hemisphere Publishing, Harper & Row, Washington.

Stacey, F.D. & Banerjee, S.K., 1974. *The Physical Principles of Rock Magnetism,* Elsevier, Amsterdam.

Stuart, A., Ord, K. & Arnold, S., 1999. *Kendall's Advanced Theory of Statistics, Volume 2A, Classical Inference and the Linear Model,* Arnold, London.

Tanaka, H., 1999. Circular asymmetry of the paleomagnetic directions observed at low latitude volcanic sites, *Earth Planets Space,* **51,** 1279–1286.

Tanaka, H. & Kono, M., 1991. Preliminary results and reliability of palaeointensity studies on historical and ^{14}C dated Hawaiian lavas, *J. Geomagn. Geoelectr.,* **43,** 375–388.

Tanaka, H., Kono, M. & Uchimura, H., 1995a. Some global features of palaeointensity in geological time, *Geophys. J. Int.,* **120**, 97–102.

Tanaka, H., Athanassopoulos, J.D.E., Dunn, J.R. & Fuller, M., 1995b. Paleointensity determinations with measurements at high temperature, *J. Geomagn. Geoelectr.,* **47**, 103–113.

Tauxe, L., 1998. *Paleomagnetic Principles and Practice,* Kluwer Academic Publishers, Dordrecht.

Tauxe, L. & Love, J.J., 2003. Paleointensity in HSDP2: results from submarine basaltic glass, **4,** 10.1029/2001GC000276.

Teanby, N., Laj, C., Gubbins, D. & Pringle, M.S., 2002. A detailed palaeointensity and inclination record from drill core SOH1 on Hawaii, *Phys. Earth planet. Inter.,* **131,** 101–140.

Tsunakawa, H., 1988. Geomagnetic secular variation during the Brunhes Epoch inferred from the paleomagnetism and the last 200 years geomagnetic field, *J. Geomagn. Geoelectr.,* **40,** 1365–1385.

Tsunakawa, H. & Shaw, J., 1994. The Shaw method of palaeointensity determinations and its application to recent volcanic rocks, *Geophys. J. Int.,* **118,** 781–787.

Ueno, N. & Kono, M., 1977. Determination of geomagnetic paleointensities from the historical lava flows of Hawaii, *Rock Magnetism Paleogeophys.,* **4,** 73–75.

Valet, J.P., Tric, E., Herrero-Bervera, E., Meynadier, L. & Lockwood, J.P., 1998. Absolute paleointensity from Hawaiian lavas younger than 35 ka, *Earth planet. Sci. Lett.,* **161,** 19–32.

Watkins, N.D., 1973. Brunhes epoch geomagnetic secular variation on Reunion Island, *J. geophys. Res.,* **78,** 7763–7768.

Watkins, N.D., Hajash, A. & Abranson, C.E., 1972. Geomagnetic secular variation during the Brunhes epoch in the Indian and Atlantic Ocean region, *Geophys. J. R. Astr. Soc.,* **28,** 1–25.

Watson, G.S. & Irving, E., 1957. Statistical methods in rock magnetism, *Month. Not. R. Astr. Soc. Geophys. Suppl.,* **7,** 289–300.

Watson, G.S., 1965. Equatorial distributions on a sphere, *Biometrika,* **52,** 193–201.

Wilson, R.L., 1970. Permanent aspects of the Earth's non-dipole magnetic field over the Upper Tertiary times, *Geophys. J. R. Astr. Soc.,* **19,** 417–437.

APPENDICES

Following are mathematical formulae for the various marginal probability density functions corresponding to the Gaussian and bi-Gaussian distributions, eqs (10) and (16), along with corresponding results (when applicable) for the Fisher and Bingham distributions, relevant for directional data, and the normal and Maxwell distributions, relevant for intensity data. For the 1-D marginal distributions of intensity, inclination, declination, and off-axis angle, we also present the cumulative distributions, the expected values, and the variances. The mathematical expressions that depend on the orientation of the distribution relative to a fixed coordinate system, namely those involving inclination and declination, are complicated. Fortunately, for many applications the most useful results are those for intensity, Appendix D, and off-axis angle, Appendix E, for which the mathematical expressions are relatively more simple, being expressed in terms of either special functions or infinite sums of special functions.

APPENDIX A: INCLINATION AND DECLINATION

A1 Marginal density function

For the Gaussian distribution, and for the case of palaeomagnetic measurements from fully oriented samples, but for which intensities are not available, the relevant directional probability density function for inclination and declination is obtained by integrating (10) over all intensities. Using 3.462.7 of Gradshteyn & Ryzhik (1980) the marginal density function for inclination and declination is

$$p_{g_1}\left(I, D \mid I_\mu, D_\mu, (\sigma/F_\mu)^2\right) = \int_0^\infty p_{g_1}(F, I, D)\, dF$$
$$= \frac{1}{4\pi}\cos I \exp\left[-\frac{1}{2}\left(\frac{F_\mu}{\sigma}\right)^2\right]\left\{\left[1+\left(\frac{F_\mu}{\sigma}\right)^2\rho^2\right]\exp\left[\frac{1}{2}\left(\frac{F_\mu}{\sigma}\right)^2\rho^2\right]\left[1+\operatorname{erf}\left[\frac{1}{\sqrt{2}}\left(\frac{F_\mu}{\sigma}\right)\rho\right]\right]+\left(\frac{2}{\pi}\right)^{\frac{1}{2}}\left(\frac{F_\mu}{\sigma}\right)\rho\right\}. \tag{A1}$$

The off-axis angle θ between a particular unit magnetic vector $\hat{\mathbf{x}}$ and the mean unit vector $\hat{\mathbf{x}}_\mu$ is defined so that

$$\rho = \hat{\mathbf{x}}\cdot\hat{\mathbf{x}}_\mu = \cos\theta = \cos I \cos I_\mu \cos(D - D_\mu) + \sin I \sin I_\mu. \tag{A2}$$

A result equivalent to (A1) has been given, in a somewhat cumbersome series form, by Bingham (1983); a related result, a generalization for anisotropic variance, was been found by Khokhlov *et al.* (2001). Note that with directional data alone the vectorial variance of the Gaussian distribution can only be determined in a relative sense, measured by $(\sigma/F_\mu)^2$. In the limiting case where the relative vectorial dispersion is substantially less than one, $\sigma/F_\mu \ll 1$, the Gaussian inclination-declination density function (A1) is approximately that for a Fisher distribution expressed in terms of inclination and declination,

$$p_f\left(I, D \mid I_\mu, D_\mu, (\sigma/F_\mu)^2\right) = \frac{1}{4\pi}\left(\frac{F_\mu}{\sigma}\right)^2\left\{\sinh\left[\left(\frac{F_\mu}{\sigma}\right)^2\right]\right\}^{-1}\cos I \exp\left[\left(\frac{F_\mu}{\sigma}\right)^2\rho\right]. \tag{A3}$$

In the opposite limiting case, where the relative vectorial dispersion is substantially greater than one, $\sigma/F_\mu \gg 1$, the Gaussian inclination-declination density function is approximately that for a spherically-uniform distribution of directions,

$$p_u(I, D) = \frac{1}{4\pi}\cos I. \tag{A4}$$

For the bi-Gaussian distribution, the directional probability density function for inclination and declination is obtained by integrating (16) over all intensities,

$$p_{g_2}\left(I, D \mid I_\mu, D_\mu, (\sigma/F_\mu)^2\right) = \int_0^\infty p_{g_2}(F, I, D)\, dF = \frac{1}{4\pi}\cos I\left[1+\left(\frac{F_\mu}{\sigma}\right)^2\rho^2\right]\exp\left[\frac{1}{2}\left(\frac{F_\mu}{\sigma}\right)^2(\rho^2-1)\right]. \tag{A5}$$

In the limiting case where the relative vectorial dispersion is substantially less than one, $\sigma/F_\mu \ll 1$, the bi-Gaussian inclination-declination density function (A5) is approximately that for a Bingham distribution expressed in terms of inclination and declination,

$$p_b\left(I, D \mid I_\mu, D_\mu, (\sigma/F_\mu)^2\right) = \frac{1}{4\pi}\left\{{}_1F_1\left[\begin{matrix}\frac{1}{2}\\ \frac{3}{2}\end{matrix}; \frac{1}{2}\left(\frac{F_\mu}{\sigma}\right)^2\right]\right\}^{-1}\cos I \exp\left[\frac{1}{2}\left(\frac{F_\mu}{\sigma}\right)^2\rho^2\right]. \tag{A6}$$

The hypergeometric function is a special case of

$${}_iF_j\left[\begin{matrix}a_1, \cdots, a_i\\ c_1, \cdots, c_j\end{matrix}; z\right] = \frac{\Gamma(c_1)\cdots\Gamma(c_j)}{\Gamma(a_1)\cdots\Gamma(a_i)}\sum_{k=0}^{\infty}\frac{\Gamma(a_1+k)\cdots\Gamma(a_i+k)}{\Gamma(c_1+k)\cdots\Gamma(c_j+k)}\frac{z^k}{k!}; \tag{A7}$$

for reference see Abramowitz & Stegun (1965) or Spanier & Oldham (1987); for a comprehensive mathematical discussion of hypergeometric functions see Slater (1966). In the opposite limiting case, where the relative vectorial dispersion is substantially greater than one, $\sigma/F_\mu \gg 1$, the bi-Gaussian inclination-declination density function is approximately that for a uniform distribution of directions, (A4).

APPENDIX B: INTENSITY AND DECLINATION

B1 Marginal density function

We know of no situation where palaeomagnetic data consist of intensity-declination pairs, that is where only inclinations are unavailable. However, for the sake of completeness, for the Gaussian distribution, we obtain the probability density functions for intensity and declination by integrating (10) over all inclinations. After expanding the exponential function in terms of an infinite series, making binomial expansions, using 3.621.5 of Gradshteyn & Ryzhik (1980), then summing, the marginal density function for intensity and declination is

$$p_{g_1}\left(F, D \mid F_\mu, I_\mu, D_\mu, \sigma^2\right) = \int_{-\frac{\pi}{2}}^{+\frac{\pi}{2}} p_{g_1}(F, I, D)\, dI = \frac{2}{(2\pi)^{\frac{3}{2}}\sigma}\left(\frac{F}{\sigma}\right)^2 \exp\left[-\frac{1}{2}\left(\frac{F}{\sigma}\right)^2 - \frac{1}{2}\left(\frac{F_\mu}{\sigma}\right)^2\right]$$
$$\times \left\{\sum_{m=0}^{\infty} \frac{\sin^{2m} I_\mu}{(2m+1)!}\left(\frac{FF_\mu}{\sigma^2}\right)^{2m} {}_2F_1\left[\begin{matrix}1, -m \\ \frac{1}{2}\end{matrix}; -\cot^2 I_\mu \cos^2(D - D_\mu)\right]\right.$$
$$\left. + \left(\frac{\pi}{2}\right)\frac{\cos I_\mu \cos(D - D_\mu)}{\sqrt{\cos^2 I_\mu \cos^2(D - D_\mu) + \sin^2 I_\mu}} I_1\left[\left(\frac{FF_\mu}{\sigma^2}\right)\sqrt{\cos^2 I_\mu \cos^2(D - D_\mu) + \sin^2 I_\mu}\right]\right\}. \tag{B1}$$

Hypergeometric functions with negative integer argument $(-m)$ are defined by extension of 15.4.1 of Abramowitz & Stegun (1965) or 60:4:10 of Spanier & Oldham (1987),

$${}_iF_j\left[\begin{matrix}a_1, \cdots, a_{i-1}, -m \\ c_1, \cdots, c_j\end{matrix}; z\right] = \frac{\Gamma(c_1)\cdots\Gamma(c_j)}{\Gamma(a_1)\cdots\Gamma(a_{i-1})}\sum_{k=0}^{m}\binom{m}{k}\frac{\Gamma(a_1 + k)\cdots\Gamma(a_{i-1} + k)}{\Gamma(c_1 + k)\cdots\Gamma(c_j + k)}(-z)^k. \tag{B2}$$

The modified Bessel function is I_1; for reference see Abramowitz & Stegun or Spanier & Oldham.

For the bi-Gaussian distribution, the probability density function for intensity and declination is obtained by integrating (16) over all inclinations,

$$p_{g_2}\left(F, D \mid F_\mu, I_\mu, D_\mu, \sigma^2\right) = \int_{-\frac{\pi}{2}}^{+\frac{\pi}{2}} p_{g_2}(F, I, D)\, dI$$
$$= \frac{2}{(2\pi)^{\frac{3}{2}}\sigma}\left(\frac{F}{\sigma}\right)^2 \exp\left[-\frac{1}{2}\left(\frac{F}{\sigma}\right)^2 - \frac{1}{2}\left(\frac{F_\mu}{\sigma}\right)^2\right]\sum_{m=0}^{\infty}\frac{\sin^{2m} I_\mu}{(2m+1)!}\left(\frac{FF_\mu}{\sigma^2}\right)^{2m} {}_2F_1\left[\begin{matrix}1, -m \\ \frac{1}{2}\end{matrix}; -\cot^2 I_\mu \cos^2(D - D_\mu)\right]. \tag{B3}$$

APPENDIX C: INTENSITY AND INCLINATION

C1 Marginal density function

For the Gaussian distribution, for intensity and inclination palaeomagnetic data taken from an azimuthally-unoriented borecore, such as that from the Hawaiian Scientific Drilling Project (HSDP), the appropriate marginal probability density function is obtained by integrating (10) over all declinations. After using 3.937.2 of Gradshteyn & Ryzhik (1980) the marginal density function for intensity and inclination is

$$p_{g_1}\left(F, I \mid F_\mu, I_\mu, \sigma^2\right) = \int_0^{2\pi} p_{g_1}(F, I, D)\, dD$$
$$= \frac{1}{\sqrt{2\pi}\sigma}\left(\frac{F}{\sigma}\right)^2 \cos I \exp\left[-\frac{1}{2}\left(\frac{F}{\sigma}\right)^2 - \frac{1}{2}\left(\frac{F_\mu}{\sigma}\right)^2\right]\exp\left[\left(\frac{FF_\mu}{\sigma^2}\right)\sin I \sin I_\mu\right] I_0\left[\left(\frac{FF_\mu}{\sigma^2}\right)\cos I \cos I_\mu\right], \tag{C1}$$

where I_0 is the modified Bessel function; for reference see Abramowitz & Stegun (1965) or Spanier & Oldham (1987).

For the bi-Gaussian distribution, the probability density function for intensity and inclination is obtained by integrating (16) over all declinations,

$$p_{g_2}\left(F, I \mid F_\mu, I_\mu, \sigma^2\right) = \int_0^{2\pi} p_{g_2}(F, I, D)\, dD$$
$$= \frac{1}{\sqrt{2\pi}\sigma}\left(\frac{F}{\sigma}\right)^2 \cos I \exp\left[-\frac{1}{2}\left(\frac{F}{\sigma}\right)^2 - \frac{1}{2}\left(\frac{F_\mu}{\sigma}\right)^2\right]\cosh\left[\left(\frac{FF_\mu}{\sigma^2}\right)\sin I \sin I_\mu\right] I_0\left[\left(\frac{FF_\mu}{\sigma^2}\right)\cos I \cos I_\mu\right], \tag{C2}$$

which is similar, but not identical, to the corresponding result for the Gaussian distribution, (C1).

APPENDIX D: INTENSITY

D1 Marginal density function

For the Gaussian distribution, the intensity probability density function is obtained by integrating (10) over all angles. From (B1), and after expanding the hypergeometric and Bessel functions in terms of power series, using 3.661.1 and 2 of Gradshteyn & Ryzhik (1980) to integrate term-by-term, then summing, the marginal density function for intensity is

$$p_{g_1}\left(F \mid F_\mu, \sigma^2\right) = \int_0^{2\pi}\int_{-\frac{\pi}{2}}^{+\frac{\pi}{2}} p_{g_1}(F, I, D)\, dI\, dD = \sigma^{-1}\left(\frac{2}{\pi}\right)^{\frac{1}{2}}\left(\frac{F}{F_\mu}\right)\exp\left[-\frac{1}{2}\left(\frac{F}{\sigma}\right)^2 - \frac{1}{2}\left(\frac{F_\mu}{\sigma}\right)^2\right]\sinh\left[\frac{FF_\mu}{\sigma^2}\right], \tag{D1}$$

which, as we discuss in Section 4, is a special case of the generalized Rayleigh–Rician density function. In Fig. 2(a) we show examples of the intensity density function, given different vectorial dispersions σ. In the limiting case where the vectorial dispersion is substantially less than

the intensity of the mean vector, $\sigma \ll F_\mu$, the Gaussian intensity probability density function (D1) is approximately that for a 1-D normal distribution,

$$p_n\left(F \mid F_\mu, \sigma^2\right) = \frac{1}{\sqrt{2\pi}\sigma} \exp\left[-\frac{1}{2}\left(\frac{F - F_\mu}{\sigma}\right)^2\right]. \tag{D2}$$

In the opposite limiting case, where the vectorial dispersion is substantially greater than the intensity of the mean vector, $\sigma \gg F_\mu$, the Gaussian intensity probability density function is approximately that for a Maxwell distribution,

$$p_m\left(F \mid \sigma^2\right) = \sigma^{-1}\left(\frac{2}{\pi}\right)^{\frac{1}{2}}\left(\frac{F}{\sigma}\right)^2 \exp\left[-\frac{1}{2}\left(\frac{F}{\sigma}\right)^2\right]. \tag{D3}$$

For more discussion of these limiting properties, see Section 4 and Fig. 6.

For the bi-Gaussian distribution, the intensity probability density function, corresponding to (16), is identical to that for the Gaussian distribution,

$$p_{g_2}\left(F \mid F_\mu, \sigma^2\right) = p_{g_1}\left(F \mid F_\mu, \sigma^2\right). \tag{D4}$$

Obviously, the limiting forms of the intensity density function for the bi-Gaussian distribution are identical to those of the Gaussian distribution as well.

D2 Relative intensity

For the case where intensity data are only relative, which is usually the case for palaeomagnetic data coming from sedimentary deposits, then (F, F_μ, σ) are arbitrary to within a multiplicative constant. The probability density function is obtained by the transformation

$$p_g\left(F, I, D \mid F_\mu, I_\mu, D_\mu, \sigma^2\right) \rightarrow p_g\left(aF, I, D \mid aF_\mu, I_\mu, D_\mu, a^2\sigma^2\right), \tag{D5}$$

or more succinctly,

$$p_g\left(\mathbf{x} \mid \mathbf{x}_\mu, \sigma^2\right) \rightarrow p_g\left(a\mathbf{x} \mid a\mathbf{x}_\mu, a^2\sigma^2\right), \tag{D6}$$

where a is an arbitrary constant. Similarly, the differential volume is obtained by

$$dFdIdD \rightarrow adFdIdD. \tag{D7}$$

In any case, the total probability remains unchanged under these transformations,

$$\int_0^{2\pi}\int_{-\frac{\pi}{2}}^{\frac{\pi}{2}}\int_0^{\infty} p_g(\mathbf{x})\, dFdIdD = \int_0^{2\pi}\int_{-\frac{\pi}{2}}^{\frac{\pi}{2}}\int_0^{\infty} p_g\left(a\mathbf{x} \mid a\mathbf{x}_\mu, a^2\sigma^2\right) adFdIdD = 1. \tag{D8}$$

This is not to say, however, that the mean intensity F_μ and the variance σ^2 are dependent quantities; in fact, the relative variance $(\sigma/F_\mu)^2$ is identical for either of the cases of relative or absolute intensity data.

D3 Cumulative distribution

For the Gaussian intensity probability density function (D1), the corresponding cumulative distribution gives the probability that an intensity lies on the interval $[0, F]$. After expanding the hyperbolic-sine function in terms of a power series, using 313.1, 2, and 3c of Gröbner & Hofreiter (1965b), then summing, the intensity cumulative distribution is

$$\begin{aligned} P_{g_1}\left(F \mid F_\mu, \sigma^2\right) &= \int_0^F p_{g_1}\left(F'\right)\, dF' \\ &= \frac{1}{2}\left\{\operatorname{erf}\left[\frac{F - F_\mu}{\sqrt{2}\sigma}\right] + \operatorname{erf}\left[\frac{F + F_\mu}{\sqrt{2}\sigma}\right]\right\} - \frac{1}{\sqrt{2\pi}}\frac{\sigma}{F_\mu}\left\{\exp\left[-\frac{1}{2}\left(\frac{F - F_\mu}{\sigma}\right)^2\right] - \exp\left[-\frac{1}{2}\left(\frac{F + F_\mu}{\sigma}\right)^2\right]\right\}. \end{aligned} \tag{D9}$$

As expected, since $\operatorname{erf}(\infty) = 1$,

$$P_{g_1}\left(\infty \mid F_\mu, \sigma^2\right) = 1. \tag{D10}$$

In Fig. 2(b) we show examples of the intensity cumulative distribution, given different vectorial dispersions σ. In the limiting case where the vectorial dispersion is substantially less than the intensity of the mean vector, $\sigma \ll F_\mu$, the Gaussian intensity cumulative distribution function (D9) is approximately that for a 1-D normal distribution. From (D2) and using 8.250.1 of Gradshteyn & Ryzhik (1980) we have

$$P_n\left(F \mid F_\mu, \sigma^2\right) = \int_{-\infty}^F p_n(F')\, dF' = \frac{1}{2} + \frac{1}{2}\operatorname{erf}\left[\frac{F - F_\mu}{\sqrt{2}\sigma}\right]. \tag{D11}$$

In the opposite limiting case, where the vectorial dispersion is substantially greater than the intensity of the mean vector, $\sigma \gg F_\mu$, the Gaussian intensity cumulative distribution function is approximately that for a Maxwell distribution. From (D3), and after integrating by parts and using 8.250.1 of Gradshteyn & Ryzhik, we have

$$P_m(F \mid \sigma^2) = \int_0^F p_m(F')\, dF' = \operatorname{erf}\left[\frac{1}{\sqrt{2}}\left(\frac{F}{\sigma}\right)\right] - \left(\frac{2}{\pi}\right)^{\frac{1}{2}}\left(\frac{F}{\sigma}\right)\exp\left[-\frac{1}{2}\left(\frac{F}{\sigma}\right)^2\right]. \tag{D12}$$

For the bi-Gaussian distribution, the cumulative intensity distribution, corresponding to (16), is identical to that for the Gaussian distribution,

$$P_{g_2}\left(F \mid F_\mu, \sigma^2\right) = P_{g_1}\left(F \mid F_\mu, \sigma^2\right). \tag{D13}$$

D4 Expected value

From the Gaussian intensity density function (D1), and after expanding the hyperbolic-sine function in terms of a power series, using 3.461.3 of Gradshteyn & Ryzhik (1980), then summing, the expected (average) intensity is

$$E_{g_1}\left(F \mid F_\mu, \sigma^2\right) = \int_0^\infty p_{g_1}(F)\, F dF = \sigma\left\{\left(\frac{2}{\pi}\right)^{\frac{1}{2}}\exp\left[-\frac{1}{2}\left(\frac{F_\mu}{\sigma}\right)^2\right] + \left(\frac{\sigma}{F_\mu} + \frac{F_\mu}{\sigma}\right)\operatorname{erf}\left[\frac{1}{\sqrt{2}}\left(\frac{F_\mu}{\sigma}\right)\right]\right\}. \tag{D14}$$

This average intensity should not be confused with F_μ, the intensity of the mean vector. In fact, the difference between the two quantities is one of the biases discussed in Section 5. In Fig. 9(a) we show examples of the intensity bias,

$$\delta F_{g_1} = E_{g_1}(F) - F_\mu, \tag{D15}$$

as a function of the vectorial dispersion σ, given different mean vectorial intensities F_μ. In the limiting case where the vectorial dispersion is substantially less than the intensity of the mean vector, $\sigma \ll F_\mu$, the Gaussian expected intensity (D14) is approximately that for a 1-D normal distribution. From (D2) and using 3.462.6 of Gradshteyn & Ryzhik we have the well known result

$$E_n(F \mid F_\mu) = \int_{-\infty}^\infty p_n(F)\, F dF = F_\mu. \tag{D16}$$

In the opposite limiting case, where the vectorial dispersion is substantially greater than the intensity of the mean vector, $\sigma \gg F_\mu$, the Gaussian expected intensity is approximately that for a Maxwell distribution. From (D3) and using 3.461.3 of Gradshteyn & Ryzhik we have

$$E_m(F \mid \sigma^2) = \int_0^\infty p_m(F) F\, dF = 2\left(\frac{2}{\pi}\right)^{\frac{1}{2}}\sigma; \tag{D17}$$

for reference see, for example, Papoulis & Pillai (2002).

For the bi-Gaussian distribution, the expected intensity, corresponding to (16), is identical to that for the Gaussian distribution,

$$E_{g_2}\left(F \mid F_\mu, \sigma^2\right) = E_{g_1}\left(F \mid F_\mu, \sigma^2\right). \tag{D18}$$

D5 Variance

From the Gaussian intensity density function (D1), and after expanding the hyperbolic-sine function in terms of a power series, using 3.461.2 of Gradshteyn & Ryzhik (1980), then summing, the expected value for the square of the intensity is the surprisingly compact expression

$$E_{g_1}\left(F^2 \mid F_\mu, \sigma^2\right) = \int_0^\infty p_{g_1}(F)\, F^2 dF = F_\mu^2 + 3\sigma^2. \tag{D19}$$

Of course, with this result the variance of the intensity about its expected value is just

$$V_{g_1}\left(F \mid F_\mu, \sigma^2\right) = E_{g_1}(F^2) - \left[E_{g_1}(F)\right]^2, \tag{D20}$$

where the last term comes from (D14). The variance of the intensity should not be confused with vectorial variance about the mean vector. In Fig. 9(b) we show examples of the standard deviation of the intensity,

$$S_{g_1}\left(F \mid F_\mu, \sigma^2\right) = \left[V_{g_1}(F)\right]^{\frac{1}{2}}, \tag{D21}$$

as a function of the vectorial dispersion σ, given different mean vectorial intensities F_μ. In the limiting case where the vectorial dispersion is substantially less than the intensity of the mean vector, $\sigma \ll F_\mu$, the variance of the intensity (D19) is approximately that for a 1-D normal distribution. From (D2) and using 3.462.6 and 8 of Gradshteyn & Ryzhik we have the well known result

$$V_n(F \mid \sigma^2) = \int_{-\infty}^\infty p_n(F)(F - F_\mu)^2\, dF = \sigma^2. \tag{D22}$$

In the opposite limiting case, where the vectorial dispersion is substantially greater than the intensity of the mean vector, $\sigma \gg F_\mu$, the variance of the intensity is approximately that for a Maxwell distribution. From (D3) and (D17), and using 3.461.2 of Gradshteyn & Ryzhik, we have

$$V_m(F \mid \sigma^2) = \int_0^\infty p_m(F)\, F^2 dF - \left[E_m\left(F \mid \sigma^2\right)\right]^2 = \sigma^2 \left\{3 - \frac{8}{\pi}\right\}; \tag{D23}$$

for reference see, for example, Papoulis & Pillai (2002).

For the bi-Gaussian distribution, the variance of intensity, corresponding to (16), is identical to that for the Gaussian distribution,

$$V_{g_2}\left(F \mid F_\mu, \sigma^2\right) = V_{g_1}\left(F \mid F_\mu, \sigma^2\right). \tag{D24}$$

APPENDIX E: OFF-AXIS ANGLE

E1 Marginal Density Function

For the Gaussian distribution, the probability density function for the off-axis angle θ can be obtained from (A1). After specializing to $I_\mu = \pi/2$, making a transformation from inclination to co-inclination (off-axis angle), $\theta = \pi/2 - I$, then integrating over all declinations, which gives a factor of 2π, we have

$$p_{g_1}\left(\theta \mid (\sigma/F_\mu)^2\right) = \frac{1}{2}\sin\theta \exp\left[-\frac{1}{2}\left(\frac{F_\mu}{\sigma}\right)^2\right]$$
$$\times \left\{\left[1 + \left(\frac{F_\mu}{\sigma}\right)^2 \cos^2\theta\right] \exp\left[\frac{1}{2}\left(\frac{F_\mu}{\sigma}\right)^2 \cos^2\theta\right]\left[1 + \operatorname{erf}\left[\frac{1}{\sqrt{2}}\left(\frac{F_\mu}{\sigma}\right)\cos\theta\right]\right] + \left(\frac{2}{\pi}\right)^{\frac{1}{2}}\left(\frac{F_\mu}{\sigma}\right)\cos\theta\right\}. \tag{E1}$$

Alternatively, this equation can be obtained from (F1) with $I_\mu = \pi/2$, for which the hypergeometric functions equal unity. A general discussion of the product of exponential and error functions, such as those in (E1), can be found in Chapter 41 of Spanier & Oldham (1987). In Fig. 2(g) we show examples of the off-axis angular density function for the Gaussian distribution, given different relative vectorial dispersions σ/F_μ. In the limiting case where the relative vectorial dispersion is substantially less than one, $\sigma/F_\mu \ll 1$, the Gaussian off-axis angular density function (E1) is approximately that for a Fisher distribution,

$$p_f\left(\theta \mid (\sigma/F_\mu)^2\right) = \frac{1}{2}\left(\frac{F_\mu}{\sigma}\right)^2 \left\{\sinh\left[\left(\frac{F_\mu}{\sigma}\right)^2\right]\right\}^{-1} \sin\theta \exp\left[\left(\frac{F_\mu}{\sigma}\right)^2 \cos\theta\right]. \tag{E2}$$

It is worth noting that for this limiting case, the Fisher dispersion parameter,

$$\kappa = \left(\frac{F_\mu}{\sigma}\right)^2, \tag{E3}$$

is simply related to the relative vectorial variance of our Gaussian distribution. In the opposite limiting case, where the relative vectorial dispersion is substantially greater than one, $\sigma/F_\mu \gg 1$, the off-axis angular density function is approximately that for a spherically-uniform distribution of directions,

$$p_u(\theta) = \frac{1}{2}\sin\theta. \tag{E4}$$

For more discussion of these limiting properties, see Section 4 and Fig. 7.

For the bi-Gaussian distribution, the off-axis angular probability density function is obtained from (A5),

$$p_{g_2}\left(\theta \mid (\sigma/F_\mu)^2\right) = \frac{1}{2}\sin\theta \exp\left[-\frac{1}{2}\left(\frac{F_\mu}{\sigma}\right)^2 \sin^2\theta\right]\left[1 + \left(\frac{F_\mu}{\sigma}\right)^2 \cos^2\theta\right]. \tag{E5}$$

In Fig. 4(g) we show examples of the off-axis angular density function for the bi-Gaussian distribution, given different relative vectorial dispersions σ/F_μ. In the limiting case where the relative vectorial dispersion is substantially less than one, $\sigma/F_\mu \ll 1$, then the bi-Gaussian off-axis angular density function (E5) is approximately that for a Bingham distribution,

$$p_b\left(\theta \mid (\sigma/F_\mu)^2\right) = \frac{1}{2}\left\{{}_1F_1\left[\tfrac{1}{2}; \tfrac{3}{2}; \frac{1}{2}\left(\frac{F_\mu}{\sigma}\right)^2\right]\right\}^{-1} \sin\theta \exp\left[\frac{1}{2}\left(\frac{F_\mu}{\sigma}\right)^2 \cos^2\theta\right], \tag{E6}$$

where the hypergeometric function is given by (A7). It is worth noting that for this limiting case, the Bingham dispersion parameter,

$$\kappa = \frac{1}{2}\left(\frac{F_\mu}{\sigma}\right)^2, \tag{E7}$$

is simply related to the relative vectorial variance of our bi-Gaussian distribution. In the opposite limiting case, where the relative vectorial dispersion is substantially greater than one, $\sigma/F_\mu \gg 1$, the bi-Gaussian off-axis angular density function is approximately that for a spherically-uniform distribution of directions, (E4). See Section 4 and Fig. 8.

E2 Cumulative distribution

For the Gaussian off-axis angular probability density function (E1), the corresponding cumulative distribution gives the probability that the off-axis angle lies on the interval $[0, \theta]$. After expanding the exponential and exponential-error functions in terms of power series, integrating term-by-term, then summing, the off-axis cumulative distribution is

$$P_{g_1}\left(\theta \,|\, (\sigma/F_\mu)^2\right) = \int_0^\theta p_{g_1}(\theta')\, d\theta' = \frac{1}{2}\left[1 + \operatorname{erf}\left[\frac{1}{\sqrt{2}}\left(\frac{F_\mu}{\sigma}\right)\right] - \cos\theta \exp\left[-\frac{1}{2}\left(\frac{F_\mu}{\sigma}\right)^2 \sin^2\theta\right]\left\{1 + \operatorname{erf}\left[\frac{1}{\sqrt{2}}\left(\frac{F_\mu}{\sigma}\right)\cos\theta\right]\right\}\right]. \tag{E8}$$

As expected,

$$P_{g_1}\left(\pi \,|\, (\sigma/F_\mu)^2\right) = 1. \tag{E9}$$

In Fig. 2(h) we show examples of the Gaussian off-axis cumulative distribution, given different relative vectorial dispersions σ/F_μ. In the limiting case where the relative vectorial dispersion is substantially less than one, $\sigma/F_\mu \ll 1$, the Gaussian off-axis cumulative distribution (E8) is approximately that for a Fisher distribution. From (E2) we have, almost trivially,

$$P_f\left(\theta \,|\, (\sigma/F_\mu)^2\right) = \int_0^\theta p_f\left(\theta'\right) d\theta' = \frac{1}{2}\left\{\sinh\left[\left(\frac{F_\mu}{\sigma}\right)^2\right]\right\}^{-1}\left\{\exp\left[\left(\frac{F_\mu}{\sigma}\right)^2\right] - \exp\left[\left(\frac{F_\mu}{\sigma}\right)^2 \cos\theta\right]\right\}. \tag{E10}$$

In the opposite limiting case, where the relative vectorial dispersion is substantially greater than one, $\sigma/F_\mu \gg 1$, the Gaussian off-axis cumulative distribution is approximately that for a spherically-uniform distribution of directions. From (E4) we have

$$P_u(\theta) = \int_0^\theta p_u\left(\theta'\right) d\theta' = \frac{1}{2} - \frac{1}{2}\cos\theta. \tag{E11}$$

For the bi-Gaussian off-axis angular probability density function (E5), the corresponding cumulative distribution is just

$$P_{g_2}\left(\theta \,|\, (\sigma/F_\mu)^2\right) = \int_0^\theta p_{g_2}\left(\theta'\right) d\theta' = \frac{1}{2} - \frac{1}{2}\cos\theta \exp\left[-\frac{1}{2}\left(\frac{F_\mu}{\sigma}\right)^2 \sin^2\theta\right]. \tag{E12}$$

In Fig. 4(h) we show examples of the bi-Gaussian off-axis cumulative distribution, given different relative vectorial dispersions σ/F_μ. In the limiting case where the relative vectorial dispersion is substantially less than one, $\sigma/F_\mu \ll 1$, the bi-Gaussian off-axis angular cumulative distribution (E12) is approximately that for a Bingham distribution. From (E6) we have

$$P_b\left(\theta \,|\, (\sigma/F_\mu)^2\right) = \int_0^\theta p_b\left(\theta'\right) d\theta' = \frac{1}{\sqrt{2}}\left(\frac{\sigma}{F_\mu}\right)\left\{{}_1F_1\left[\begin{matrix}\frac{1}{2}\\ \frac{3}{2}\end{matrix}; \frac{1}{2}\left(\frac{F_\mu}{\sigma}\right)^2\right]\right\}^{-1}$$
$$\times\left\{\exp\left[\frac{1}{2}\left(\frac{F_\mu}{\sigma}\right)^2\right]\operatorname{daw}\left[\frac{1}{\sqrt{2}}\left(\frac{F_\mu}{\sigma}\right)\right] - \exp\left[\frac{1}{2}\left(\frac{F_\mu}{\sigma}\right)^2 \cos^2\theta\right]\operatorname{daw}\left[\frac{1}{\sqrt{2}}\left(\frac{F_\mu}{\sigma}\right)\cos\theta\right]\right\}. \tag{E13}$$

Dawson's integral is given by

$$\operatorname{daw}(t) = \int_0^t \exp(s^2 - t^2)\, ds = t\sum_{j=0}^{\infty}\frac{(-2t^2)^j}{(2j+1)!!}; \tag{E14}$$

for reference see Abramowitz & Stegun (1965) or Spanier & Oldham (1987). In the opposite limiting case, where the relative vectorial dispersion is substantially greater than one, $\sigma/F_\mu \gg 1$, the bi-Gaussian off-axis cumulative distribution is approximately that for a spherically-uniform distribution of directions, (E11).

E3 Expected value

With the Gaussian off-axis angular density function (E1), and after expanding the exponential and exponential-error functions in terms of power series, using 2.512.2 and 3 of Gradshteyn & Ryzhik (1980) to integrate term-by-term, then summing, the expected off-axis angle is

$$E_{g_1}\left(\theta \,|\, (\sigma/F_\mu)^2\right) = \int_0^\pi p_{g_1}(\theta)\,\theta d\theta = \frac{\pi}{2}\left\{1 - \operatorname{erf}\left[\frac{1}{\sqrt{2}}\left(\frac{F_\mu}{\sigma}\right)\right]\right\} + \left(\frac{\pi}{2}\right)^{\frac{1}{2}}\left(\frac{\sigma}{F_\mu}\right)\left\{1 - \exp\left[-\frac{1}{2}\left(\frac{F_\mu}{\sigma}\right)^2\right]\right\}. \tag{E15}$$

In Fig. 9(g) we show examples of the expected off-axis angle for a Gaussian distribution as a function of relative vectorial dispersion σ/F_μ. In the limiting case where the relative vectorial dispersion is substantially less than one, $\sigma/F_\mu \ll 1$, the Gaussian expected off-axis angle (E15) is approximately that for a Fisher distribution. From (E2) the expected off-axis angle is

$$E_f\left(\theta \,|\, (\sigma/F_\mu)^2\right) = \int_0^\pi p_f(\theta)\,\theta d\theta = \frac{\pi}{2}\left\{\sinh\left[\left(\frac{F_\mu}{\sigma}\right)^2\right]\right\}^{-1}\left\{I_0\left[\left(\frac{F_\mu}{\sigma}\right)^2\right] - \exp\left[-\left(\frac{F_\mu}{\sigma}\right)^2\right]\right\}, \tag{E16}$$

where I_0 is the modified Bessel function; for reference see Abramowitz & Stegun (1965) or Spanier & Oldham (1987). In the opposite limiting case where the relative vectorial dispersion is substantially greater than one, $\sigma/F_\mu \gg 1$, the expected off-axis angle is approximately that for a spherically-uniform distribution of directions. From (E4) we have

$$E_u(\theta) = \int_0^\pi p_u(\theta)\,\theta\,d\theta = \frac{\pi}{2}, \tag{E17}$$

which can be easily checked.

For the bi-Gaussian off-axis angular density function (E5), the expected off-axis angle is just

$$E_{g_2}(\theta) = \int_0^\pi p_{g_2}(\theta)\,\theta\,d\theta = \frac{\pi}{2}, \tag{E18}$$

which can be deduced by consideration of symmetry. The expected off-axis angle for the Bingham distribution is identical,

$$E_b(\theta) = \int_0^\pi p_b(\theta)\,\theta\,d\theta = \frac{\pi}{2}. \tag{E19}$$

E4 Variance

With the Gaussian off-axis angular density function (E1), and after expanding the exponential and exponential-error functions in terms of power series, using 2.512.2 and 3 of Gradshteyn & Ryzhik (1980) to integrate by parts and term-by-term, then summing, the expected square of the off-axis angle is

$$E_{g_1}\left(\theta^2 \,|\, (\sigma/F_\mu)^2\right) = \int_0^\pi p_{g_1}(\theta)\,\theta^2\,d\theta = \pi\left[\left\{\left(\frac{\pi}{2}\right)^{\frac{1}{2}}\left(\frac{\sigma}{F_\mu}\right) + \frac{\pi}{2}\right\} - \left\{\left(\frac{\pi}{2}\right)^{\frac{1}{2}}\left(\frac{\sigma}{F_\mu}\right) + \frac{\pi}{2}\right\}\mathrm{erf}\left[\frac{1}{\sqrt{2}}\left(\frac{F_\mu}{\sigma}\right)\right]\right.$$
$$\left. - \exp\left[-\frac{1}{2}\left(\frac{F_\mu}{\sigma}\right)^2\right]\left\{\left(\frac{\pi}{2}\right)^{\frac{1}{2}}\left(\frac{\sigma}{F_\mu}\right) - \sum_{m=0}^{\infty}\frac{(2m+1)!!}{(2m+2)!!(2m+2)!!}\left(\frac{F_\mu}{\sigma}\right)^{2m}{}_3F_2\left[\begin{matrix}\frac{1}{2}, m+1, m+\frac{3}{2}\\ m+2, m+2\end{matrix}; 1\right]\right\}\right]. \tag{E20}$$

where the hypergeometric functions are given by (A7). With this result, the variance of the off-axis angle about its expected value is just

$$V_{g_1}\left(\theta \,|\, (\sigma/F_\mu)^2\right) = E_{g_1}(\theta^2) - \left[E_{g_1}(\theta)\right]^2. \tag{E21}$$

In Fig. 9(h) we show examples of the standard deviation of the off-axis angle for a Gaussian distribution,

$$S_{g_1}\left(\theta \,|\, (\sigma/F_\mu)^2\right) = \left[V_{g_1}(\theta)\right]^{\frac{1}{2}}, \tag{E22}$$

as a function of relative vectorial dispersion σ/F_μ. In the limiting case where the relative vectorial dispersion is substantially less than one, $\sigma/F_\mu \ll 1$, the Gaussian expected square of the off-axis angle (E20) is approximately that for a Fisher distribution. From (E2) the expected square of the off-axis angle is

$$E_f\left(\theta^2 \,|\, (\sigma/F_\mu)^2\right) = \int_0^\pi p_f(\theta)\,\theta^2 d\theta = \pi\left\{\sinh\left[\left(\frac{F_\mu}{\sigma}\right)^2\right]\right\}^{-1}\left\{\left(\frac{\pi}{2}\right)I_0\left[\left(\frac{F_\mu}{\sigma}\right)^2\right] - \left(\frac{\pi}{2}\right)\exp\left[-\left(\frac{F_\mu}{\sigma}\right)^2\right]\right.$$
$$\left. - \left(\frac{F_\mu}{\sigma}\right)^2{}_1F_2\left[\begin{matrix}1\\ \frac{3}{2}, \frac{3}{2}\end{matrix}; \frac{1}{4}\left(\frac{F_\mu}{\sigma}\right)^4\right] + \left(\frac{F_\mu}{\sigma}\right)^2\sum_{m=0}^{\infty}\frac{1}{(2m+2)!!(2m+2)!!}\left(\frac{F_\mu}{\sigma}\right)^{4m}{}_3F_2\left[\begin{matrix}\frac{1}{2}, m+1, m+\frac{3}{2}\\ m+2, m+2\end{matrix}; 1\right]\right\}. \tag{E23}$$

The modified Bessel function is I_0; for reference see Abramowitz & Stegun (1965) or Spanier & Oldham (1987). In the opposite limiting case where the relative vectorial dispersion is substantially greater than one, $\sigma/F_\mu \gg 1$, the Gaussian expected square of the off-axis angle is approximately that for a spherically-uniform distribution of directions. From (E4) we have

$$E_u(\theta^2) = \int_0^\pi p_u(\theta)\,\theta^2\,d\theta = \frac{1}{2}\pi^2 - 2, \tag{E24}$$

which can be easily checked.

For the bi-Gaussian off-axis angular density function (E5), the variance of the off-axis angle is obtained using the expected square of the angle,

$$E_{g_2}\left(\theta^2 \,|\, (\sigma/F_\mu)^2\right) = \int_0^\pi p_{g_2}(\theta)\,\theta^2\,d\theta = \pi\left\{\frac{\pi}{2} - \left(\frac{\pi}{2}\right)^{\frac{1}{2}}\left(\frac{\sigma}{F_\mu}\right)\mathrm{erf}\left[\frac{1}{\sqrt{2}}\left(\frac{F_\mu}{\sigma}\right)\right]\right.$$
$$\left. + \exp\left[-\frac{1}{2}\left(\frac{F_\mu}{\sigma}\right)^2\right]\sum_{m=0}^{\infty}\frac{(2m+1)!!}{(2m+2)!!(2m+2)!!}\left(\frac{F_\mu}{\sigma}\right)^{2m}{}_3F_2\left[\begin{matrix}\frac{1}{2}, m+1, m+\frac{3}{2}\\ m+2, m+2\end{matrix}; 1\right]\right\}. \tag{E25}$$

In the limiting case where the relative vectorial dispersion is substantially less than one, $\sigma/F_\mu \ll 1$, the bi-Gaussian expected square of the off-axis angle (E25) is approximately that for a Bingham distribution. From (E6) the expected square of the off-axis angle is

$$E_b\left(\theta^2 \,|\, (\sigma/F_\mu)^2\right) = \int_0^\pi p_b(\theta)\,\theta^2 d\theta = \pi\left\{{}_1F_1\left[\begin{matrix}\frac{1}{2}\\ \frac{3}{2}\end{matrix}; \frac{1}{2}\left(\frac{F_\mu}{\sigma}\right)^2\right]\right\}^{-1}\left\{\frac{\pi}{\sqrt{2}}\left(\frac{\sigma}{F_\mu}\right)\exp\left[\frac{1}{2}\left(\frac{F_\mu}{\sigma}\right)^2\right]\mathrm{daw}\left[\frac{1}{\sqrt{2}}\left(\frac{F_\mu}{\sigma}\right)\right]\right.$$
$$\left. - {}_2F_2\left[\begin{matrix}\frac{1}{2}, 1\\ \frac{3}{2}, \frac{3}{2}\end{matrix}; \frac{1}{2}\left(\frac{F_\mu}{\sigma}\right)^2\right] + \sum_{m=0}^{\infty}\frac{(2m-1)!!}{(2m+2)!!(2m+2)!!}\left(\frac{F_\mu}{\sigma}\right)^{2m}{}_3F_2\left[\begin{matrix}\frac{1}{2}, m+1, m+\frac{3}{2}\\ m+2, m+2\end{matrix}; 1\right]\right\} \tag{E26}$$

where Dawson's integral is given by (E15). In the opposite limiting case, where the relative vectorial dispersion is substantially greater than one, $\sigma/F_\mu \gg 1$, the bi-Gaussian expected square of the off-axis angle is approximately that for a spherically-uniform distribution of directions, (E24).

APPENDIX F: INCLINATION

F1 Marginal density function

The case of inclination-only data is relevant to studies of azimuthally-unoriented borecores. For the Gaussian distribution, the probability density function is obtained by integrating (10) over all intensities and declinations. From (C1), and after expanding the last exponential function in terms of an infinite series, then using 6.631.1 of Gradshteyn & Ryzhik (1980) to integrate term-by-term, the marginal density function for inclination is

$$p_{g_1}\left(I \mid I_\mu, (\sigma/F_\mu)^2\right) = \int_0^{2\pi}\int_0^{\infty} p_{g_1}(F, I, D)\, dF dD = \cos I \exp\left[-\frac{1}{2}\left(\frac{F_\mu}{\sigma}\right)^2\right]$$
$$\times \sum_{m=0}^{\infty}\left\{\frac{1}{2}\frac{(2m+1)}{(2m)!!}\left(\frac{F_\mu}{\sigma}\right)^{2m}\sin^{2m} I \sin^{2m} I_\mu\, {}_1F_1\left[\begin{matrix} m+\frac{3}{2} \\ 1 \end{matrix}; \frac{1}{2}\left(\frac{F_\mu}{\sigma}\right)^2 \cos^2 I \cos^2 I_\mu\right]\right.$$
$$\left. + \frac{1}{\sqrt{2\pi}}\frac{(2m+2)}{(2m+1)!!}\left(\frac{F_\mu}{\sigma}\right)^{2m+1}\sin^{2m+1} I \sin^{2m+1} I_\mu\, {}_1F_1\left[\begin{matrix} m+2 \\ 1 \end{matrix}; \frac{1}{2}\left(\frac{F_\mu}{\sigma}\right)^2 \cos^2 I \cos^2 I_\mu\right]\right\}, \quad \text{(F1)}$$

where the hypergeometric functions are given by (A7). Note that with inclination-only data the vectorial variance of the Gaussian distribution can only be determined in a relative sense, measured by $(\sigma/F_\mu)^2$. We show examples of the inclination density function for the Gaussian distribution in Fig. 2(c), given different relative vectorial dispersions σ/F_μ, and in Fig. 3(c), given different mean vectorial inclinations I_μ. In the limiting case where the relative vectorial dispersion is substantially less than one, $\sigma/F_\mu \ll 1$, the Gaussian inclination density function (F1) is approximately that for a Fisher distribution. From (A3) and using 3.915.2 of Gradshteyn & Ryzhik we have

$$p_f\left(I \mid I_\mu, (\sigma/F_\mu)^2\right) = \int_0^{2\pi} p_f(I, D)\, dD = \frac{1}{2}\left(\frac{F_\mu}{\sigma}\right)^2 \left\{\sinh\left[\left(\frac{F_\mu}{\sigma}\right)^2\right]\right\}^{-1} \cos I \exp\left[\left(\frac{F_\mu}{\sigma}\right)^2 \sin I \sin I_\mu\right] I_0\left[\left(\frac{F_\mu}{\sigma}\right)^2 \cos I \cos I_\mu\right], \quad \text{(F2)}$$

which is a result first obtained by Briden & Ward (1966). This should be compared with eq. (C1), the intensity-inclination density function for the Gaussian distribution. In the opposite limiting case, where the relative vectorial dispersion is substantially greater than one, $\sigma/F_\mu \gg 1$, the Gaussian inclination density function is approximately that for a spherically-uniform distribution of directions. From (A4) we have

$$p_u(I) = \int_0^{2\pi} p_u(I, D)\, dD = \frac{1}{2}\cos I. \quad \text{(F3)}$$

For the bi-Gaussian distribution, the inclination probability density function is obtained by integrating (16) over all intensities and declinations,

$$p_{g_2}\left(I \mid I_\mu, (\sigma/F_\mu)^2\right) = \int_0^{2\pi}\int_0^{\infty} p_{g_2}(F, I, D)\, dF dD$$
$$= \frac{1}{2}\cos I \exp\left[-\frac{1}{2}\left(\frac{F_\mu}{\sigma}\right)^2\right] \sum_{m=0}^{\infty}\frac{(2m+1)}{(2m)!!}\left(\frac{F_\mu}{\sigma}\right)^{2m}\sin^{2m} I \sin^{2m} I_\mu\, {}_1F_1\left[\begin{matrix} m+\frac{3}{2} \\ 1 \end{matrix}; \frac{1}{2}\left(\frac{F_\mu}{\sigma}\right)^2 \cos^2 I \cos^2 I_\mu\right]. \quad \text{(F4)}$$

We show examples of the inclination density function for the bi-Gaussian distribution in Fig. 4(c), given different relative vectorial dispersions σ/F_μ, and in Fig. 5(c), given different mean vectorial inclinations I_μ. In the limiting case where the relative vectorial dispersion is substantially less than one, $\sigma/F_\mu \ll 1$, the bi-Gaussian inclination density function (F4) is approximately that for a Bingham distribution. From (A6), and after expanding the exponential function in terms of nested infinite series, using 331.25 of Gröbner & Hofreiter (1965a) to integrate term-by-term, then summing, we have

$$p_b\left(I \mid I_\mu, (\sigma/F_\mu)^2\right) = \int_0^{2\pi} p_b(I, D)\, dD = \frac{1}{2}\left\{{}_1F_1\left[\begin{matrix} \frac{1}{2} \\ \frac{3}{2} \end{matrix}; \frac{1}{2}\left(\frac{F_\mu}{\sigma}\right)^2\right]\right\}^{-1} \cos I \exp\left[\frac{1}{2}\left(\frac{F_\mu}{\sigma}\right)^2 \sin^2 I \sin^2 I_\mu\right]$$
$$\times \sum_{m=0}^{\infty}\frac{1}{(2m)!!(2m)!!}\left(\frac{F_\mu}{\sigma}\right)^{4m}\cos^{2m} I \cos^{2m} I_\mu \sin^{2m} I \sin^{2m} I_\mu\, {}_1F_1\left[\begin{matrix} m+\frac{1}{2} \\ m+1 \end{matrix}; \frac{1}{2}\left(\frac{F_\mu}{\sigma}\right)^2 \cos^2 I \cos^2 I_\mu\right]. \quad \text{(F5)}$$

In the opposite limiting case, where the relative vectorial dispersion is substantially greater than one, $\sigma/F_\mu \gg 1$, the bi-Gaussian inclination density function is approximately that for a spherically-uniform distribution of directions, (F3).

F2 Cumulative distribution

For the Gaussian inclination probability density function (F1), the corresponding cumulative distribution gives the probability that an inclination lies on the interval $[-\pi/2, I]$. After expanding the hypergeometric functions in terms of power series, using 2.511.4 of Gradshteyn & Ryzhik (1980) to integrate term-by-term, then summing, the inclination cumulative distribution is

$$P_{g_1}\left(I \mid I_\mu, (\sigma/F_\mu)^2\right) = \int_{-\frac{\pi}{2}}^{I} p_{g_1}\left(I'\right) dI' = \frac{1}{2}\left\{1 - \mathrm{erf}\left[\frac{1}{\sqrt{2}}\left(\frac{F_\mu}{\sigma}\right)\sin I_\mu\right]\right\} + \exp\left[-\frac{1}{2}\left(\frac{F_\mu}{\sigma}\right)^2\right]$$
$$\times \sum_{m=0}^{\infty}\sum_{n=0}^{\infty}\left\{\frac{1}{2}\frac{(2m+2n-1)!!}{(2m)!!(2m)!!(2n)!}\left(\frac{F_\mu}{\sigma}\right)^{2m+2n}\cos^{2m} I \cos^{2m} I_\mu \sin^{2n+1} I \sin^{2n} I_\mu {}_2F_1\left[\begin{matrix}1, -m\\ \frac{1}{2} - m - n\end{matrix}; \sec^2 I\right]\right.$$
$$\left. + \frac{1}{\sqrt{2\pi}}\frac{(2m+2n)!!}{(2m)!!(2m)!!(2n+1)!}\left(\frac{F_\mu}{\sigma}\right)^{2m+2n+1}\cos^{2m} I \cos^{2m} I_\mu \sin^{2n+2} I \sin^{2n+1} I_\mu {}_2F_1\left[\begin{matrix}1, -m\\ -m - n\end{matrix}; \sec^2 I\right]\right\}. \quad \text{(F6)}$$

The first set of hypergeometric functions are given by (B2), for which we use the property

$$\Gamma\left[\frac{1}{2} - n\right] = \frac{(-2)^n\sqrt{\pi}}{(2n-1)!!} \quad \text{for} \quad n = 0, 1, 2, ...; \quad \text{(F7)}$$

see 43:4:3 of Spanier & Oldham (1987). With this,

$${}_2F_1\left[\begin{matrix}1, -m\\ \frac{1}{2} - n\end{matrix}; z\right] = \sum_{j=0}^{m}\frac{(2m)!!(2n-2j-1)!!}{(2n-1)!!(2m-2j)!!}z^j. \quad \text{(F8)}$$

The second set of hypergeometric functions are defined using 15.4.2 of Abramowitz & Stegun (1965),

$${}_2F_1\left[\begin{matrix}1, -m\\ -n\end{matrix}; z\right] = \sum_{j=0}^{m}\frac{(2m)!!(2n-2j)!!}{(2n)!!(2m-2j)!!}z^j. \quad \text{(F9)}$$

As expected,

$$P_{g_1}\left(\frac{\pi}{2} \mid I_\mu, (\sigma/F_\mu)^2\right) = 1, \quad \text{(F10)}$$

which we have checked numerically. We show examples of the Gaussian inclination cumulative distribution in Fig. 2(c), given different relative vectorial dispersions σ/F_μ, and in Fig. 3(c), given different mean vectorial inclinations I_μ. In the limiting case where the relative vectorial dispersion is substantially less than one, $\sigma/F_\mu \ll 1$, the Gaussian inclination cumulative distribution (F6) is approximately that for a Fisher distribution. From (F2) the inclination cumulative distribution is

$$P_f\left(I \mid I_\mu, (\sigma/F_\mu)^2\right) = \int_{-\frac{\pi}{2}}^{I} p_f\left(I'\right) dI' = \frac{1}{2}\left(\frac{F_\mu}{\sigma}\right)^2\left\{\sinh\left[\left(\frac{F_\mu}{\sigma}\right)^2\right]\right\}^{-1}$$
$$\times\left[\sum_{m=0}^{\infty}\left\{\frac{\cos^{2m} I_\mu}{(2m)!!(2m+1)!!}\left(\frac{F_\mu}{\sigma}\right)^{4m}{}_1F_2\left[\begin{matrix}1\\ 1, m+\frac{3}{2}\end{matrix}; \frac{1}{4}\left(\frac{F_\mu}{\sigma}\right)^4\sin^2 I_\mu\right]\right.\right.$$
$$\left.\left. - \frac{\cos^{2m} I_\mu \sin I_\mu}{(2m)!!(2m+2)!!}\left(\frac{F_\mu}{\sigma}\right)^{4m+2}{}_1F_2\left[\begin{matrix}1\\ \frac{3}{2}, m+2\end{matrix}; \frac{1}{4}\left(\frac{F_\mu}{\sigma}\right)^4\sin^2 I_\mu\right]\right\}\right.$$
$$+ \sum_{m=0}^{\infty}\sum_{n=0}^{\infty}\left\{\frac{\cos^{2m} I \cos^{2m} I_\mu \sin^{2n+1} I \sin^{2n} I_\mu}{(2m)!!(2m)!!(2n)!(2m+2n+1)}\left(\frac{F_\mu}{\sigma}\right)^{4m+4n}{}_2F_1\left[\begin{matrix}1, -m\\ \frac{1}{2} - m - n\end{matrix}; \sec^2 I\right]\right.$$
$$\left.\left. + \frac{\cos^{2m} I \cos^{2m} I_\mu \sin^{2n+2} I \sin^{2n+1} I_\mu}{(2m)!!(2m)!!(2n+1)!(2m+2n+2)}\left(\frac{F_\mu}{\sigma}\right)^{4m+4n+2}{}_2F_1\left[\begin{matrix}1, -m\\ -m - n\end{matrix}; \sec^2 I\right]\right\}\right], \quad \text{(F11)}$$

which is probably the most unpleasant formula in this paper. Some re-expression can be made in terms of modified Bessel functions, but we have not been able to reduce (F11) to a more compact or more symmetrical form. The hypergeometric functions are given by (A7), (B2), (F8), and (F9). In the opposite limiting case, where the relative vectorial dispersion is substantially greater than one, $\sigma/F_\mu \gg 1$, the Gaussian inclination cumulative distribution is approximately that for a spherically-uniform distribution of directions. From (F3) we have

$$P_u(I) = \int_{-\frac{\pi}{2}}^{I} p_u\left(I'\right) dI' = \frac{1}{2} + \frac{1}{2}\sin I. \quad \text{(F12)}$$

For the bi-Gaussian inclination probability density function (F4), the corresponding cumulative distribution is just

$$P_{g_2}\left(I \mid I_\mu, (\sigma/F_\mu)^2\right) = \int_{-\frac{\pi}{2}}^{I} p_{g_2}\left(I'\right) dI' = \frac{1}{2} + \frac{1}{2}\exp\left[-\frac{1}{2}\left(\frac{F_\mu}{\sigma}\right)^2\right]$$
$$\times \sum_{m=0}^{\infty}\sum_{n=0}^{\infty}\frac{(2m+2n-1)!!}{(2m)!!(2m)!!(2n)!}\left(\frac{F_\mu}{\sigma}\right)^{2m+2n}\cos^{2m} I \cos^{2m} I_\mu \sin^{2n+1} I \sin^{2n} I_\mu {}_2F_1\left[\begin{matrix}1, -m\\ \frac{1}{2} - m - n\end{matrix}; \sec^2 I\right]. \quad \text{(F13)}$$

We show examples of the bi-Gaussian inclination cumulative distribution in Fig. 4(d), given different relative vectorial dispersions σ/F_μ, and in Fig. 5(d), given different mean vectorial inclinations I_μ. In the limiting case where the relative vectorial dispersion is substantially less

than one, $\sigma/F_\mu \ll 1$, the bi-Gaussian inclination cumulative distribution (F13) is approximately that for a Bingham distribution. From (F5) the inclination cumulative distribution is

$$P_b\left(I \mid I_\mu, (\sigma/F_\mu)^2\right) = \int_{-\frac{\pi}{2}}^{I} p_b\left(I'\right) dI' = \frac{1}{2} + \frac{1}{2}\left\{ {}_1F_1\left[\begin{matrix}\frac{1}{2}\\ \frac{3}{2}\end{matrix}; \frac{1}{2}\left(\frac{F_\mu}{\sigma}\right)^2\right]\right\}^{-1}$$
$$\times \sum_{m=0}^{\infty}\sum_{n=0}^{\infty}\sum_{j=0}^{\infty} \frac{(2m+2n-1)!!}{(2m)!!(2j)!!(2m+2n)!!(2n)!(2m+4n+2j+1)} \left(\frac{F_\mu}{\sigma}\right)^{2m+4n+2j}$$
$$\times \cos^{2m+2n} I \cos^{2m+2n} I_\mu \sin^{2n+2j+1} I \sin^{2n+2j} I_\mu \, {}_2F_1\left[\begin{matrix}1, -m-n\\ \frac{1}{2}-m-2n-j\end{matrix}; \sec^2 I\right]. \tag{F14}$$

In the opposite limiting case, where the relative vectorial dispersion is substantially greater than one, $\sigma/F_\mu \gg 1$, the bi-Gaussian inclination cumulative distribution is approximately that for a spherically-uniform distribution of directions, (F12).

F3 Expected value

With the Gaussian inclination density function (F1), and after expanding the hypergeometric functions in terms of power series, using 2.511.1 and 4 of Gradshteyn & Ryzhik (1980) to integrate by parts and term-by-term, then summing, the expected inclination is

$$E_{g_1}\left(I \mid I_\mu, (\sigma/F_\mu)^2\right) = \int_{-\frac{\pi}{2}}^{+\frac{\pi}{2}} p_{g_1}(I)\, I dI = \left(\frac{\pi}{2}\right)^{\frac{1}{2}} \exp\left[-\frac{1}{2}\left(\frac{F_\mu}{\sigma}\right)^2\right]$$
$$\times \sum_{m=0}^{\infty}\sum_{n=0}^{\infty} \frac{(2m+1)!!(2m+2n+2)!!}{(2m+2)!!(2m+2)!!(2m)!!(2n+1)!} \left(\frac{F_\mu}{\sigma}\right)^{2m+2n+1} \cos^{2m} I_\mu \sin^{2n+1} I_\mu \, {}_3F_2\left[\begin{matrix}m+1, m+\frac{3}{2}, -n\\ m+2, m+2\end{matrix}; 1\right], \tag{F15}$$

where the hypergeometric functions are given by (B2). This average inclination should not be confused with I_μ, the inclination of the mean vector. In Fig. 9(c) we show examples of the inclination bias,

$$\delta I_{g_1} = E_{g_1}(I) - I_\mu, \tag{F16}$$

as a function of the relative vectorial dispersion σ/F_μ, given different mean vectorial inclinations I_μ. In the limiting case where the relative vectorial dispersion is substantially less than one, $\sigma/F_\mu \ll 1$, the Gaussian expected inclination density function (F15) is approximately that for a Fisher distribution. From (F2) the expected inclination is

$$E_f\left(I \mid I_\mu, (\sigma/F_\mu)^2\right) = \int_{-\frac{\pi}{2}}^{+\frac{\pi}{2}} p_f(I) I dI = \frac{\pi}{2}\left(\frac{F_\mu}{\sigma}\right)^2 \left\{\sinh\left[\left(\frac{F_\mu}{\sigma}\right)^2\right]\right\}^{-1}$$
$$\times \sum_{m=0}^{\infty}\sum_{n=0}^{\infty} \frac{(2m+1)!!}{(2m+2)!!(2m+2)!!(2m)!!(2n+1)!} \left(\frac{F_\mu}{\sigma}\right)^{4m+4n+2} \cos^{2m} I_\mu \sin^{2n+1} I_\mu \, {}_3F_2\left[\begin{matrix}m+1, m+\frac{3}{2}, -n\\ m+2, m+2\end{matrix}; 1\right]. \tag{F17}$$

In the opposite limiting case, where the relative vectorial dispersion is substantially greater than one, $\sigma/F_\mu \gg 1$, the Gaussian inclination density function is approximately that for a spherically-uniform distribution of directions. From (F3) we have

$$E_u(I) = \int_{-\frac{\pi}{2}}^{\frac{\pi}{2}} p_u(I) I dI = 0. \tag{F18}$$

For the bi-Gaussian inclination density function (F4), the expected inclination is just

$$E_{g_2}(I) = \int_{-\frac{\pi}{2}}^{+\frac{\pi}{2}} p_{g_2}(I)\, I dI = 0, \tag{F19}$$

which can be deduced by consideration of symmetry. The expected inclination for the Bingham distribution is identical,

$$E_b(I) = \int_{-\frac{\pi}{2}}^{+\frac{\pi}{2}} p_b(I)\, I dI = 0. \tag{F20}$$

F4 Variance

With the Gaussian inclination probability density function (F1), and after expanding the hypergeometric functions in terms of power series, using 2.511.1 and 4 of Gradshteyn & Ryzhik (1980) to integrate by parts and term-by-term, then summing, the expected value for the square of the inclination is

$$E_{g_1}\left(I^2 \mid I_\mu, (\sigma/F_\mu)^2\right) = \int_{-\frac{\pi}{2}}^{+\frac{\pi}{2}} p_{g_1}(I)\, I^2 dI = \frac{2}{\sqrt{\pi}} \exp\left[-\frac{1}{2}\left(\frac{F_\mu}{\sigma}\right)^2\right] \sum_{m=0}^{\infty}\sum_{n=0}^{\infty}\sum_{j=0}^{\infty}\left(-\frac{1}{2}\right)^n \Gamma\left[j-n+\frac{1}{2}\right]$$
$$\times \frac{(2m+2n+1)!!(2m+2j)!!}{(2m)!!(2m)!!(2n)!!(2m+2j+3)!!j!(2m+2j+3)} \left(\frac{F_\mu}{\sigma}\right)^{2m+2n} \cos^{2m} I_\mu \sin^{2n} I_\mu$$
$$\times {}_3F_2\left[\begin{matrix}\frac{1}{2}, m+j+\frac{3}{2}, m+j+2 \\ m+j+\frac{5}{2}, m+j+\frac{5}{2}\end{matrix}; 1\right], \tag{F21}$$

where we use (F7) and where the hypergeometric functions are given by (A7). Of course, with this result the variance of the inclination about its expected value is just

$$V_{g_1}\left(I \mid I_\mu, (\sigma/F_\mu)^2\right) = E_{g_1}(I^2) - \left[E_{g_1}(I)\right]^2, \tag{F22}$$

where the last term comes from (F15). In Fig. 9(d) we show examples of the standard deviation of inclination for a Gaussian distribution,

$$S_{g_1}\left(I \mid I_\mu, (\sigma/F_\mu)^2\right) = \left[V_{g_1}(I)\right]^{\frac{1}{2}}, \tag{F23}$$

as a function of the relative vectorial dispersion σ/F_μ and for different mean vectorial inclinations I_μ. In the limiting case where the relative vectorial dispersion is substantially less than one, $\sigma/F_\mu \ll 1$, the Gaussian expected square of the inclination (F21) is approximately that for a Fisher distribution. From (F2) the expected value for the square of the inclination is

$$E_f\left(I^2 \mid I_\mu, (\sigma/F_\mu)^2\right) = \int_{-\frac{\pi}{2}}^{+\frac{\pi}{2}} p_f(I)\, I^2 dI = \frac{2}{\sqrt{\pi}}\left(\frac{F_\mu}{\sigma}\right)^2 \left\{\sinh\left[\left(\frac{F_\mu}{\sigma}\right)^2\right]\right\}^{-1} \sum_{m=0}^{\infty}\sum_{n=0}^{\infty}\sum_{j=0}^{\infty}\left(-\frac{1}{2}\right)^n \Gamma\left[j-n+\frac{1}{2}\right]$$
$$\times \frac{(2m+2j)!!}{(2m)!!(2m)!!(2n)!!(2m+2j+3)!!j!(2m+2j+3)} \left(\frac{F_\mu}{\sigma}\right)^{4m+4n} \cos^{2m} I_\mu \sin^{2n} I_\mu$$
$$\times {}_3F_2\left[\begin{matrix}\frac{1}{2}, m+j+\frac{3}{2}, m+j+2 \\ m+j+\frac{5}{2}, m+j+\frac{5}{2}\end{matrix}; 1\right]. \tag{F24}$$

In the opposite limiting case, where the relative vectorial dispersion is substantially greater than one, $\sigma/F_\mu \gg 1$, the Gaussian inclination density function is approximately that for a spherically-uniform distribution of directions. From (F3) we have

$$E_u(I^2) = \int_{-\frac{\pi}{2}}^{+\frac{\pi}{2}} p_u(I)\, I^2\, dI = \left(\frac{\pi}{2}\right)^2 - 2, \tag{F25}$$

which should be compared with that for the off-axis angle, (E24).

For the bi-Gaussian inclination density function (F4), the variance of the inclination is just

$$V_{g_2}\left(I \mid I_\mu, (\sigma/F_\mu)^2\right) = E_{g_1}\left(I^2 \mid I_\mu, (\sigma/F_\mu)^2\right), \tag{F26}$$

which can be deduced by consideration of symmetry and the fact that the expected inclination for such a distribution is zero, (F19). In the limiting case where the relative vectorial dispersion is substantially less than one, $\sigma/F_\mu \ll 1$, the bi-Gaussian expected square of the inclination (F21) is approximately that for a Bingham distribution. From (F5) the expected value for the square of the inclination is

$$E_b\left(I^2 \mid I_\mu, (\sigma/F_\mu)^2\right) = \int_{-\frac{\pi}{2}}^{+\frac{\pi}{2}} p_b(I)\, I^2 dI = \frac{2}{\sqrt{\pi}}\left\{{}_1F_1\left[\frac{1}{2}; \frac{1}{2}\left(\frac{F_\mu}{\sigma}\right)^2\right]\right\}^{-1} \sum_{m=0}^{\infty}\sum_{n=0}^{\infty}\sum_{j=0}^{\infty}\sum_{k=0}^{\infty}\left(-\frac{1}{2}\right)^{m+n} \Gamma\left[k-m-n+\frac{1}{2}\right]$$
$$\times \frac{(2m+2n-1)!!(2m+2j+2k)!!(2m+2j-1)!!}{(2n)!!(2j)!!(2m+2j)!!(2m+2j+2k+3)!!(2m)!k!(2m+2j+2k+3)} \left(\frac{F_\mu}{\sigma}\right)^{4m+2n+2j} \cos^{2m+2j} I_\mu \sin^{2m+2n} I_\mu$$
$$\times {}_3F_2\left[\begin{matrix}\frac{1}{2}, m+j+k+\frac{3}{2}, m+j+k+2 \\ m+j+k+\frac{5}{2}, m+j+k+\frac{5}{2}\end{matrix}; 1\right]. \tag{F27}$$

In the opposite limiting case, where the relative vectorial dispersion is substantially greater than one, $\sigma/F_\mu \gg 1$, the bi-Gaussian inclination density function is approximately that for a spherically-uniform distribution of directions, (F25).

APPENDIX G: DECLINATION

G1 Marginal density function

We know of no situation where palaeomagnetic data consist of only declinations, that is where neither intensities nor inclinations are available. However, for the sake of completeness, for the Gaussian distribution, we obtain the declination probability density functions by integrating (10) over all intensities and inclinations. From (B1), and after expanding the hypergeometric and Bessel functions in terms of power series,

making binomial expansions, using 3.461.2 and 3 of Gradshteyn & Ryzhik (1980) to integrate term-by-term, then summing, the marginal density function for declination is

$$p_{g_1}\left(D \mid I_\mu, D_\mu, (\sigma/F_\mu)^2\right) = \int_{-\frac{\pi}{2}}^{+\frac{\pi}{2}} \int_0^\infty p_{g_1}(F, I, D)\, dF dI$$
$$= \frac{1}{2\pi} \exp\left[-\frac{1}{2}\left(\frac{F_\mu}{\sigma}\right)^2\right] \sum_{m=0}^{\infty} \frac{\sin^{2m} I_\mu}{(2m)!!} \left(\frac{F_\mu}{\sigma}\right)^{2m} {}_2F_1\left[\begin{matrix}1, -m \\ \frac{1}{2}\end{matrix}; -\cot^2 I_\mu \cos^2(D - D_\mu)\right]$$
$$+ \frac{1}{2\sqrt{2\pi}} \left(\frac{F_\mu}{\sigma}\right) \cos I_\mu \cos(D - D_\mu) \exp\left[-\frac{1}{2}\left(\frac{F_\mu}{\sigma}\right)^2 \cos^2 I_\mu \sin^2(D - D_\mu)\right], \tag{G1}$$

where the hypergeometric functions are given by (B2). Note that with declination-only data the vectorial variance of the Gaussian distribution can only be determined in a relative sense, measured by $(\sigma/F_\mu)^2$. We show examples of the declination density function for the Gaussian distribution in Fig. 2(e), given different relative vectorial dispersions σ/F_μ, and in Fig. 3(e), given different mean vectorial inclinations I_μ. In the limiting case where the relative vectorial dispersion is substantially less than one, $\sigma/F_\mu \ll 1$, the Gaussian declination density function (G1) is approximately that for a Fisher distribution. From (A3) we have

$$p_f\left(D \mid I_\mu, D_\mu, (\sigma/F_\mu)^2\right) = \int_0^{2\pi} p_f(I, D)\, dD = \frac{1}{2\pi}\left(\frac{F_\mu}{\sigma}\right)^2 \left\{\sinh\left[\left(\frac{F_\mu}{\sigma}\right)^2\right]\right\}^{-1}$$
$$\times \left\{\sum_{m=0}^{\infty} \frac{\sin^{2m} I_\mu}{(2m+1)!} \left(\frac{F_\mu}{\sigma}\right)^{4m} {}_2F_1\left[\begin{matrix}1, -m \\ \frac{1}{2}\end{matrix}; -\cot^2 I_\mu \cos^2(D - D_\mu)\right]\right.$$
$$\left. + \left(\frac{\pi}{2}\right) \frac{\cos I_\mu \cos(D - D_\mu)}{\sqrt{\cos^2 I_\mu \cos^2(D - D_\mu) + \sin^2 I_\mu}} I_1\left[\left(\frac{F_\mu}{\sigma}\right)^2 \sqrt{\cos^2 I_\mu \cos^2(D - D_\mu) + \sin^2 I_\mu}\right]\right\}, \tag{G2}$$

where the integration performed is like that used to derive (B1). The modified Bessel function is I_1; for reference see Abramowitz & Stegun (1965) or Spanier & Oldham (1987). In the opposite limiting case, where the relative vectorial dispersion is substantially greater than one, $\sigma/F_\mu \gg 1$, the Gaussian declination density function is approximately that for a spherically-uniform distribution of directions,

$$p_u(D) = \frac{1}{2\pi}. \tag{G3}$$

For the bi-Gaussian distribution, the declination probability density function is obtained by integrating (16) over all intensities and inclinations,

$$p_{g_2}\left(D \mid I_\mu, D_\mu, (\sigma/F_\mu)^2\right) = \int_{-\frac{\pi}{2}}^{+\frac{\pi}{2}} \int_0^\infty p_{g_2}(F, I, D)\, dF dI$$
$$= \frac{1}{2\pi} \exp\left[-\frac{1}{2}\left(\frac{F_\mu}{\sigma}\right)^2\right] \sum_{m=0}^{\infty} \frac{\sin^{2m} I_\mu}{(2m)!!} \left(\frac{F_\mu}{\sigma}\right)^{2m} {}_2F_1\left[\begin{matrix}1, -m \\ \frac{1}{2}\end{matrix}; -\cot^2 I_\mu \cos^2(D - D_\mu)\right]. \tag{G4}$$

We show examples of the declination density function for the bi-Gaussian distribution in Fig. 4(e), given different relative vectorial dispersions σ/F_μ, and in Fig. 5(e), given different mean vectorial inclinations I_μ. In the limiting case where the relative vectorial dispersion is substantially less than one, $\sigma/F_\mu \ll 1$, the bi-Gaussian declination density function (G4) is approximately that for a Bingham distribution. From (A6), and after expanding the exponential function in terms of a power series, making binomial expansions, using 2.511.4 of Gradshteyn & Ryzhik to integrate term-by-term, then summing, we have

$$p_b\left(D \mid I_\mu, D_\mu, (\sigma/F_\mu)^2\right) = \int_0^{2\pi} p_b(I, D)\, dD$$
$$= \frac{1}{2\pi}\left\{{}_1F_1\left[\begin{matrix}\frac{1}{2} \\ \frac{3}{2}\end{matrix}; \frac{1}{2}\left(\frac{F_\mu}{\sigma}\right)^2\right]\right\}^{-1} \sum_{m=0}^{\infty} \frac{\sin^{2m} I_\mu}{(2m)!!(2m+1)} \left(\frac{F_\mu}{\sigma}\right)^{2m} {}_2F_1\left[\begin{matrix}1, -m \\ \frac{1}{2}\end{matrix}; -\cot^2 I_\mu \cos^2(D - D_\mu)\right]. \tag{G5}$$

In the opposite limiting case, where the relative vectorial dispersion is substantially greater than one, $\sigma/F_\mu \gg 1$, the bi-Gaussian declination density function is approximately that for a spherically-uniform distribution of directions, (G3).

G2 Cumulative Distribution

For the Gaussian declination probability density function (G1), the corresponding cumulative distribution gives the probability that a declination lies on the interval $[\beta, \beta + D]$,

$$P_{g_1}\left(D, \beta \mid I_\mu, D_\mu, (\sigma/F_\mu)^2\right) = \int_\beta^{\beta+D} p_{g_1}(D')\, dD'. \tag{G6}$$

Note that, because of the periodic nature of declination, the choice of the angle β defines this cumulative distribution for all arbitrary shifts and parameterizations on the circle. Expanding the hypergeometric and exponential functions in terms of power series, then using 2.512.2 and 3 of Gradshteyn & Ryzhik (1980) to integrate term-by-term, we obtain

$$Q_{g_1}\left(D' \mid I_\mu, (\sigma/F_\mu)^2\right) = \frac{D'}{2\pi} + \frac{1}{4}\mathrm{erf}\left[\frac{1}{\sqrt{2}}\left(\frac{F_\mu}{\sigma}\right)\cos I_\mu \sin D'\right] + \frac{1}{2\pi}\exp\left[-\frac{1}{2}\left(\frac{F_\mu}{\sigma}\right)^2\right]\tan D'$$
$$\times \sum_{m=0}^{\infty}\sum_{n=0}^{m}\sum_{j=0}^{n-1}\frac{(2n-2j-2)!!}{(2n)!!(2m-2n)!!(2n-2j-1)!!}\left(\frac{F_\mu}{\sigma}\right)^{2m}\sin^{2m} I_\mu \cot^{2n} I_\mu \cos^{2n} D' \sec^{2j} D', \tag{G7}$$

so that the cumulative distribution is

$$P_{g_1}\left(D, \beta \mid I_\mu, D_\mu, (\sigma/F_\mu)^2\right) = Q_{g_1}(D - D_\mu) - Q_{g_1}(\beta - D_\mu). \tag{G8}$$

As expected,

$$P_{g_1}\left(2\pi, \beta \mid I_\mu, D_\mu, (\sigma/F_\mu)^2\right) = 1, \tag{G9}$$

which we have checked numerically. We show examples of the Gaussian declination cumulative distribution in Fig. 2(f), given different relative vectorial dispersions σ/F_μ, and in Fig. 3(f), given different mean vectorial inclinations I_μ. In the limiting case where the relative vectorial dispersion is substantially less than one, $\sigma/F_\mu \ll 1$, the Gaussian declination cumulative distribution (G6) is approximately that for a Fisher distribution. From (G2) the declination cumulative distribution is just

$$P_f\left(D, \beta \mid I_\mu, D_\mu, (\sigma/F_\mu)^2\right) = \int_\beta^{\beta+D} p_f\left(D'\right) dD', \tag{G10}$$

which can be obtained using

$$Q_f\left(D' \mid I_\mu, (\sigma/F_\mu)^2\right) = \frac{D'}{2\pi} + \frac{1}{2\pi}\left(\frac{F_\mu}{\sigma}\right)^2\left\{\sinh\left[\left(\frac{F_\mu}{\sigma}\right)^2\right]\right\}^{-1}\sin D'\sum_{m=0}^{\infty}\sum_{n=0}^{m}\frac{\sin^{2m} I_\mu \cot^{2n} I_\mu \cos^{2n} D'}{(2m-2n)!!}\left(\frac{F_\mu}{\sigma}\right)^{4m}$$
$$\times\left\{\sum_{j=0}^{n-1}\frac{(2n-2j-2)!!}{(2n)!!(2n-2j-1)!!(2m+1)!!}\sec^{2j+1} D' + \left(\frac{\pi}{2}\right)\frac{(2n-1)!!}{(2m+2)!!(2n+1)!}\left(\frac{F_\mu}{\sigma}\right)^2\cos I_\mu {}_2F_1\left[\begin{matrix}1, -n\\ \frac{1}{2} - n\end{matrix}; \sec^2 D'\right]\right\}, \tag{G11}$$

where the hypergeometric functions are given by (F8). In the opposite limiting case, where the relative vectorial dispersion is substantially greater than one, $\sigma/F_\mu \gg 1$, the Gaussian declination cumulative distribution is approximately that for a spherically-uniform distribution of directions. From (G3) we have

$$P_u(D) = \int_\beta^{\beta+D} p_u(D')\, dD' = \frac{D}{2\pi}. \tag{G12}$$

For the bi-Gaussian declination probability density function (G4), the corresponding cumulative distribution is just

$$P_{g_2}\left(D, \beta \mid I_\mu, D_\mu, (\sigma/F_\mu)^2\right) = \int_\beta^{\beta+D} p_{g_2}(D')\, dD', \tag{G13}$$

which can be obtained using

$$Q_{g_2}\left(D' \mid I_\mu, (\sigma/F_\mu)^2\right) = \frac{D'}{2\pi} + \frac{1}{2\pi}\exp\left[-\frac{1}{2}\left(\frac{F_\mu}{\sigma}\right)^2\right]\tan D'$$
$$\times \sum_{m=0}^{\infty}\sum_{n=0}^{m}\sum_{j=0}^{n-1}\frac{(2n-2j-2)!!}{(2n)!!(2m-2n)!!(2n-2j-1)!!}\left(\frac{F_\mu}{\sigma}\right)^{2m}\sin^{2m} I_\mu \cot^{2n} I_\mu \cos^{2n} D' \sec^{2j} D'. \tag{G14}$$

We show examples of the bi-Gaussian declination cumulative distribution in Fig. 4(f), given different relative vectorial dispersions σ/F_μ, and in Fig. 5(f), given different mean vectorial inclinations I_μ. In the limiting case where the relative vectorial dispersion is substantially less than one, $\sigma/F_\mu \ll 1$, the bi-Gaussian declination cumulative distribution (G6) is approximately that for a Bingham distribution. From (G5) the declination cumulative distribution is just

$$P_b\left(D, \beta \mid I_\mu, D_\mu, (\sigma/F_\mu)^2\right) = \int_\beta^{\beta+D} p_b(D')\, dD', \tag{G15}$$

which can be obtained using

$$Q_b\left(D' \mid I_\mu, (\sigma/F_\mu)^2\right) = \frac{D'}{2\pi} + \frac{1}{2\pi}\left\{{}_1F_1\left[\begin{matrix}\frac{1}{2}\\ \frac{3}{2}\end{matrix}; \frac{1}{2}\left(\frac{F_\mu}{\sigma}\right)^2\right]\right\}^{-1}\tan D'$$
$$\times \sum_{m=0}^{\infty}\sum_{n=0}^{m}\sum_{j=0}^{n-1}\frac{(2n-2j-2)!!}{(2n)!!(2m-2n)!!(2n-2j-1)!!(2m+1)}\left(\frac{F_\mu}{\sigma}\right)^{2m}\sin^{2m} I_\mu \cot^{2n} I_\mu \cos^{2n} D' \sec^{2j} D'. \tag{G16}$$

In the opposite limiting case, where the relative vectorial dispersion is substantially greater than one, $\sigma/F_\mu \gg 1$, the bi-Gaussian declination cumulative distribution is approximately that for a spherically-uniform distribution of directions, (G12).

G3 Expected value

From the Gaussian declination density function (G1), the expected declination is obtained by integration,

$$E_{g_1}\left(D \mid I_\mu, D_\mu, (\sigma/F_\mu)^2\right) = \int_0^{2\pi} p_{g_1}(D)\, D\, dD. \tag{G17}$$

In fact, performing this integration is not necessary, since by symmetry we know that

$$E_{g_1}\left(D \mid I_\mu, D_\mu, (\sigma/F_\mu)^2\right) = D_\mu, \tag{G18}$$

unless, of course, $I_\mu = \pm 90^\circ$, in which case the mean declination is indeterminate. Furthermore, as one might expect, in the limit as the relative vectorial dispersion goes to infinity, the expected declination becomes that for a spherically-uniform distribution of directions; in other words, it becomes indeterminate, which we have checked numerically. The declination bias, such as it is, for a Gaussian distribution, is shown in Fig. 9(e).

For the bi-Gaussian declination density function (G4), the expected declination $E_{g_2}(D)$ is indeterminate for all mean inclinations I_μ, which can be deduced by consideration of symmetry. What this means, in practice, is that an arithmetic mean of a set of declinations drawn from a bi-Gaussian distribution is not likely to be an accurate estimate of $\pm D_\mu$, and furthermore, the mean will be unstable to the addition of data. Such estimation difficulties do not exist, however, if one adopts a maximum-likelihood approach for estimating the declination of the mean vector, namely $\pm D_\mu$, although because of symmetry the result is arbitrary to within some multiple of π.

G4 Variance

With the Gaussian declination probability density function (G1), and after expanding the hypergeometric and exponential functions in terms of power series, then using 1.320.5, 7 and 3.761.10 of Gradshteyn and Ryzhik 1980 to integrate term-by-term, the variance of the declination about the mean declination is

$$V_{g_1}\left(D \mid I_\mu, (\sigma/F_\mu)^2\right) = \int_{D_\mu-\pi}^{D_\mu+\pi} p_{g_1}(D)(D-D_\mu)^2\, dD = \frac{1}{3}\pi^2 + 4\exp\left[-\frac{1}{2}\left(\frac{F_\mu}{\sigma}\right)^2\right] \sum_{m=0}^{\infty}\sum_{n=0}^{m} \frac{\sin^{2m} I_\mu \cot^{2n} I_\mu}{(2m-2n)!!}\left(\frac{F_\mu}{\sigma}\right)^{2m}$$
$$\times\left\{\sum_{j=0}^{n-1}\frac{(2n)!!}{(2j)!!(4n-2j)!!(2n-2j)^2} - \left(\frac{\pi}{2}\right)^{\frac{1}{2}}\sum_{j=0}^{n}\frac{(2n+1)!!}{(2j)!!(4n-2j+2)!!(2n-2j+1)^2}\left(\frac{F_\mu}{\sigma}\right)\cos I_\mu\right\}. \tag{G19}$$

Since the variance is defined relative to the mean declination, this result is independent of D_μ. In Fig. 9(f) we show examples of the Gaussian standard deviation of declination,

$$S_{g_1}\left(D \mid I_\mu, (\sigma/F_\mu)^2\right) = \left[V_{g_1}(D)\right]^{\frac{1}{2}}, \tag{G20}$$

as a function of the relative vectorial dispersion σ/F_μ, given different mean vectorial inclinations I_μ. In the limiting case where the relative vectorial dispersion is substantially less than one, $\sigma/F_\mu \ll 1$, the Gaussian declination variance (G19) is approximately that for a Fisher distribution. From (G2) the declination variance is

$$V_f\left(D \mid I_\mu, (\sigma/F_\mu)^2\right) = \int_{D_\mu-\pi}^{D_\mu+\pi} p_f(D)(D-D_\mu)^2\, dD = \frac{1}{3}\pi^2 + 4\left(\frac{F_\mu}{\sigma}\right)^2\left\{\sinh\left[\left(\frac{F_\mu}{\sigma}\right)^2\right]\right\}^{-1}\sum_{m=0}^{\infty}\sum_{n=0}^{m}\frac{\sin^{2m} I_\mu \cot^{2n} I_\mu}{(2m-2n)!!}\left(\frac{F_\mu}{\sigma}\right)^{4m}$$
$$\times\left\{\sum_{j=0}^{n-1}\frac{(2n)!!}{(2m+1)!!(2j)!!(4n-2j)!!(2n-2j)^2} - \left(\frac{\pi}{2}\right)\sum_{j=0}^{n}\frac{(2n+1)!!}{(2m+2)!!(2j)!!(4n-2j+2)!!(2n-2j+1)^2}\left(\frac{F_\mu}{\sigma}\right)^2\cos I_\mu\right\}. \tag{G21}$$

In the opposite limiting case, where the relative vectorial dispersion is substantially greater than one, $\sigma/F_\mu \gg 1$, the Gaussian declination variance is approximately that for a spherically-uniform distribution of directions. From (G3) we have

$$V_u(D) = \int_{D_\mu-\pi}^{D_\mu+\pi} p_u(D)(D-D_\mu)^2 dD = \frac{1}{3}\pi^2. \tag{G22}$$

For the bi-Gaussian declination probability density function (G4), the variance of the declination about the mean declination is just

$$V_{g_2}\left(D \mid I_\mu, (\sigma/F_\mu)^2\right) = \int_{D_\mu-\pi}^{D_\mu+\pi} p_{g_2}(D)(D-D_\mu)^2\, dD$$
$$= \frac{1}{3}\pi^2 + 4\exp\left[-\frac{1}{2}\left(\frac{F_\mu}{\sigma}\right)^2\right]\sum_{m=0}^{\infty}\sum_{n=0}^{m}\sum_{j=0}^{n-1}\frac{(2n)!!}{(2m-2n)!!(2j)!!(4n-2j)!!(2n-2j)^2}\left(\frac{F_\mu}{\sigma}\right)^{2m}\sin^{2m} I_\mu \cot^{2n} I_\mu. \tag{G23}$$

In the limiting case where the relative vectorial dispersion is substantially less than one, $\sigma/F_\mu \ll 1$, the bi-Gaussian declination variance (G23) is approximately that for a Bingham distribution. From (G5) the declination variance is

$$V_b\left(D \mid I_\mu, (\sigma/F_\mu)^2\right) = \int_{D_\mu-\pi}^{D_\mu+\pi} p_b(D)\,(D-D_\mu)^2\,dD$$

$$= \left\{ {}_1F_1\left[\begin{matrix}\frac{1}{2}\\ \frac{3}{2}\end{matrix}; \frac{1}{2}\left(\frac{F_\mu}{\sigma}\right)^2\right]\right\}^{-1}\left\{\frac{\sqrt{2}}{3}\pi^2\left(\frac{\sigma}{F_\mu}\right)\exp\left[\frac{1}{2}\left(\frac{F_\mu}{\sigma}\right)^2\right]\mathrm{daw}\left[\frac{1}{\sqrt{2}}\left(\frac{F_\mu}{\sigma}\right)\right]\right.$$

$$\left. + 4\sum_{m=0}^{\infty}\sum_{n=0}^{m}\sum_{j=0}^{n-1}\frac{(2n)!!}{(2m-2n)!!(2j)!!(4n-2j)!!(2m+1)(2n-2j)^2}\left(\frac{F_\mu}{\sigma}\right)^{2m}\sin^{2m}I_\mu\cot^{2n}I_\mu\right\}, \tag{G24}$$

where Dawson's integral is given by (E14). In the opposite limiting case, where the relative vectorial dispersion is substantially greater than one, $\sigma/F_\mu \gg 1$, the bi-Gaussian declination density function is approximately that for a spherically-uniform distribution of directions, (G22).